Application of Dynamic Energy Budgets to xenobiotic kinetics in *Mytilus edulis* and population dynamics of *Globodera pallida*

R.J.F. van Haren

Application of Dynamic Energy Budgets to xenobiotic kinetics in *Mytilus edulis* and population dynamics of *Globodera pallida*

cover-design by Katinka Bijvoet

ipo-dlo

Application of Dynamic Energy Budgets to xenobiotic kinetics in *Mytilus edulis* and population dynamics of *Globodera pallida*

ACADEMISCH PROEFSCHRIFT

ter verkrijging van de graad van doctor aan
de Vrije Universiteit te Amsterdam,
op gezag van de rector magnificus
prof.dr E. Boeker,
in het openbaar te verdedigen
ten overstaan van de promotiecommissie
van de faculteit der biologie
op maandag 12 juni 1995 te 13.45 uur
in het hoofdgebouw van de universiteit,
De Boelelaan 1105

door

Robertus Johannes Franciscus van Haren

geboren te Nijmegen

Promotor: prof.dr S.A.L.M. Kooijman
Copromotor: dr ir C.J.H. Booij
Referent: prof.dr M.W. Sabelis

aan Katinka
aan mijn ouders

Contents

Chapter 1

General introduction

1.1 Introduction

The living world is characterized by an overwhelming diversity of species. Each species has its own specific way to survive and reproduce. The diversity of species, and the diversity of relations between the species and the abiotic environment leads to an enormous complexity which is too large to grasp immediately.

The individual organism is a relative simple object to study amidst this world of complexity. I take here a realistic viewpoint in which natural objects, as individual organisms are, are directly accessible to us. The study of the individual therefore takes a central place in this thesis. The individual is used as point of reference for further investigations into uptake, elimination and internal compartimentation of xenobiotics in individuals and into population dynamics of individuals.

First, I will give a brief introduction into the history of the notion 'individual organism', together with some ideas concerning the central role of 'individual organism' in biology. After this I will amplify the notion of 'individual organism' by an introduction into the theory of Dynamic Energy Budgets (DEB) for individuals [125].

1.1.1 History of Biology: the concept individual

Current biological knowledge and theory is founded to a large extent on the study of individual organisms. What we now call natural history together with anatomical study of individuals has dominated biological science throughout the greater part of its history. These disciplines initially focused their attention merely on the pure structure of the object. The discovery of the blood circulation by Harvey in 1628 is a landmark in the integrative study of structure and function. Physiological knowledge has increased in the next few centuries by coupling structure and function. A gradual shift in attention has occurred from static structures to dynamic processes. The functional approach has implicitly introduced the notion of time (physical time) into biology. The introduction of the 'idea of time' superimposed on the 'idea of structure' has changed biology.

The word 'organism' as the locus of synthesis of structure and function has been used for the first time in the early eighteenth century, by the German anatomist E.G. Stahl (1660-1734). He describes the living body as 'organism' which is composed of different organs, with each their own function and structure, which in their turn are composed of different parts. The discovery of the 'cell' in 1665 by R. Hooke and M. Malpighi in 1675, the cell nucleus in 1831 by R. Brown and other cell organelles, proteins etc. in the twentieth century has resulted in a cascade of 'organizational levels' down to the smallest parts. On the other hand a cascade up to the biggest entities starts with early studies of populations by Malthus (1798) and Verhulst (1838), stepping stones to the notions of ecosystem, community and global systems. This development resulted in a diverging amount of subdisciplines arranged according to their hierarchical level of organization. The notion of 'organism' ended up as one of the many levels of organization in biology.

The 'idea of time' has changed considerably by the introduction of the 'idea of evolution' by Darwin (1859). The physical notion of time as 'something passing by' is altered by the 'idea of evolution' into a notion of 'change' or 'transition'. The 'idea of evolution' has been a very fruitful one and has developed into an autonomous branch of biology by the rediscovery of the Mendelian inheritance laws and the discovery of DNA as the locus of inheritance. While the time-scale of evolution is in terms of many generations, is the time-scale physiology is operating on, geared to cell division cycles, heart strokes or individual development.

Thus we end up with a hierarchy of structures with fractions at each level. Relations between structures and between hierarchical levels are in first studied as qualitative functional relations. Functional relations are insufficient to lead to a full comprehension of relations acting on structures. Therefore quantitative notions of 'relation' have to be introduced in order to comprehend more completely the relations between structures. The first quantitative notion recognized is the law of conservation of masses found by Lavosier which states that during chemical transformations no mass gets lost. The second notion is the law of conservation of energy, which states that no energy gets lost. These two notions makes it possible to trace and quantify relations between structures and between hierarchical levels. I define relations quantified in this way as processes. The notions of hierarchy, structure, and relation can be summarized in the 'idea of organization' which is 'a hierarchy of structures with fractions at each level which are in qualitative and quantitative relation to each other'. The 'idea of organization' has to be fleshed out with the different notions of time i.e. the physical constant time ('passing by') and the biological changing time ('active time') summarized in the 'idea of evolution or change'.

These two ideas are manifested in each entity of the hierarchy i.e. genes, cell, tissue, organism, population etc. These entities can be regarded as the intersections between the 'idea of organization' and the 'idea of change'. Only some entities strike us as selfsustaining. These entities conserve their organization and pass it over through time (generations). By choosing the individual organism as point of reference one has the additional advantages that it is directly accessible for observation and experimentation, it is somewhere midway in the hierarchical structure and it is already studied a long time in biological history.

1.1.2   The Dynamic Energy Budget model

Kooijman is one of the first who explicitly developed a model of individual (organismal) organization based on energy dynamics which aims to serve as point of reference for both sub- and supra-organismal organization [125]. This individual model is non-specific and can be used to analyze populations and food chains/webs on the basis of individuals. The individual model synthesizes (physiological) subprocesses underlying the parameters of the model. The Dynamic Energy Budget (DEB model) can therefore be used as framework of a research program for regauging biological dynamics. A brief description of the DEB model is given below.

The energy flows through an animal according to the DEB model are shown in figure 1.1. The DEB model describes the energy flows, and changes therein, in environments with varying food densities and temperatures. The DEB model distinguishes three life stages: embryos which do neither feed nor reproduce, juveniles which feed but do not reproduce and adults which both feed and reproduce. The model distinguishes also three main body fractions for an animal: (1) structural biovolume (somatic tissue) (2) stored energy reserves and (3) gonads and/or stored energy reserves allocated to reproduction. The contribution of these body fractions to total biovolume changes with time although homeostasis for each fraction is assumed. The food uptake rate hyperbolically depends on the food density in the environment, it is a type II functional response according to Holling.

The proportion of incoming energy stored is proportional to the surface area of the structural biovolume with a constant turnover (assimilation efficiency) of food into energy. Energy utilization from these reserves is allocated to (a) growth, (b) maintenance and (c) reproduction. A fixed fraction of the utilized energy $(1 - \kappa)$ is allocated to reproduction while the remainder is allocated to growth and maintenance (κ). Energy demands for maintenance have priority over those for growth, which ceases when food densities are low. The energy costs of maintenance are proportional to structural biovolume. At constant food densities, the stored energy reserves are in equilibrium with the environment and consequently growth of structural biovolume is a weighed difference between surface area and volume.

Energy allocated to reproduction is used for maturation in embryos and juveniles, while in adults it is used for maintenance of the degree of maturation and egg production. When the animal becomes adult, the energy spent on development of a certain degree of maturation is then used for reproduction. This energy may be stored temporarily in a buffer which is emptied at oviposition [268].

Because body size and reserves play an important role in the DEB model, a more detailed discussion on body size is appropriate here.

1.1.3   Body size measures

The volume of the organism consists of the structural biovolume, the volume of the stored energy reserves and the volume of reproductive storage or eggs. It depends on the biology of the organism how size measures should be interpreted. Two conditions have to be
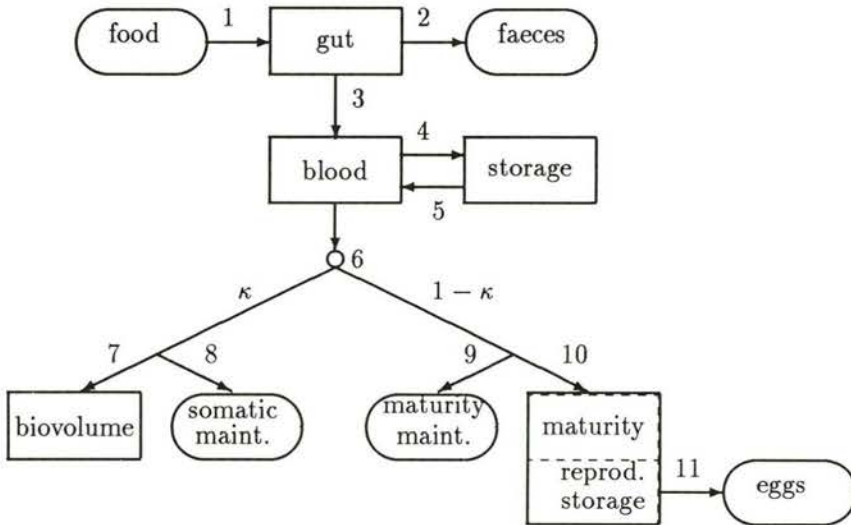
Figure 1.1: Energy flow through an organism. Rates: 1 ingestion (uptake), 2 defecation, 3 assimilation, 4 demobilization, 5 mobilization, 6 utilization, 7 growth, 8 maintenance, 9 maturation maintenance, 10 maturation, 11 reproduction. The rounded boxes indicate sources or sinks, the squares indicate state variables.

fulfilled before size measures can be interpreted in a simple way. Firstly, the contribution to total volume of stored energy reserves and reproductive storage or eggs has to be small compared to structural biovolume. Secondly, the shape of the organism must not change during development. More realistic assumptions about the contributions of reserves to volume and/or weight have been worked out [125], but complicate the interpretation of body size. Size can be measured under these two conditions as length or wet weight, *i.e.* the weight of a living organism without adhering water. Wet weights can be converted to volumes by division by a fixed specific density which is generally close to 1 g.cm^{-3}. An appropriate length measure can be converted to volume when length is multiplied by a fixed dimensionless shape coefficient and the result is raised to the third power. The shape coefficient, which is defined as volume$^{1/3}$.length^{-1}, is specific for the particular way the length measure has been chosen. A simple way to obtain an approximate value for the shape coefficient is to divide the cubed root of wet weight by the length measure under the assumption that the specific density is 1 g.cm^{-3}. The shape coefficient is a measure for the surface area/volume ratio of the organism.

1.2 Aims of research

The aims of research in this thesis were to test the practical applicability of the DEB model. The practical applications reported in this thesis have been instigated by demands from the Dutch government. The first application concerns the extension of the DEB model to uptake, internal distribution and elimination of xenobiotics in the marine mussel *Mytilus edulis* (L.) in estuarine environments. The second application concerns the development of a population dynamic model of the potato cyst nematodes *Globodera pallida* (Stone) and *Globodera rostochiensis* (Woll.), major soil-borne plant pathogens, as an alternative for existing population dynamic models.

1.2.1 The marine mussel and its xenobiotics

The Western Scheldt estuary is a severely polluted estuary. The ministry of Transport, Public Works and Water Management has initiated a major research project (System Analysis Western Scheldt Estuary, SAWES) at the Tidal waters Division (now National Institute for Coastal and Marine Management, RIKZ) in close cooperation with Delft Hydraulics in order to evaluate effects of reductions of loads of different components varying from sewage effluents to heavy metals and organochlorines. The system analytical approach aims to integrate the current knowledge of hydraulics, chemistry and biology in a simulation model for the Western Scheldt estuary. This simulation model has been used for calculation of different scenarios of load reduction for the Western Scheldt estuary. These scenario studies have been used in the negotiations between The Netherlands and Belgium concerning the water treaties.

The DEB model suits the analysis of complex interactions between the marine mussel and ambient xenobiotics and available nutrients. The entwining of xenobiotic kinetics with the individual mussel physiology can only be disentangled by using a physiologically structured model as the DEB model.

The model predicts, for example, the cadmium concentration in the mussel as a function of ambient dissolved and particulate adsorbed cadmium fairly well, see chapter 3. It also appeared from model studies that the bioconcentration factor (BCF) is a function of variables of the model. The BCF depends on the physiological variables size, stored energy density and the reproductive phase of the mussel together with the physico-chemical properties of the xenobiotic. The BCF therefore can not be applied to toxico-kinetic studies of organisms inhabiting highly dynamic environments such as estuaries.

Monitoring studies such as the Mussel Watch are hampered by the physiological interaction of the mussel with its environment. Usually mussels are sampled in length cohorts in order to reduce the variability between different locations. The variability, however, is still considerable. Model studies show that it is produced by different growth rates of mussels of the different locations. Combination of the current monitoring procedures with measurements of growth, as for instance annual rings on the mussel shells, should improve the interpretation of monitoring results. Ambient xenobiotic concentrations can straightforwardly be reconstructed with the additional growth measurements and the developed

DEB based toxico-kinetic model.

1.2.2   Management of the potato cyst nematode

The potato cyst nematode (PCN) is a highly persistent soil borne pathogen in Dutch agricultural practice. Yield losses of the potato crop up to 80% have been recorded due to PCN. Control of potato cyst nematodes highly depends on chemical soil disinfection, crop rotation and growing of resistant potato cultivars. Despite this intensive control PCN remain problematic, due to multiplication on volunteer potatoes (plants growing from potato tubers left behind), loss of resistance to virulent populations and insufficient effectiveness of chemical disinfection.

Although the use of disinfectants have been reduced considerably, pesticides still play a dominant role in control of PCN. Soil disinfectants are the main pesticides used for arable farming in the Netherlands (10.2 million kg active ingredients on a total of 20.0 million kg in 1988 and 6.8 on a total of 15.9 million kg a.i. in 1992 [101]). Public awareness of environmental problems of pesticide application in Dutch agricultural practice, especially its effects on surface and ground water, urged the Dutch government to initiate the Multi-Year Crop Protection plan. Reductions of the use of soil disinfectant fumigants are set at 48% in 1995 and 75% for the year 2000. Preventive soil disinfection will be forbidden in 1997 [4]. As a result of this policy the control of PCN will increasingly rely on crop rotation and the use of resistant potato cultivars.

Development of such cropping systems requires knowledge of the plant-nematode interactions and its environmental dependency. Recorded multiplication rates of PCN on susceptible potato cultivars varies between 2.5 and 150 times in field experiments [214]. This variation is largely unexplained. Schans [204] has initiated system analytical research towards an improved understanding of the plant-nematode interaction in order to reduce the observed variability. His research counterbalances the wide-spread use of purely descriptive models which were developed in the mid-sixties [161, 216, 215]. Schans has focused his research on the early events of the infection process from the plants perspective. His crop growth model is further developed by van Oijen [158, 160, 159]. The DEB model is applied to infection process from the PCN perspective. The DEB model can be used in combination with potato crop growth models as extended by van Oijen [158] and Schans [204].

Application of the DEB model has shown that individual based modelling is feasible for PCN. Population dynamics of PCN is predicted properly in both mesocosm and field conditions. Properties of individuals, such as growth and fecundity measured in controlled laboratory conditions, can be extrapolated straightforwardly to predict population dynamics in the field. Experimental methods have been developed in cooperation with the Centre of Plant Biotechnology and Biochemistry of the University of Leeds, UK, in concordance with the DEB model to assess individual growth and fecundity for different host plants under controlled laboratory conditions.

1.3 Summary

Chapters 2 and 3 show the application of the DEB model to toxico-kinetics of xenobiotics in the marine mussel *M. edulis*. Chapter 2 shows the application to the physiology of the mussel preceding the development of the toxico-kinetic model. Filtering, ingestion, assimilation, respiration, growth and reproduction are successfully described in terms of the DEB model. The relation between oxygen consumption rate and ingestion rate has been derived from elementary model assumptions. Parameters of the DEB model which are estimated for laboratory situations are applied to field data. The varying growth rates in the field have been described by taking account of changes in food density and quality, and temperature, on the basis of the Arrhenius relation. A methodology is given to reconstruct ambient food densities from observed growth curves. This can be used to assess the nutritive value of measured substances such as POM (particulate organic matter) or chlorophyll. The concept of Scope For Growth is discussed in terms of the DEB model.

The DEB model is applied to describe uptake and elimination kinetics of xenobiotics in the mussel *M. edulis* in chapter 3. A multi-compartment pharmaco-kinetic model is used in simultaneous non-linear regression analysis of existing experiments. Data on Cd, PCB's and PAH's are analyzed. The contribution of physiologically determined variables as body size and tissue composition are evaluated on their influence on the pharmaco-kinetics of the xenobiotics. Internal partitioning over body fractions is related to octanol-water partition coefficients (log K_{ow} values) of the organic compounds. Values of the bioconcentration factor (BCF) are evaluated in relation to physiologically determined variables such as body size, stored energy reserves and accumulated reproductive output.

Chapters 4, 5, 6 and 7 show the application of the DEB model to population dynamics of *G. pallida*. Chapter 4 shows an overview of the possibilities of the DEB application. Individual growth and fecundity is directly given by the DEB model. Population dynamics is based on a simple model for resource partitioning between competing females. In this model it is assumed that each nematode ingests a constant fraction of the available nutrients which decreases progressively with increasing numbers of nematodes.

Growth curves of vermiform nematodes and the saccate sedentary plant parasitic nematode, *G. pallida* are compared in chapter 5. They are based on the DEB model and the von Bertalanffy growth model derived from it. Saccate females of *G. pallida* internally cumulate the energy investment allocated to reproduction with a change in their form during growth which accommodates this process. Morphometrical data for the female provide a basis for defining modified growth curves of the Bertalanffy type. It is proposed that many host cultivars of *G. pallida* can be ranked with respect to their level of resistance from measurements of ultimate size made on adult females.

Feeding rates of the potato cyst nematode are studied by apoplastic application of the fluorescence dye fluorescein to the apical root meristem (chapter 6). The increase in fluorescence intensity is studied by low-lux cameras attached to a digital image analysis system, which takes up apoplast real-time analysis of the processed signals. It is found that *G. pallida* by an one-compartied fluorescein. Fluorescent tracer uptake by *G. pallida* is described tracer uptake model. Estimated tracer uptake rates are assumed

to be equivalent to nutrient ingestion rates since ingestion is the only likely tracer uptake route. The measured ingestion rates of adult females are found to vary between 0.16 and 0.75 $mm^3.d^{-1}$. The measured ingestion rates are compared with predicted ingestion rates, based on diameters of the feeding pump in the metacorpal bulb and the feeding pump pulsation frequency. It has appeared that the predicted ingestion rates are lower then the measured ingestion rates. A possible source of error for the predicted ingestion rates is the neglect of pressure differences between syncytium and nematode.

The DEB model is used to analyze the population dynamics of the potato cyst nematode *G. pallida* and to reveal the modes of intraspecific competition (chapter 7). A partitioning model for plant resources that are available to the nematodes is developed which is based upon root growth dynamics and adverse reactions of nematodes on the plant. This model is applied to experiments performed in the field and a mesocosm for different initial population densities and on host cultivars differing in nematode resistance and tolerance. Final population densities and size distributions at these densities are determined after the growing season. The combined models of resource partitioning and individual energy dynamics are applied to these data. It appears that for the interaction with potato cultivar Darwina the model gives a good fit for both the population dynamics and the size distributions of the individuals. The fit for the interaction with potato cultivar Elles is satisfying for the population dynamics but the size distributions are not predicted correctly. Possible reasons for the disagreement are discussed in relation to intraspecific competition.

Part I

The marine mussel

Chapter 2

Mussel Energetics

2.1   Introduction

The dynamics of the energy budget of *Mytilus edulis* (L.) are of interest for several reasons. It is an important species in estuarine environments, which calls for a close analysis of its role in terms of energetics. It is commercially valuable, so it is useful to elaborate harvesting programs that can be maintained for long periods. The species is also used as a monitor organism for environmental pollution. The uptake and elimination behaviour of xenobiotics, especially the lipophilic ones like PCB's, depend on feeding conditions, and so on energetics [131]. Results of environmental monitoring programs such as the "Mussel Watch Program" [81, 172, 17] are therefore difficult to interpret without a toxico-kinetic model based on physiology which can handle fluctuating conditions in the environment.

Modelling physiological energetics in *M. edulis* is usually based on the widely applied Scope For Growth (SFG) concept and allometric relations between body size and physiological rates [16, 23, 248, 14, 124]. The SFG concept is based on the energy balance of a mussel in steady state conditions. The amount of energy gained by the individual under such conditions equals the amount of energy lost due to maintenance, growth and reproduction. The SFG is the difference between energy gained by feeding and energy lost by respiration (supposedly a measure of maintenance). When this difference is positive, energy is available for growth and reproduction, when it is negative, there is a (dry) weight loss due to the utilization of energy reserves [23]. One problem with this approach is that it does not distinguish storage of energy reserves (i.e. lipids, glycogen) from 'structural biomass' in its standardization for body weight.

The necessity to distinguish energy reserves from structural biomass is particularly felt in modelling seasonal variations of body composition. At reproduction mussels experience

19

a dramatic drop in lipid content. Size increase of lipid-rich biomass costs obviously much more energy than of lipid-poor biomass. This type of qualitative differences can only be modelled by separating storage from structural biomass.

The basic difference between 'structural biomass' and storage is that storage materials do not require maintenance and are readily available for use for maintenance, growth and reproduction [129]. This is most easily illustrated by a freshly produced egg, which consists of a relatively large amount of energy reserves and an infinitesimally small amount of structured body mass. As is shown for the pond snail Lymnaea stagnalis (L.), such an egg does hardly respire [102]. Structural biomass on the other hand does require maintenance, i.e. energy used for recycling of proteins, regulation of chemical composition and circulation. It is not as readily available as an energy source for production. Another problem in the application of SFG concerns the interpretation of respiration rates. Although measurements of the energy balance of a particular individual take such a short period that the change in size is negligibly small, the energy invested in growth can be substantial [258, 115]. So part of the respiration measured with a standard conversion to energy is connected with growth, while in the SFG, it is fully assigned to maintenance. This problem can be solved by using a dynamic energy budget (DEB) model, which considers an individual as an input-output system with size and stored energy as state variables.

The purpose of the present paper is to show how the DEB model can be applied to *M. edulis* under submerged conditions. The anaerobic metabolism of littoral individuals is not considered. Originally, the model was developed for *Daphnia magna* Straus [127, 60] and successfully applied to *L. stagnalis* [269] and micro–organisms [130]. It permits the description of embryo development [129, 270], growth [128] and body size scaling relations [126, 128]. Ross & Nisbet [201] argued that it is necessary to modify the model to obtain consistency with published data on mussel physiology. We reanalyzed these data and used additional ones to test the unmodified DEB model. We will first present a brief description of the model and consider the different processes which are relevant for the energetics. Subsequently we will test it against data from the literature and some unpublished data.

2.2   The DEB model

We will restrict the present discussion to the feeding stages, which can be splitted into a juvenile stage which cannot reproduce and an adult one. In these stages, the mussel does not change its shape to any significant extent. The chemical composition of the structural biomass and of stored materials is taken to be constant, so homeostasis is assumed for structural biomass as well as stored materials. Since the composition of stored materials will differ from that of structural biomass, and the storage density can fluctuate, homeostasis is not assumed for the combination of structural biomass and stored materials. A list of frequently used symbols is given in table 2.1.

Two state variables, volume, V (length^3), and storage, E (energy) are distinguished. The choice for storage as a state variable is motivated by the observation that animals undergoing a sharp change in food density adapt only gradually to a new growth rate.

This implies that there is an energy buffer [127]; see also the section on growth.

Uptake is assumed to follow a type II Holling functional response and is taken proportional to surface area (of the filtering apparatus and/or gut), so the ingestion rate is

$$I = \{I_m\}fV^{2/3} \text{ with } f = X/(K + X) \tag{2.1}$$

where X is the food density, K the saturation constant and $\{I_m\}$ the maximum surface area–specific ingestion rate. The filtering rate is $F = I/X$, on the assumption that there is complete retention of particles. The maximum filtering rate is thus $V^{2/3}\{I_m\}/K$. If the digestive system remains filled with processed food, and has a capacity of V_g, the gut passage time is V_g/I [60]. The food-energy conversion is taken to be constant, $\{A_m\}/\{I_m\}$, so the assimilation energy, i.e. the total energy input, equals $\{A_m\}fV^{2/3}$, where $\{A_m\}$ is the maximum surface area–specific assimilation rate. The incoming energy adds to the reserves. When expressed as density, $[E] = E/V$, so energy reserve per volume of body, the reserves follow a first order process. From the assumption of homeostasis for energy reserves it follows that the energy reserves in equilibrium are independent of the length of the mussel i.e.

$$\frac{de}{dt} = vV^{-1/3}(f - e) \tag{2.2}$$

where $e = [E]/[E_m]$, where $[E_m]$ is the maximum storage density and $v = \{A_m\}/[E_m]$ is by definition the energy conductance (length.time^{-1}). The latter concept is well known from plant physiology ([156] p393). The rate at which energy is utilized from the storage, is

$$
\begin{aligned}
C &= -\frac{dE}{dt}\bigg|_{f=0} = [E_m]\left(-\frac{de}{dt}\bigg|_{f=0} V - e\frac{dV}{dt}\right) \\
&= e[E_m]\left(vV^{2/3} - \frac{dV}{dt}\right)
\end{aligned} \tag{2.3}
$$

A fixed fraction κ of the utilized energy is spent on growth plus maintenance. The latter quantity is taken to be proportional to volume, $[M]V$. So $\kappa C = [M]V + [G]\frac{dV}{dt}$, where $[G]$ is the volume–specific costs for growth. Substitution gives

$$\frac{dV}{dt} = \frac{V^{2/3}ev - Vgm}{e + g} \tag{2.4}$$

where the dimensionless investment ratio, $g = [G]/\kappa[E_m]$, and the maintenance rate coefficient, $m = [M]/[G]$ are compound parameters. Growth ceases when the energy reserves drops below $e = V^{1/3}mg/v$. If the food density is constant long enough, equation 2.2 states that e tends to f and remains constant as well. This turns equation 2.4 into the well known von Bertalanffy growth equation, having the solution

$$V(t) = \left(V_\infty^{1/3} - (V_\infty^{1/3} - V_0^{1/3})e^{-\gamma t}\right)^3 \tag{2.5}$$

where $V_\infty^{1/3} = f\kappa\{A_m\}/[M]$ is the ultimate volume$^{1/3}$ and $\gamma = (3/m + 3V_\infty^{1/3}/v)^{-1}$, the von Bertalanffy growth rate. The maximum volume$^{1/3}$ is thus $V_m^{1/3} = \kappa\{A_m\}/[M] = v/gm$, which can only be reached at prolonged exposure to abundant food. The von Bertalanffy growth rate is then minimal and equals $\frac{m}{3}\frac{g}{1+g}$.

Back substitution of equation 2.4 into the storage utilization rate, equation 2.3 gives

$$C = \frac{eg[E_m]}{e+g}\left(vV^{2/3} + mV\right) \tag{2.6}$$

In the absence of feeding and digestion, respiration is taken to be proportional to this utilization rate.

The maximum starvation time, i.e. the time until death by starvation, is found by setting the utilization rate in equation 2.2 equal to the maintenance rate for $f = 0$. Neglecting the small size increase, for a well–fed individual, we arrive at a starvation time of $\frac{V^{1/3}}{v}\ln\frac{V_m^{1/3}}{\kappa V^{1/3}}$.

The energy drain to development plus reproduction equals $(1 - \kappa)C$. The maintenance of a certain degree of maturation is taken to be $\frac{1-\kappa}{\kappa}[M]\min(V, V_j)$. This choice, which is an alternative way of defining κ, makes the costs of development independent from the feeding conditions. The implication is that the cumulative energy drain to reproduction in adults, i.e. in individuals of a body volume larger than V_j, amounts to

$$R_c(t_1, t) = \int_{t_1}^t \frac{1-\kappa}{\kappa}\frac{e(s)}{e(s)+g}[G](vV(s)^{2/3} + mV(s))\, ds - \frac{1-\kappa}{\kappa}[M](t-t_1)V_j \tag{2.7}$$

When growth ceases, the cumulated energy drain to reproduction in animals that continue to allocate energy to reproduction under these circumstances becomes

$$R_c(t_1, t) = \int_{t_1}^t (e(s)\{A_m\}V(s)^{2/3} - [M]V(s))\, ds - \frac{1-\kappa}{\kappa}[M](t-t_1)V_j \tag{2.8}$$

In animals like *Mytilus*, the energy feeding the drain to reproduction accumulates during the non-reproductive seasons inside the animal, but it is assumed to be not metabolically available for other purposes, see the section on reproduction. So, glycogen and lipid in the storage pool differs from that in this one in its availability. Reproduction is upon some internal or external stimulus. For the calculation of the actual reproduction, the cumulated energy has to be divided by the energy investment into a single sperm or egg. See Kooijman, 1986c, Zonneveld & Kooijman, 1991 for expressions of these costs on the assumptions that the initial embryo volume is negligibly small and that the energy density at hatching equals that of the mother at egg formation. At spawning, we assume a reset of R_c to zero.

2.3   Size

Frequently used measures of size of mussels are shell length, wet weight, dry weight and ash free dry weight. For animals like mussels, wet weight, W_w, relates in a simple way to

Figure 2.1: The relation between fresh (wet) weight, W_w, and shell length, L. Data from Borchardt [35]; Pieters et al. [175]; Dutch contribution to ICES, Copenhagen. The least squares fitted curve is $W_w = d_w(d_m L)^3$ with $d_w = 1$ g/cm^3, $d_m^3 = 0.03692$ (SD $7.59 \cdot 10^{-5}$). It does not differ significantly from the best fitting allometric one $W_w = 0.02774 L^{3.157}$ on the basis of the likelihood ratio test ($p = 0.096$).
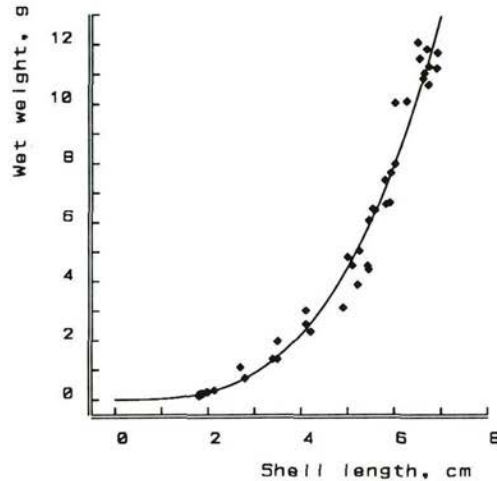
body volume, assuming a constant specific density close to $d_w = 1$ g/cm^3. The rationale is that storage compounds replace water [175] and have about the same specific density. For isomorphs, shell length relates to volume as $d_m L = V^{1/3}$, where d_m is called the shape coefficient. Figure 2.1 confirms this relation. The data represented imply that the shape coefficient $d_m = 0.333$ (SD 0.097). Kooijman [128] estimated a shape coefficient of 0.394 based on the intra shell volume.

The advantage of length above wet weight is that it allows an easy and accurate measurement which is not destructive. Dry weight or ash free dry weight of the soft parts is a weighted sum of volume, V, storage materials, E, and cumulated reproductive material, R_c. Both latter compounds vary with habitat and season [175, 267]. dry weights of the soft parts of a 4.0 cm *M. edulis* take values as extreme as 130 mg and 630 mg, and beyond [116].

The largest mussels found in nature tend to occur in subarctic and arctic regions because of the high food densities [186]. Theisen [236] and Thompson [238] report mean shell lengths of 9.2 and 9.4 cm in Greenland and Newfoundland respectively. Theisen reports shell lengths exceeding 9.2 cm. Unfortunately he gave no actual lengths because these shells went lost during the meal. The theoretical maximum will doubtless be higher, because plankton densities fall in winter.

2.4 Temperature

Acute and long–term responses of *M. edulis* to temperature changes have been described by several authors; for a review see Bayne [16] (p141) and Jørgensen [115] (p50-51). Knowledge of long term–temperature responses is needed for comparing experiments carried out under different temperature regimes. The long–term temperature response is also needed for
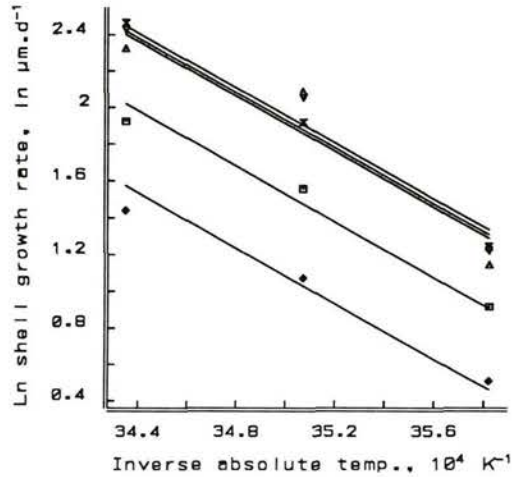
Figure 2.2: Arrhenius plot for shell length growth rates of larval mussels at 2, 5, 10, 20 and 40 cells Isochrysis/mm^3. Data from Sprung [227]. The Arrhenius temperature is 7579 (SD 167) K.

applying the model to field conditions with seasonally fluctuating temperatures.

The way rates depend on temperature is usually well described by the Arrhenius relation within a species–specific tolerance range [128]. In *M. edulis* the range is 5-20°C [256, 255]. At lower temperatures, the actual rates are lower than expected because the animal remains in a kind of resting phase until the temperature rises again [128]. At higher temperatures, animals usually die. Lethal temperatures for sublittoral *M. edulis* vary from 27°C to 40°C as a function of the exposure regime [16] (p181).

The Arrhenius temperature is estimated using growth rates of larval shell length (figure 2.2). We assume that, as a first approximation, all physiological rates are affected in the same way with deviations at temperatures exceeding 20°C. Nielsen [155] and Widdows & Bayne [256] report decreasing growth rates of (juvenile) mussels with increasing temperatures, which is in contrast with the expected increasing growth rates (figure 2.2). The explanation might be in the depletion of food at higher temperatures due to elevated metabolic rates.

Results of Widdows [254] and Widdows et al. [257] suggest that there is no long–term effect of temperature on filtration rates of *M. edulis* when rates are corrected to a standard weight of 1 g dry weight. However, during the season, food tends to covary with temperature, so does the reserves and thus the dry weights. Standardization on the basis of dry weights therefore obscures the effect of temperature, if the change rate in reserves matches with that of temperature. We use an Arrhenius temperature correction for filtering rates as well, the Arrhenius temperature being $T_A = 7600$ K. The rate at absolute temperature T_1 is thus obtained from that at T_0 according to $v_{T_1} = v_{T_0} e^{T_A(1/T_0 - 1/T_1)}$.

2.5 Food

Since energy uptake depends on food availability and quality, some remarks on food for mussels are in order, because it is hard to characterize.

Suspended particles in natural conditions are mixtures of organic and inorganic compounds which vary in size. If larger than 4 μm in diameter, they are fully retained by *M. edulis* whereas a 50% retention is reported for particles of 1 μm in diameter [246, 147]. Particles less than 1μm are poorly utilized [262, 85]. Field monitoring programs frequently use the 0.45 μm mesh sieve to distinguish 'dissolved' from particulate or suspended matter (SM). This criterion is also used in the following sections. Thus *M. edulis* will be able to retain most of the particulate matter suspended in the water column.

Particulate organic matter (POM, defined as SM minus its ash weight) is the major food component for *M. edulis*. Laane et al. [135] distinguish a refractory fraction which can not be utilized by metazoans. The non-refractory fraction of POM mainly consists of phytoplankton and detritus. POM in estuaries originates from autochthonous production and allochthonous sources, vs rivers and coastal waters. The detritus concentration in estuaries and coastal waters far exceeds the concentration of phytoplankton [135]. Rodhouse et al. [199] explained high length growth rates of *M. edulis* in winter by allochthonous detritus input into the estuary.

The nutritive value of POM can be estimated by the protein, carbohydrate and lipid contents [257, 135]. The nutritive value expressed as energy per mg SM varies considerably among estuaries and seasons. Typical yearly ranges are 22.2-24.8 J.mg SM^{-1} (Lynher estuary, U.K., [257]), 0.29-15.9 J.mg SM^{-1} (Gironde, France, [135]), 0.18-5.9 J.mg SM^{-1} (Ems-Dollard estuary, the Netherlands, [135]). The nutritive fraction of SM follows a seasonal cycle, similar to that recorded for percentage ash- free material of SM [257]. The POM concentration in water can be used as a measure of food energy for *M. edulis* after conversion of POM to its mean energy equivalent of 20.3 J.mg POM^{-1} [20].

2.6 Feeding, ingestion and assimilation

High SM concentrations (2.6-5 mg.dm^{-3}, [257]; 3.2-7.4 mg.dm^{-3}, [21]) induce the production of pseudofaeces, consisting of material cleared from suspension but rejected by the mussel before ingestion. Selection for the digestible fraction of SM is demonstrated by Kiørboe et al. [123], who used mixtures of resuspended sediments with cultured algae in their experiments. However, Foster-Smith [70] and Widdows et al. [257] found no selection. The labial palp plays a role in sorting incoming material, which is conveyed to the mouth or to the rejection tracts [16] (p.143-144). Theisen [237] has shown that palp size increases with increasing SM concentrations in water. He suggests that large palp size is an adaption to live in turbid waters.

Food intake is a function of body size, particle concentration, and pseudofaeces production [261]. A retention efficiency of 100% for POM is assumed here. This is realistic under most field conditions. We also assume that the fraction of POM in pseudofaeces is
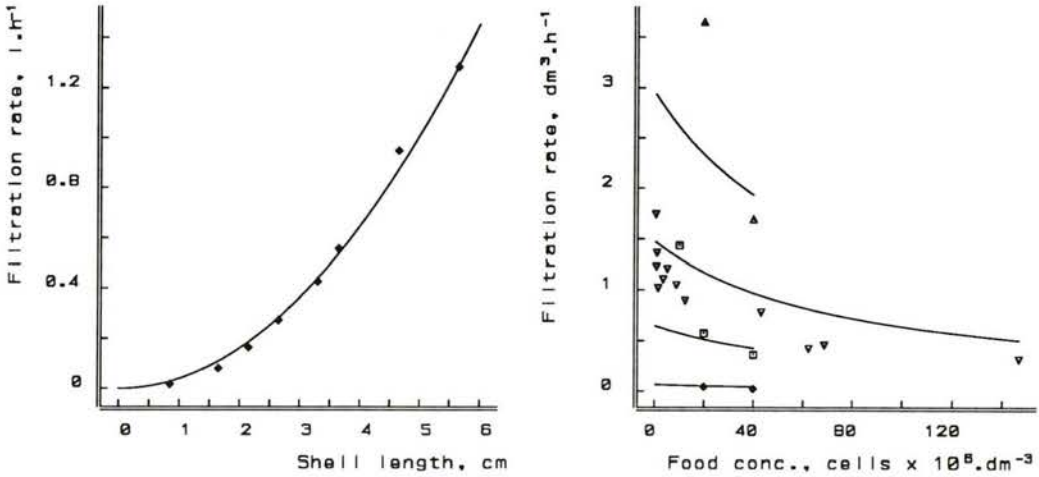
Figure 2.3: Left: The filtration rate as function of shell length, L, at constant food density ($40 \cdot 10^6$ cells.dm^{-3} *Dunaliella marina*) at 12°C. Data from Winter [260]. The least squares fitted curve is $\{F\}(d_m L)^2$, with $\{F\}= 0.041$ (SD $6.75\ 10^{-4}$) dm^3.h^{-1}.cm^{-2}, which does not differ significantly from the best fitting allometric one $0.039L^{2.03}$ on the basis of the likelihood ratio test (p =0.66). Right: The filtration rate, F, as function of food density, X, for different shell lengths, L. Rates are corrected to 15°C and shell lengths are (from bottom to top) resp. 0.85, 2.65, 4 and 5.65 cm. Data from Winter [260] and Schulte [210] (4 cm only). The simultaneously least squares fitted curves are $F = \frac{\{F_m\}(d_m L)^2}{1+X/K}$, with $\{F_m\} = 0.83$ (SD 0.098) dm^3.cm^{-2}.h^{-1} and $K = 76$ (SD 42) 10^6 cells.dm^{-3}.

negligibly small. Filtration and ingestion rates are closely related for food densities low enough to prevent pseudofaeces production. At such densities, all the filtered material is ingested.

Foster-Smith [71] found that the square root of the gill area is proportional to shell length. Figure 2.3 shows that filtering rate is proportional to squared length. Since no pseudofaeces occurred, ingestion is likely to be proportional to squared length as well. Winter [261] and Møhlenberg & Riisgård [148] reported scaling parameters for wet weights of 0.73 at constant food density of $40 \cdot 10^6$ cells.dm^{-3} and 0.66 at different food densities. In Winters' review [261] scaling parameters are reported to vary between 0.27 and 0.82 for dry weights.

At high food densities, the food handling organs (cirri, gill filaments, mucus strings, labial palp and gut) become saturated. Foster-Smith [70], Riisgård & Møhlenberg [191] and Riisgård & Randløv [192] observed decreasing filtration rates at increasing food densities. This decrease has obviously the function of providing the ingestive system with limited amounts of food it can handle. Figure 2.3 shows the fitted filtration rates at four different shell lengths as a function of food density. The rates are corrected to 15°C.
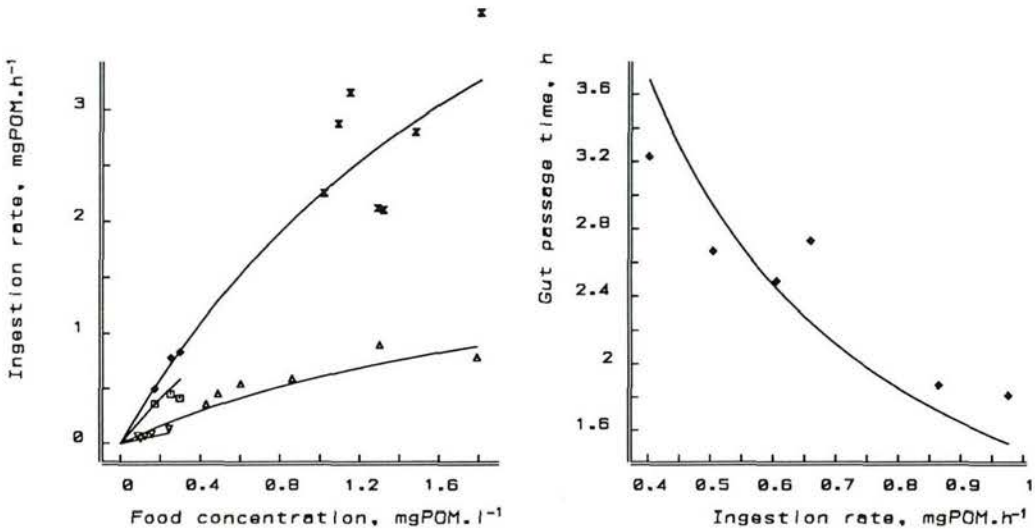
Figure 2.4: Left: The ingestion rate, I, as function of food density, X, for different shell lengths, L. Food is added as mixtures of algae or organic matter with silt (anorganic particles). Rates are corrected to 15°C and the shell lengths are resp. (from bottom to top) 1.75, 2.5, 4.25 and 4.8 cm, data from resp. Kiørboe et al., [122]; Bayne et al. [21]; Bayne et al. [20] and Smaal (pers. com.). The simultaneously least squares fitted curves are $I = \{I_m\}(d_m L)^2 X/(K + X)$, with $\{I_m\}$ = 3.0 (SD 1.0) mg POM.cm^{-2}.h^{-1} and K = 2.4 (SD 1.3) mg POM.dm^{-3}.
Right: The gut passage time as a function of ingestion rate for a 2.5 cm mussel feeding on a mixture of *Isochrysis galbana*, *Phaeodactylum tricornutum* and ashed silt at 14°C. Data from Bayne et al. [21]. The least squares fitted curve is $T = V_g/I$, with gut content $V_g = 1.48$ (SD 0.077) mg POM.

In very dilute suspensions *M. edulis* ceases filtering [16](p139). Riisgård & Randløv [192] reported a threshold food concentration of $1.5 \cdot 10^6$ *Phaeodactylum tricornutum* cells.dm^{-3} for a 2 cm mussel ($\simeq$ 0.024 mg dry weight.dm^{-3}, [122]), below which no filtration occurs due to shell closure. After a period of 24 days at a constant low or high food level, *M. edulis* reacts within an hour to changes in algal concentrations by opening or closing its shell.

Figure 2.4 shows the ingestion rate as function of food density at different shell lengths. The maximum ingestion rate coincides with the threshold concentration at which pseudofaeces production starts. Bayne et al [21] reported an maximum ingestion rate for a 2.5 cm mussel of 1.8 mg POM.h^{-1} (corresponds in his experiments with a SM concentration of 7.43 mg.dm^{-3}, 14° C) which is close to the calculated value of 1.64 mg POM.h^{-1} based on the fitted curves in figure 2.4. So the assumption of 100% sorting efficiency is corroborated by these results. Figure 2.4 confirms that the gut passage time is inversely related to ingestion rate, which implies that the food loading of the digestive system remains constant.

The assimilation efficiency of food in the gut depends on food density [16] (p.457) or

Figure 2.5: The assimilation rate as a function of ingestion rate for mussels ranging from 1.75 to 5.7 cm. Data from Bayne et al. [20, 21]; Borchardt [35]; Kiørboe et al. [122] and Hawkins & Bayne [96]. All rates are corrected to 15°C. The fitted line is $A = I\{A_m\}/\{I_m\}$ with $\{A_m\}/\{I_m\} = 11.5$ (SD 0.34) J.mg POM^{-1}.
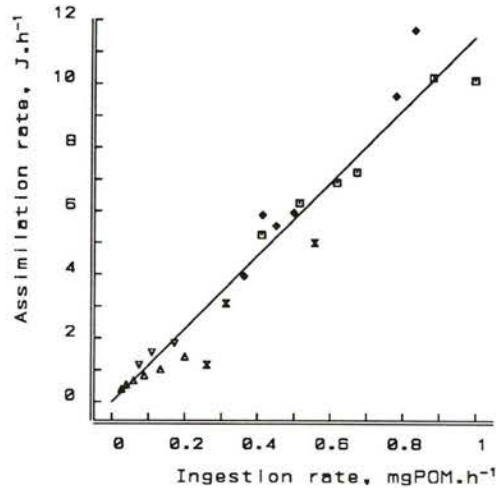
ingestion rate [70, 35]. When data from several sources are combined, these dependencies are not obvious, see figure 2.5. The presented assimilation rates were obtained by multiplication of the assimilation efficiency of Conover [42] with the ingestion rate and the 'mean' energy equivalent of POM. This leads to an average food–energy conversion of $\{A_m\}/\{I_m\}$ = 11.5 J.mg POM^{-1}, which is 0.57 times the 'mean' energy equivalent of POM.

2.7 Respiration and maintenance

The oxygen consumption rate as function of length at constant food densities is shown in figure 2.6. On the basis of the DEB model, we expect a proportionately of the oxygen consumption rate to $V + V^{2/3}v/m$, which closely resembles frequently postulated one to $W^{0.75}$ based on weight [127, 60]. The scaling parameter for *M. edulis* varies between 0.595 and 0.930 at different temperatures and dry weights [16] (p.161). Hamburger et al. [87] found a scaling parameter of 0.903 for veliger larvae and 0.663 for adult mussels. They based their calculations on dry weight instead of wet weight or shell length which bias the estimation of the scaling parameters by the fact that energy reserves do contribute substantially to dry weights, while not requiring energy for maintenance.

Three different levels of oxygen consumption rate of *M. edulis* have been empirically identified by Thompson & Bayne [239] in relation to changes in food density. The standard oxygen consumption rate is defined in the absence of food when the oxygen consumption rate declines to a steady state. The active oxygen consumption rate is reached when a starved mussel is fed. Between the limits of standard and active oxygen consumption rates the mussel can show several routine oxygen consumption rates [16]. Thompson & Bayne [240] showed that the oxygen consumption rate depends hyperbolically on the ingestion rate. This is consistent with the DEB model, if the contribution of filtration,
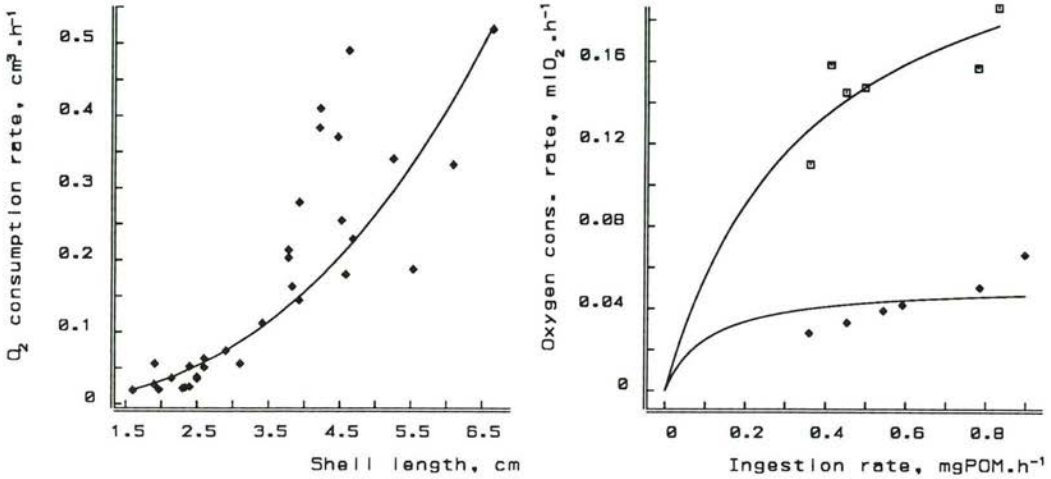
Figure 2.6: Left: The oxygen consumption rate as function of shell length, L, at constant food density at 15°C. Data from Kruger [133]. The least squares fitted curve is $O_r = [O_0](L^3 + \frac{v}{m}L^2)$ with $[O_0] = 0.022$ (SD 0.0074) cm^3 O$_2$.cm^{-3}.h^{-1} and $\frac{v}{m} = 26.5$ (SD 14.8) mm.
Right: The oxygen consumption rate as function of ingestion rate, I, for the shell lengths, L, 2.5 and 4.5 cm. Data from Bayne et al. [20, 21]. Rates are corrected to 15° C. The simultaneously least squares fitted curves are $O_r = \frac{O_s I}{(d_m L)^3} \frac{d_m L + v/m}{I(d_m L)^{-2} + g\{I_m\}}$ with $O_s(d_m L)^{-3} = 0.056$ (SD 0.025) cm^3 O$_2$.h^{-1}.cm^{-3}, $v/m = 5.3$ (SD 6.5) mm, $g\{I_m\} = 0.16$ (SD 0.07) mg POM.cm^{-2}.h^{-1}.

ingestion and digestion to respiration is negligible [258, 115]. Substitution of equation 2.1 into equation 2.6 leads to $O_r = O_s \frac{I}{V} \frac{V^{1/3} + v/m}{IV^{-2/3} + g\{I_m\}}$ where the proportionately constant O_s (cm^3 O$_2$.h^{-1}) stands for the standard oxygen consumption rate of an individual. This is so because a prolonged ingestion rate of $\{I_m\}VV_m^{-1/3}$ just balances the maintenance costs $V[M]/\kappa$. At maximally prolonged ingestion, when $I = \{I_m\}V^{2/3}$, the oxygen consumption rate thus becomes $O_r = O_s \frac{1 + V^{-1/3}v/m}{1 + g}$. This corresponds with the active oxygen consumption rate of Thompson & Bayne [239]. In figure 2.6 the oxygen consumption is related to ingestion for mussels of different sizes. The estimated parameters are not very useful because a slight deviation in the shell lengths causes a large deviation in the parameter estimates.

After the cessation of growth, oxygen consumption, O_r, during starvation is proportional to the energy spent on maintenance plus reproduction. It decreases exponentially at a rate proportional to body length [126, 60] in animals that do not change their storage dynamics and continue to allocate energy to reproduction :

$$O_r(t) = \{O_0\}V^{2/3}\exp\{-vtV^{-1/3}\} \tag{2.9}$$

where $\{O_0\}$ is the proportionately constant (cm^3 O$_2$.cm^{-2}.h^{-1}) which depends on the food history at the start of the experiment. The oxygen consumption rate and carbohydrate

Figure 2.7: The oxygen consumption rate, $\bowtie$, and the carbohydrate weight, $\square$ and $\cdots$, in starving 4.5 cm mussels at 15°C. Data from Bayne & Thompson [24]. The simultaneous least squares fitted curves are $O_r(t) = O_0 e^{-vt/d_m L}$, with $O_0 = 0.33$ (SD 0.046) cm^3 O$_2$.h^{-1} and $v = 0.25$ (SD 0.009) mm.d^{-1} and $V(t) = W_0 e^{-vt/d_m L}$, with $V_0 = 23.2$ (SD 0.55) mg.
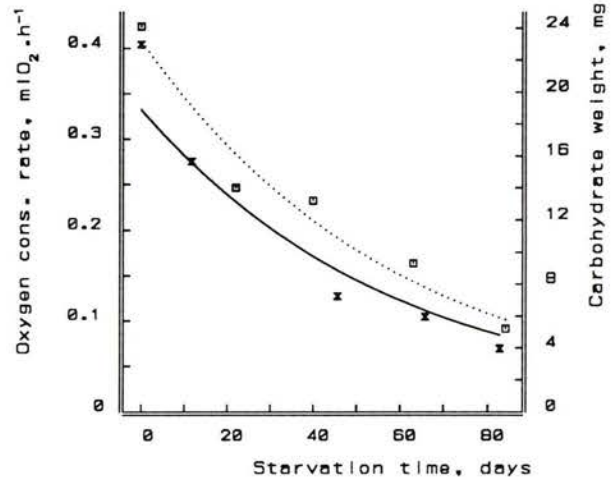
weight as a function of starvation time at two different body sizes is shown in figure 2.7. Respiration rate and dry weight decrease concomitant during starvation. Standardisation of respiration rate on dry weight of the mussel obscures the effect of starvation on respiration and results in a 'constant' respiration rate. The estimated value of the energy conductance v at 15°C, 0.25 (SD 0.009) mm.d^{-1} is close to the value of 0.22 (SD 0.018) mm.d^{-1} estimated with data of decreasing lipid weights during starvation [1].

2.8   Growth

Age is usually determined in the field on the basis of rings in the shell [140, 188], size frequencies [25], or it is known in experimental setups [119]. When food density is constant or when food is abundant, the von Bertalanffy growth curve, equation 2.5 should fit. The fit is mostly satisfying, see figure 2.8 and table 2.2. This implies that the yearly means of food density and temperature remain more or less constant at the sites of sampling (exposed rocky shores in Yorkshire, U.K., Seed, 1969b).

Sigmoid growth curves, like the age–based Gompertz growth curve, sometimes fit available data better [236, 25]. Variations in food density and/or temperature affect growth such that the solution of equations 2.2 and 2.4 can take almost any shape [128]. Kautsky [120, 119] measured the mussels individually in cages (ø10 cm) at a depth of 15 m in the Baltic at 7 S°/$_{oo}$ salinity. These data, see figure 2.8, clearly show the annual cycle in growth. Assuming that the rates depend on temperature in an Arrhenius way and that the change in food density is slow enough to approximate the energy reserves with $e = f$, equation 2.4 can be used to reconstruct the (not measured) food density. So, the predicted
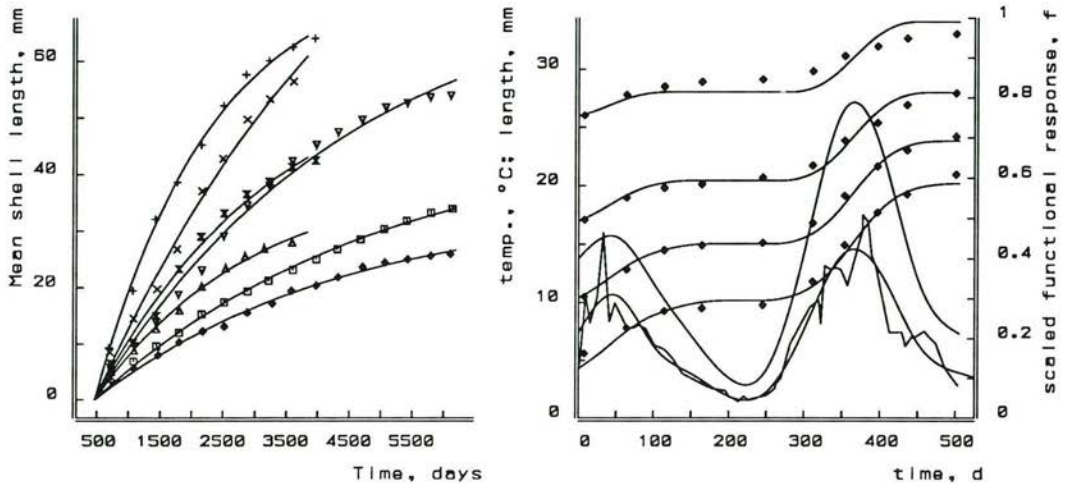
Figure 2.8: Left: The von Bertalanffy growth curves fitted to length–time data, as reported by Seed [211] on intertidal North Sea mussels. The parameter values are listed in table 2.2.
Right: The reconstruction of scaled functional response since 1 august from mean length–time data as reported by Kautsky [119], given a cubic spline description of the measured temperature. Initial lengths were 4.3, 10.4, 17 and 26 mm. Parameters: $L_m = 100$ mm, $g = 0.13$, $m_{15} = 0.03$ d^{-1}, $T_A = 7600$ K.

length is found from

$$\frac{d}{dt} L = \frac{(L_m f(t) - L)_+}{3(f(t) + g)} g m_{15}(T(t) > T_0) e^{T_A(\frac{1}{288} - \frac{1}{T(t)})} \tag{2.10}$$

where m_{15} denotes m at 15°C. We used a cubic spline function to describe temperature $T(t)$. The reconstruction of scaled food density $f(t)$ from the length– time data then amounts to the estimation of the values at chosen time points. In view of the scatter, which increases in time in the upper size class in the original data, the fit is acceptable. This illustrates that there is no need to modify equation 2.4 to describe sigmoid growth curves. The von Bertalanffy growth rate at $f = 1$ is 0.42 y^{-1} at 15°C on the basis of the parameter values given in figure 2.8. The ratio of the peaks of the scaled functional responses is 1.66. The peak temperatures differ 4°C, which corresponds with a factor 1.45 in the maximum surface–specific uptake rates of mussels as well as algae. The remaining difference in primary production could possibly be explained by an increase in received solar radiation with temperature.

Strömgren & Cary [233] found decreasing shell length growth rates during starvation. This can be described by equations 2.2 and 2.4. During the experiment, the mussels in the range of 12-22 mm grew 0.75 mm. When we neglect the change in length, equation 2.2

Figure   2.9:
The growth rate in starved mus-
sels at 21.8°C. Data from Strömgren
& Cary [233].   The fitted curve
is $\frac{d}{dt}L = \frac{v\exp\{-vt/d_mL\}-gmd_mL/e_0}{3d_m(g/e_0+\exp\{-vt/d_mL\})}$,
with the shape coefficient d_m =
0.333 and $L = 1.7$ cm. The least
squares estimates were $\frac{g}{e_0} = 12.59$
(SD 1.21), $m = 2.36$ (SD 0.99)
10^{-3} d^{-1} and $v = 2.52$ (SD 0.183)
mm.d^{-1}.
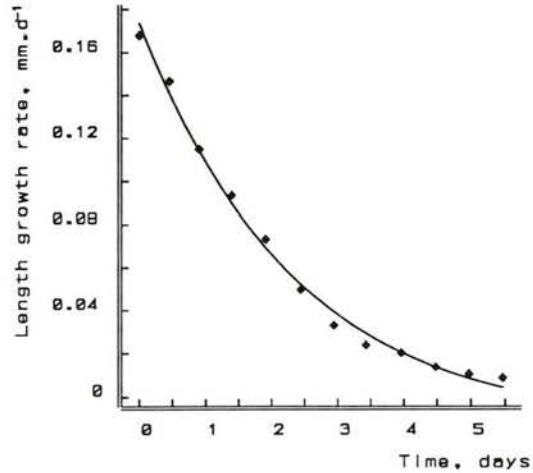
gives $e(t) = e_0\exp\{-\frac{vt}{d_mL}\}$. Substitution into equation 2.4 gives

$$\frac{dL}{dt} = \frac{v\exp\{-\frac{vt}{d_mL}\} - d_mLm\frac{g}{e_0}}{3d_m(\exp\{-\frac{vt}{d_mL}\} + \frac{g}{e_0})} \tag{2.11}$$

Figure 2.9 shows a good fit. The parameter values loose a bit of their value by the broad
length range of the mussels and the way they are selected for measurement.

We finally consider growth in situations where temperatures and food availabilities
changed and have been measured; see figure 2.10. The estimation of food density during
the season from field data is difficult, therefore a smoothed cubic spline function is used.
A length data set of *M. edulis* is chosen from available data in the Oosterschelde (Dutch
Delta area). The predicted shell lengths based on the forcing functions of temperature and
food are shown in figure 2.11.

The deviation of the measured shell lengths from the prediction approximately amount
to a factor of 2. This deviation is mainly caused by the few measurements of actual food
densities in the field, see figure 2.10, and the differences in food qualities between laboratory
and field [233]. The energy content of algae cultured in the laboratory is generally lower
than from those grown in the field. It is difficult to mimic the nutritive quality of POM in
the laboratory unless fresh seawater is used. Values of the saturation constant K and the
energy conductance v are affected by differences in food quality. When a free fit of these
parameters is allowed, the length growth curve fits satisfactorily with the measured shell
lengths. The adjusted parameter value for the saturation constant K is 1.69 (SD 0.628) mg
POC.dm^{-3} (which is equivalent to 4.23 mg POM.dm^{-3}) and for the energy conductance v
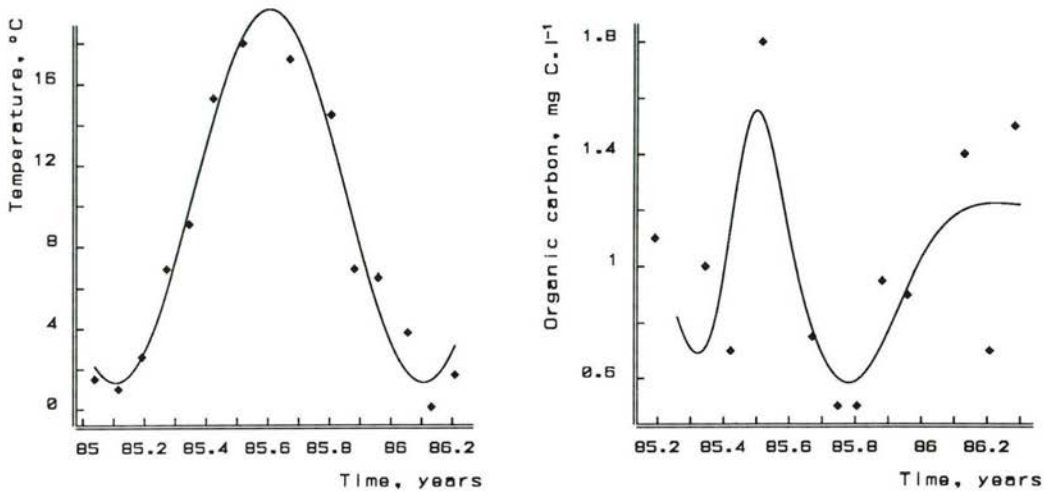is 0.59 (SD 0.07) mm.d^{-1} at 15°C.

Figure 2.10: The measured temperature (left) and POC concentrations (right) in the Ooster-schelde estuary (near the Storm Surge Barrier) during 1985 and 1986. Data from the Ministry of Public Works and Transport, Tidal Division. The curves are a least squares fitted sinus and a cubic spline.

2.9 Reproduction and spawning

Seed [212] reports lengths of fully mature mussels of 6-7 mm in areas of rapid growth and lengths of 2 mm in areas of exceptionally slow growth. Kautsky [120] reports that maturity in the slowly growing Baltic *M. edulis* is reached at sizes smaller than 6 mm. Pilar-Aguirre [176] observed lengths of fully mature mussels of 35 mm on the Spanish coast. Zonneveld & Kooijman [269] observed that the size at first maturity in the pond snail L.stagnalis depends on day-length. Simultaneous changes in growth and reproduction could be used to deduce that day length only affects the partition coefficient κ and so the energy available for maturation.

M. edulis has a pronounced annual cycle for gametogenesis with one or several spawn-ings in spring and summer [16] (p22). The annual cycle is usually described by discrete stages of gonad development, viz. resting stage, the ripe gonad and the spawning gonad. Observations by Zandee et al. [267] and Pieters et al. [174] showed that energy investment into spawning is a continuous process. They found that the lipid level in mantle tissues, where the gonads are located, increases steadily after spawning. Total lipid accounts for up to 30% of the egg dry weight [174].

Bayne et al. [19] carried out experiments with labeled ^{14}C to measure carbon incor-poration in mantle tissue of mussels fed a low and high ration (non–growing and growing mussels respectively). Their results show that more ^{14}C was transferred to the eggs at low than at high rations. This is to be expected on the basis of the DEB model, which

Figure 2.11: Fitted shell lengths in the Oosterschelde estuary during 1985 and 1986 based on measured temperature and POC concentration. Data from the Ministry of Public Works and Transport, Tidal Division. The predicted parameters based on laboratory results were $K = 0.96$ mg POC.dm^{-3}, $v_{15}=0.23$ mm/d, $g=1.03$ and $m_{15}g= 0.0052$ d^{-1}. The deviating least squares estimated parameters were $K = 1.15$ (SD 0.38) mg POC.dm^{-3} and $v_{15}=0.59$ (SD 0.07) mm/d.
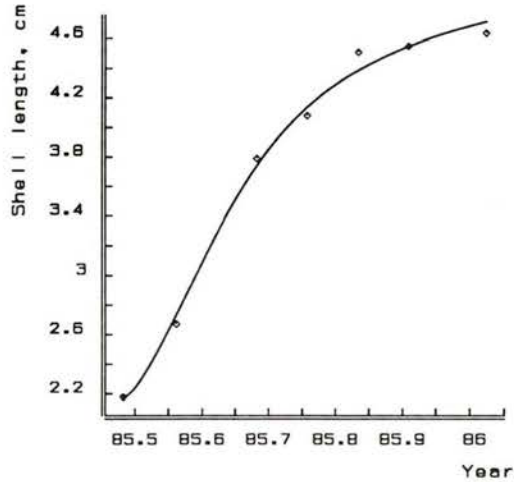
assumes an energy drain to reproduction, even under non–growth conditions. Mussels in prolonged non–growth conditions continued to develop new gametes, but some regression and resorption occurred in conditions of severe stress [22]. When gametogenesis is at an early stage, Bayne et al. [18] found that carbohydrates in the mantle connective tissue are reallocated for routine metabolism. When the development is advanced, however, the reallocation does not occur.

The ration level of adults is apparently important for the condition of their offspring. Bayne et al. [19] observed that larvae developed from the gametes of adults fed a low ration had a lower growth rate than larvae from well fed adults. This is qualitatively consistent with the DEB model [129]

Somatic production has an optimum at an intermediate age of the mussel while gonadic production increases with increasing age [25, 238, 198]. The DEB model implies that, at constant food density, the maximum body growth occurs at $V_\infty 8/27$ (Koois86a). Figure 2.12 shows the data and the curves fitted on the basis of the DEB model for three populations, in Stony Brook Harbour, New York (USA) [198], and in the Lynher and Cattewater estuaries, Morecombe Bay (U.K.) [25]. The fitted curves represent the shell length and yearly somatic and gonadic production which are fitted simultaneously with four free parameters. The trends in the data are well described by the DEB model.

The fraction κ shows marked regional differences. The value of κ in the British populations are 0.94 (SD 0.0067) and 0.99 (SD 0.0095) respectively, while the population in Stony Brook Harbour has a value of 0.71 (SD 0.050). These differences might be explained by a genetic control of fecundity [198, 99, 72].

2.10   Discussion

The DEB model provides a framework to describe a wide variety of physiological processes. Many data from the literature could not be used to test the theory and estimate the parameters, because essential information for their interpretation had not been provided. Differences in parameter values obtained from data taken from the literature are due to differences in experimental methods, temperature, salinities, water depths and food conditions and, to some extent, genetic variation. The following parameter estimates summarize the results for the tests against experimental data: $g = 1.03$, $m = 0.00517\ d^{-1}$, and $v = 0.23$ mm.d^{-1} at 15°C. This gives a maximal length of 13 cm and a maximal starvation time of 114 days for a 3 cm mussel. It is not known to which extend populations differ genetically in their parameter values or how the parameter values depend on environmental variables like salinity.

The early budget studies simply describe growth as proportional to the difference between assimilated and respired energy. The SFG concept conceives growth as the sum of somatic and gonadic production. These approaches do not allow for variations in internal states such as storage, which makes it impossible to accommodate results like those presented in figure 2.9. When SFG is expressed on a dry weight basis, changes in the energy buffer affect the SFG which give a false impression of actual growth in transient situations such as recovery from starvation. No concept seems so simple as body size at first glance and proved to be so difficult afterwards. The DEB model is based on volume, in which light the custom of standardization to fixed dry weights gives misleading results.

The models developed for mussel or filter feeder growth are usually based on allometric scaling relations and SFG calculations. Ross & Nisbet [201] modified the DEB model in order to explain the observed length and dry weight patterns in the size range 5-35 mm, to account for sigmoid growth. They dropped the proportionately of assimilation rate to surface area. The data here tested against the DEB model gave no reason to alter the underlying assumptions. Sigmoid growth curves are expected on the basis of the DEB model when food densities and temperatures vary through the seasons.

Table 2.1: Variables, primary and compound parameters

symbol	dimension	interpretation
variables		
t	time	time
X	weight.length^{-3}	food density
V	length^3	body volume
E	energy	energy storage
e	energy.length^{-3}	scaled energy storage density: $E/[E_m]V$
R_c	energy	cumulated energy investment into reproduction
primary parameters		
V_b	length^3	volume at birth
V_j	length^3	volume at start reproductive stage
K	weight.length^3	saturation constant
$\{F_m\}$	length^3.length^{-2}.time^{-1}	maximum surface area–specific filtration rate
$\{I_m\}$	weight.length^{-2}.time^{-1}	maximum surface area–specific ingestion rate
$\{A_m\}$	energy.length^{-2}.time^{-1}	maximum surface area–specific assimilation rate
$[E_m]$	energy.length^{-3}	maximum storage density
$[M]$	energy.length^{-3}.time^{-1}	volume–specific maintenance costs per unit of time
$[G]$	energy.length^{-3}	volume–specific costs for growth
κ		fraction of utilized energy spent on maintenance plus growth
d_m		shape coefficient
compound parameters		
v	length.time^{-1}	energy conductance: $\{A_m\}/[E_m]$
m	time^{-1}	maintenance rate constant: $[M]/[G]$
g		energy investment ratio: $[G]/\kappa[E_m]$

Table 2.2: Ultimate shell lengths and von Bertalanffy growth rates (with SD).

source	sample method[†]	temp. °C	L_∞ cm	γ d^{-1}
Rodhouse et al. [199]	c	11	9.60 (0.157)	$2.95 \ 10^{-4} \ (1.13 \ 10^{-5})$
	c	11	7.46 (0.296)	$3.45 \ 10^{-4} \ (2.53 \ 10^{-5})$
	c	11	6.01 (0.429)	$3.39 \ 10^{-4} \ (4.38 \ 10^{-5})$
Page & Hubbard [167]	b	14.8	9.07 (0.043)	$5.26 \ 10^{-3} \ (5.45 \ 10^{-5})$
Bayne & Worrall [25]	a	10[‡]	10.8 (2.61)	$3.74 \ 10^{-4} \ (1.30 \ 10^{-4})$
Seed [211]	c		3.46 (0.282)	$2.56 \ 10^{-4} \ (3.61 \ 10^{-5})$
	c		4.70 (0.360)	$2.24 \ 10^{-4} \ (2.80 \ 10^{-5})$
	c		3.97 (0.461)	$4.14 \ 10^{-4} \ (7.96 \ 10^{-5})$
	c		7.48 (0.313)	$2.48 \ 10^{-4} \ (1.81 \ 10^{-5})$
	c		6.19 (0.485)	$3.52 \ 10^{-4} \ (4.56 \ 10^{-5})$
	c		12.2 (1.74)	$2.05 \ 10^{-4} \ (3.89 \ 10^{-5})$
	c		7.68 (0.245)	$5.44 \ 10^{-4} \ (3.87 \ 10^{-5})$

‡ estimated mean temperature at site of sampling
† a: size frequency; b: measured age; c: shell rings

Figure 2.12: Shell length, $\Diamond$, $\Box$,—, and production of somatic, $\triangle$, $\triangledown$, ..., and reproductive tissue, $\times$, $+$,. . . ., in three populations. Data from Rodhouse et al. [198] (top) and Bayne & Worrall [25] (bottom) on the Lynher, $\Diamond$, $\triangle$, $\times$ and Cattewater, $\Box$, $\triangledown$, $+$, site. The estimated parameters in the left figure at presumably 15°C are $g = 1.01$ (SD 0.19), $mg = 4.2$ (SD 0.7) 10^{-3} d^{-1} and $\kappa = 0.71$ (0.074), given $v_{15} = 0.23$ mm.d^{-1} and $f = 0.49$, a dry weight–wet weight conversion of 0.12, with $e(0) = 0.46$, $V(0) = 1$ cm^3 at 12°C. For the right figure: $g = 1.05$ (SD 0.073), $mg = 5.0$ (SD 0.1) 10^{-3} d^{-1} and $\kappa_1 = 0.94$ (SD 0.01) and $\kappa_2 = 0.99$ (SD 0.01) with $e_{0,1} = 0.4, W_{0,1} = 6.16$ mm^3, $f_1 = 0.59$, $e_{0,2} = 0.3, W_{0,2} = 4.36$ mm^3, $f_2 = 0.51$ and $v_{15} = 0.19$ mm.d^{-1}.
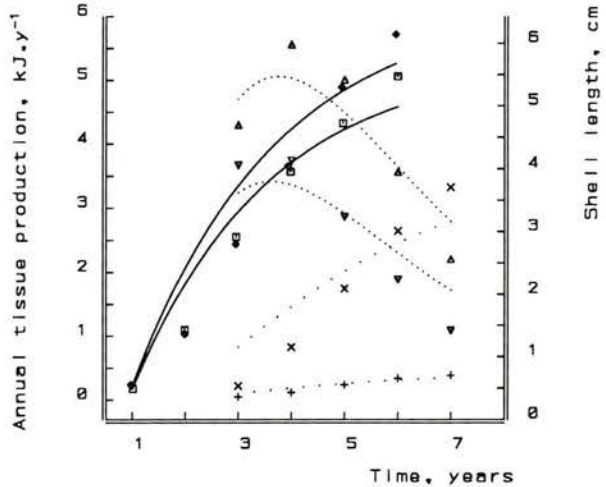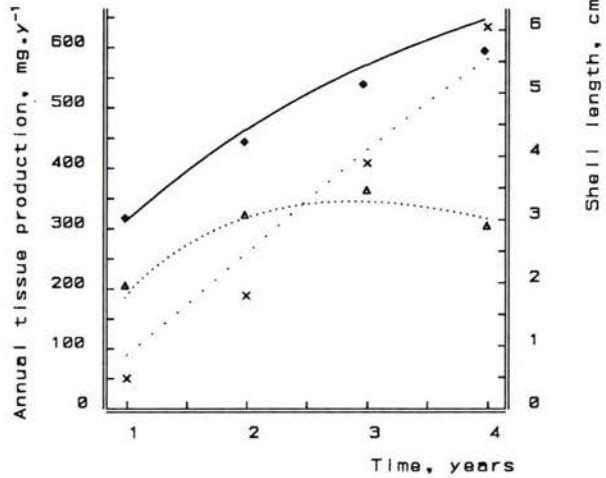
Chapter 3

Mussel toxico-kinetics

3.1 Introduction

Interpretation of environmental monitoring and ecotoxicological data is improved by knowledge on the relationship between concentrations of xenobiotics in the environment and in tissues of biota. Most of the studies on the uptake and elimination kinetics of xenobiotics assume implicitly steady-state conditions for the other physiological processes in the organism. Experimental and field monitoring data are therefore most of the time analyzed with one-compartment uptake and elimination models. These models do not always give a good fit with data, especially in those conditions where the organism changes its physiological condition (*i.e.* size, energy reserves and reproductive cycle) at a rate comparable to the uptake/elimination of the xenobiotic [145].

Monitoring programs, like the 'Mussel Watch' [82], are subject to fluctuating conditions of the xenobiotic but also in large extent to fluctuating food densities and temperatures. The kinetics and concentrations of the xenobiotic are affected by the changing physiological condition of the mussel *Mytilus edulis* through the seasons [171], [2], [145], [45], [165]. So reconstruction of ambient xenobiotic concentration based on xenobiotic body burden is only feasible when the effect of food density and/or temperature on the physiological condition of the mussel is known.

Many physiological variables affect for instance the cadmium burden of *M.edulis*. Borchardt and Riisgard, [105], [34], [35], [190], report correlations of cadmium burdens in mussels of the same size with food densities. Cadmium body burden is also affected by temperature [171], size [223], [45], [32] and reproductive cycle [223], [165], [45]. Cadmium concentrations in the mussel are usually expressed on tissue dry weights. Since tissue dry weights covary with season and temperature [92], seasonal variations of cadmium concen-

trations are hard to interpret. Fisher [65] proposed to relate cadmium body burden to shell weight which is less variable then soft tissue dry weight. Shell weight is determined mainly by size of the mussel, while soft tissue dry weight reflect partly gonad and stored energy condition and partly size of the mussel.

Organic micro contaminants like PAH's (Polycyclic Aromatic Hydrocarbons) and PCB's (PolyChlorinated Biphenyls) accumulate quite easily in mussels [76], [235], [118], [145] due to their lipophilic character. Variation in lipid content during the season in the mussel obviously affects PCB concentrations [145]. Increasing lipophility of individual PCB congeners expressed as the n-octanol-water partition coefficient, causes decreasing elimination rates for the specific compound in the green-lipped mussel *Perna viridis* [235]. Steric properties also affect toxico-kinetics. Non-ortho chlorine substituted coplanar PCB congeners exhibit slow uptake and clearance relative to many other PCB isomers [118]. In addition PCB body burden increases with increasing shell length [134] and decreases with spawning of gametes [104].

The uptake/elimination model that was proposed by Kooijman & van Haren [131] has been designed to account for change in the physiological (feeding/lipid) conditions of the organism. It rests on the Dynamic Energy Budget (DEB) model, [127], [128], [125], which describes growth, energy dynamics and reproduction as function of body size.

Uptake is via food and/or directly from the environment and elimination is via reproduction (gametes) and/or directly to the environment. The uptake and elimination rates depend on lipid content, that can change in time, so the body burden can change in time, even when the ambient concentration is constant [131].

The purpose of the present paper is to show how the DEB–based model for xenobiotic kinetics can be applied to *M.edulis* in laboratory and field conditions. The applicability of the DEB–model to *M.edulis* has been demonstrated in van Haren & Kooijman [92]. Data from uptake-elimination experiments of cadmium, several PAH and PCB congeners are used to estimate the compound–specific parameters of the model. The model is then applied to interpret field data.

It is here assumed, for simplicity's sake, that the physiological condition itself is not effected by the compounds. Although the DEB–based model offers a useful basis to describe such effects [125]. Exposure of 16.5 mm mussels to 100 $\mu g.l^{-1}$ cadmium for 17 days has no effect on physiological processes like ingestion, respiration or growth [177]. The concentrations for cadmium considered in this paper are much less.

Biotransformation of organic xenobiotics can affect elimination kinetics [130]. Organisms with MFO (Mixed Function Oxygenase) systems have the possibility to transform organic xenobiotics. MFO and BaPMO (Benzo(a)Pyrene-MonoOxygenase) activities in the mussel *Mytilus galloproviciales* correlate with a PAH pollution gradient [154]. This indicates that biotransformation might occur. Biotransformation increases the complexity of the analysis of the already complicated toxico-kinetic studies. Therefore, to simplify the analysis we start to study toxico-kinetics without biotransformation.

3.2 The DEB model

To make the paper self contained, a summary is first given of the DEB–model and DEB–based kinetics as far as relevant to the present application. For more detailed accounts we refer to [131], [92] and [125].

3.2.1 Physiological energetics

The present discussion is restricted to the feeding stages, which can be splitted into a non–reproducing juvenile stage and a reproducing adult stage. Four separate body fractions are distinguished as is shown in figure 3.1: the aqueous fraction (*e.g.* blood), the structural component of the body, stored energy reserves, and a component set aside to reproduction (mussels loose 40–70% of their wet weight at spawning, which they restore during the rest of the year) . The chemical composition of the structural biovolume, and of stored materials, is taken to be constant, so homeostasis is assumed for structural biovolume as well as stored materials. Since the composition of stored materials will differ from that of structural biovolume, and the storage density can fluctuate, homeostasis is not assumed for the combination of structural biovolume and stored materials.

Uptake of food is proportional to the surface area (of the filtering apparatus and/or gut) of the mussel and is assumed to follow a type II Holling functional response [266]:

$$f = \frac{X}{K + X} \tag{3.1}$$

where f denotes the scaled functional response, X the environmental food density and K the saturation constant. The food–energy conversion in the gut is taken to be constant. The incoming energy adds to the energy reserves, which follow a first order process:

$$\frac{d}{dt}e = vV^{-1/3}(f - e) \tag{3.2}$$

where e is the scaled storage density, V is structural biovolume (length^3) and v is the energy conductance (length.time^{-1}) (*i.e.* a resistance measure for the energy flow from energy acquisition to energy utilization).

Energy is utilized from storage in which a fixed fraction κ is spent on growth plus maintenance. Maintenance is taken proportional to structural biovolume. Consequently, growth is given by a weighted difference between surface area and volume:

$$\frac{d}{dt}V = \frac{V^{2/3}ev - Vgm}{e + g} \tag{3.3}$$

where g is the dimensionless investment ratio (costs for new biovolume relative to maximal available energy for growth plus maintenance) and m the maintenance rate constant (time^{-1}) (ratio of costs for maintenance and biovolume synthesis). Growth ceases when the energy reserves drop below:

$$e < V^{1/3}mg/v \tag{3.4}$$

A fraction $1 - \kappa$ of the energy that is utilized from storage is spent on development plus reproduction. Maintenance of the mature state is taken to be $(1 - \kappa)gmV_j$, where V_j is the size at first maturation (length^3), (see Kooijman, [125], and Zonneveld & Kooijman, [270], for arguments). From this allocation rule it follows that reproduction investment is given by:

$$\frac{d}{dt}R = \frac{(1 - \kappa)e}{e + g}\left(vgV^{2/3} + gmV\right) - (1 - \kappa)gmV_j \tag{3.5}$$

and for non-growing organisms:

$$\frac{d}{dt}R = evV^{2/3} - \kappa gmV - (1 - \kappa)gmV_j \tag{3.6}$$

where R is the volume of gonads and gametes (length^3). Reproductive output is first stored in a buffer, that is emptied once a year at spawning. This causes substantial change of lipid content over the seasons inside the mussel. The cumulated reproductive output, R_c, is not metabolically available for other purposes, so:

$$R_c(t) = \int_{t_r}^{t} \frac{d}{dt}R(s)\,ds \tag{3.7}$$

where t_r denotes the time of the latest spawning. The reproduction volume density, $r = R/V$ while the change in reproduction volume density is:

$$\frac{d}{dt}r = V^{-2}(V\frac{d}{dt}R - R\frac{d}{dt}V) = V^{-1}\frac{d}{dt}R - RV^{-2}\frac{d}{dt}V \tag{3.8}$$

3.2.2 xenobiotic kinetics

The xenobiotic compounds are, once taken up in the aqueous fraction, instantaneously partitioned over the body fractions according to the chemical affinity of the xenobiotic, see figure 3.1 and [131] for an extensive discussion. Uptake as well as elimination are assumed to be proportional to the surface area, $V^{2/3}$, of the organism. So uptake via water (*e.g.* gills) and uptake via food (*e.g.* gut) are both proportional to the surface area. The resulting differential equation for the concentration on basis of wet weight is (#.mass^{-1} in which # denotes number or weight of molecules):

$$\frac{d}{dt}c_{ww} = \frac{r_{da}c_d + r_{pa}fc_p}{d_s(1 + \alpha_e^{-1} + r)V^{1/3}} - c_{ww}\left(\frac{r_{ad}}{hV^{1/3}} + V^{-1}\frac{d}{dt}V + (1 + \alpha_e^{-1} + r)^{-1}\frac{d}{dt}r\right) \tag{3.9}$$

r_{da} and r_{pa} are the uptake rate constants for water and food respectively and r_{ad} is the elimination rate constant (length.time^{-1}). The constants d_s and α_e are the specific density of soft tissue and the maximum volume of energy reserves as fraction of body size. The compound variable h equals:

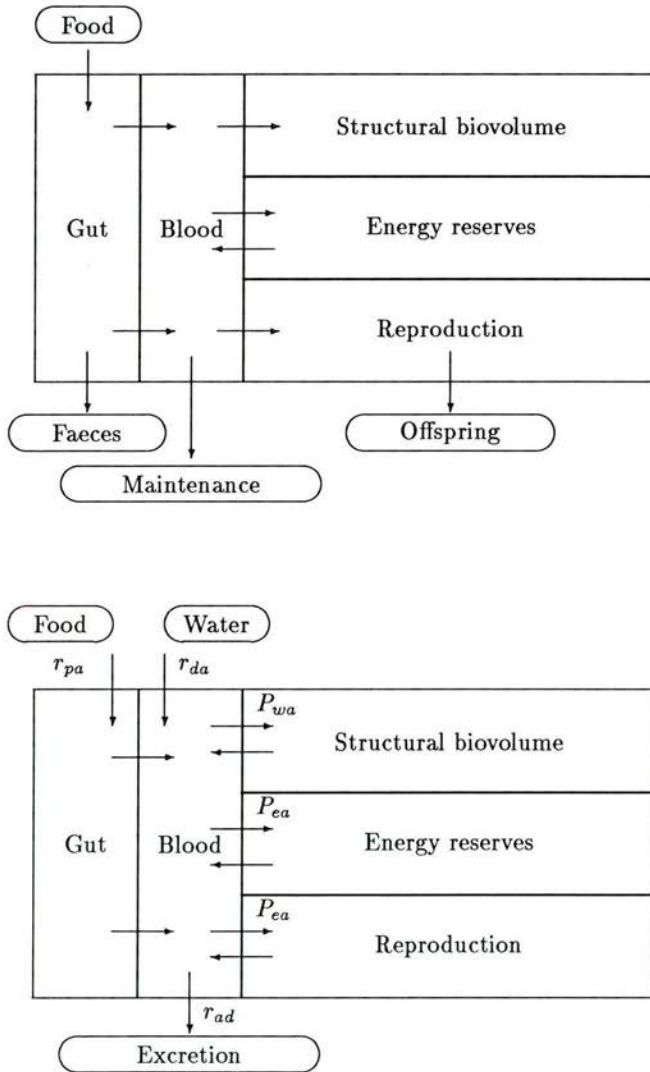$$h = \gamma + (P_{ea} - 1)e + P_{ea}r \tag{3.10}$$

Figure 3.1: Schematic representation of the energy flow (upper figure) through and xenobiotics partitioning (lower figure) in the body compartments of an individual.

in which P_{ea} is the partition coefficient of a xenobiotic between the aqueous fraction and the stored energy body compartment and γ is a compound constant in which the partition coefficient of a xenobiotic between the aqueous fraction and the structural biovolume compartment is incorporated. When $P_{ea} \gg 1$ then

$$h = \gamma + P_{ea}(e + r) \tag{3.11}$$

The variables c_d and c_p are the environmental dissolved and particulate adsorbed xenobiotic concentration (#.length^{-3}). The dimensions of the dissolved and particulate concentrations can be chosen as μg.l^{-1} or #.(gram C)$^{-1}$ for instance. These concentrations can taken to be forcing functions for generating smoothed input variables during relevant periods.

3.3 Parameter estimation

3.3.1 Estimation procedures

The data are obtained from tables in the literature, or by means of a x,y tablet from figures. We use a fourth order Adams Predictor-Corrector method [37] to integrate equations 3.2–3.9 and cubic hermite spline, to interpolate between time points of integration. The derivatives of total sum of squares (TSS) with respect to the parameters (*i.e.* the normal equations) are approximated by the forward difference method. The roots of the normal equations are solved with the Gauss-Newton method for systems of nonlinear equations [189]. Standard deviations of the parameters are estimated according to the large sample theory of maximum likelihood estimators [46], where a normal distribution for the scatter around the deterministic model is assumed. When data are available for more than one set of environmental conditions (xenobiotic concentration, food density, temperature etc.), a simultaneous fitting procedure is applied.

The number of parameters is reduced assuming that $P_{ea} \gg 1$ in equation 3.9. Since P_{ea} can be interpreted in terms of the *n*-octanol-water partition coefficient for the xenobiotic (which are of many orders of magnitude larger than 1, especially for lipophilic compounds) this assumption seems appropriate. By dividing r_{ad} and the compound parameter h by γ, two new compound parameters are formed r_{ad}/γ and P_{ea}/γ) and r_{ad} disappears as a free parameter as long as $P_{ea} \gg 1$. The new equation then becomes:

$$\frac{d}{dt}c_{ww} = \frac{r_{da}c_d + r_{pa}fc_p}{d_s(1 + \alpha_e^{-1} + r)V^{1/3}}$$
$$- c_{ww}\left(\frac{r_{ad}/\gamma}{(1 + P_{ea}/\gamma(e+r))V^{1/3}} + V^{-1}\frac{d}{dt}V + (1 + \alpha_e^{-1} + r)^{-1}\frac{d}{dt}r\right) \tag{3.12}$$

The parameters of equations 3.2–3.6 are estimated separately from data concerning physiology only in van Haren and Kooijman [92] and are set at fixed values when fitting the parameters of the toxicant kinetics. The parameter values are listed in table 3.2.

Table 3.1: The parameters and main variables of the xenobiotic and the energy budget model.
# denotes the number (moles) or weight (g) of molecules, see for further details [131]

Par.	Var.	Dimension	Interpretation
	c_d	#.length^{-3}	concentration xenobiotic in water
	c_p	#.length^{-3}	concentration xenobiotic food (as volume)
	c_{ww}	#.mass^{-1}	concentration xenobiotic in mussel on basis of wet weight
	Q_m	#	amount of xenobiotic in mussel: $Q_m \equiv c_{ww}V_{ww}$
r_{da}		length.time^{-1}	uptake rate from water
r_{pa}		length.time^{-1}	uptake rate from food
r_{ad}		length.time^{-1}	elimination rate constant
P_{ea}		-	partition coeff. energy reserves/aqueous fraction
γ		-	compound parameter
	f	-	functional response: $f = \frac{X}{K+X}$
	X	mass.length^{-3}	food density
	V	length^3	structural biovolume
	V_{ww}	mass	wet weight of mussel: $V_{ww} \equiv d_sV(1 + \alpha_e(1 + r))$
	L	length	shell length: $V_{ww} \approx d_s(d_m L)^3$
	e	-	energy reserves/max.energy reserves
	R_c	length^3	reproductive investment
	r	-	scaled reproduction density: $r \equiv \frac{R}{V}$
K		mass.length^{-3}	saturation constant
v		length.time^{-1}	energy conductance
g		-	costs of growth/κ max.energy density
m		time^{-1}	maintenance rate constant
κ		-	fraction utilized energy to growth + maintenance
α_e		-	max.vol.reserves/vol.body
d_s		mass.length^{-3}	specific density of the body
d_m		-	shape coefficient
V_b		length^3	body size at hatching
V_j		length^3	body size at first maturation
t_r		time	time at spawning or reproduction, $r = 1, 2, ..$

Table 3.2: Values of parameters of the Dynamic Energy Budget model

Parameter values at 15 °C, estimated in van Haren & Kooijman [92]			
	description	dimension	value
g	investment ratio	–	1.03
m	maintenance rate	d^{-1}	0.00517
v	energy conductance	$cm.d^{-1}$	0.023
K	saturation constant	mg POM.l^{-1}	2.4
I_m	max. ingestion rate	mg POM.d^{-1}	72
V_j	mature size	cm	1.2
κ		–	0.95
d_m	shape coefficient	–	0.33
d_s	specific density	$g.cm^{-3}$	1
T_A	Arrhenius temperature correction	Kelvin	7600

The xenobiotic kinetics model has two additional physiological parameters: d_s and α_e. The specific density of the soft tissue of the mussel d_s is close to 1 g.cm^{-3}. The maximum volume of energy reserves as fraction of body size α_e is derived by dividing the maximum storage density of the mussel of 30 kJ.cm^{-3} with the lowest calorific content of a mussel during the season (after spawning) which amounts 1.43 kJ.cm^{-3} [267] plus the maximum storage density: $\alpha_e = \frac{30}{30+1.43} = 0.95$.

The relation between wet weight V_{ww} of a mussel with the structural biovolume V is by definition, see [131], [125]:

$$V_{ww} \equiv d_s V(1 + \alpha_e(1 + r)) \tag{3.13}$$

The wet weight can be approximated by

$$V_{ww} \approx d_s(d_m L)^3 \tag{3.14}$$

in which d_m is the shape coefficient and L is the shell length. The shape coefficient is estimated to be 0.33, for an extensive discussion see [92].

3.3.2 Temperature correction

All rate constants depend on the temperature and are continuously adjusted by an Arrhenius type correction with an Arrhenius temperature of $T_A = 7600$ K, which would be approximately the same as a correction with a Q_{10} of 3. The estimates are given for a reference temperature of 15°C. A typical rate parameter p, is adjusted for temperature T, (in K) as follows:

$$p(T) = p_{ref} \exp\{T_A(T_{ref}^{-1} - T^{-1})\} \tag{3.15}$$

The rate constants v and m in the physiological equations, and r_{da}, r_{pa} and r_{ad} in the toxico-kinetics equation are corrected for fluctuating temperatures.

3.4 Cadmium

The main cadmium species that are taken up by the mussel are the water dissolved species [34], [190], [95]. Borchardt [34] and Riisgard [190] suggest that uptake of particle adsorbed cadmium species, ingested via food, is of minor importance. The bioavailable dissolved cadmium species depends on the mechanism of uptake. Passive diffusion [95] or facilitated diffusion via Ca^{2+}–channels [247] across the lipid bilayer are believed to be the most likely uptake processes. So the main cadmium species to consider are the small ionized forms, the chlorides and hydroxides [222] [142]. Once inside the organism (cell), cadmium is complexed to specialized proteins, the metallothioneins (MT), or proteins with active sulfhydryl groups [100], [247], [250], [249], [200]. Cadmium is subsequently internally distributed. Specialized structures (tertiary lysosomes) inside the kidney are the main sinks [73], [75], [74].

3.4.1 Cadmium kinetics in the laboratory

Cadmium kinetics of mussels of different size classes and at different feeding regimes are re-analyzed with the present model. Therefore, data from two uptake and elimination experiments of cadmium, from Borchardt [34], [35] and Adema [1], have to be combined in the parameter estimation procedure. Starving mussels of 4.5 cm shell length are exposed to dissolved cadmium for 25 days and allowed to eliminate for 7 days [1]. Different radio tracer labelled dissolved and particulate adsorbed cadmium is used in another study using 17-18 mm shell length mussels. This differential labelling technique was used to distinguish the different uptake routes of cadmium [34] [35].

Regression analysis is first performed on available physiological data: mussel growth [35] and lipid decrease [1] during the experiments. Results are shown in figure 3.2. The length increase of the feeding mussels at different food amounts and the lipid decrease of the starving mussels are described by equations 3.3 and 3.2, with $f = 0$ for the starving mussels. The scaled functional responses, f, for the fed mussels are: 0.11, 0.076, 0.051, 0.034, 0.023, 0.015. The estimated values of the energy conductance v and the product of maintenance rate constant and energy investment ration, gm, are in agreement with the 'mean' estimates for the mussel [92].

The results of the regression on data of the two uptake/elimination experiments are also shown in figure 3.2. The small mussels are exposed to water containing radio active labelled dissolved Cd-115m and adsorbed Cd-109 on food particles. The seawater was replaced after 33 days with clean water and the mussels were subsequently kept in it for 42 days. Borchardt [34] gives regression functions of the dissolved and adsorbed cadmium concentrations during the experiments that are based on the food quantity, FQ, added daily to the mussels. The dissolved cadmium concentrations are given by two functions in which FQ is respectively: 120.0, 80.0, 53.3, 35.6, 23.7, 15.8 $\times 10^6$ *Isochrysis galbana* per day per mussel and t is the time in days:

$$c_{Cd\text{-}115m}(t) = 0.0403 \exp\left(-37.10^{-4} - 31.10^{-12}FQ\right)t \qquad \mu g.ml^{-1} \qquad (3.16)$$

$$c_{Cd\text{-}109}(t) = 5.9.10^{-3}(-38 + 10.10^{-6}FQ)t^{0.72}/14406 \qquad ng.ml^{-1} \qquad (3.17)$$

The dissolved Cd-109 originates from desorption of the particulate bounded cadmium supplied via the algae. The Cd-109 concentration adsorbed to the algae is 1.36 μg.g^{-1} dry weight.

The 4.5 cm mussels are exposed to cadmium in filtered seawater with dissolved concentrations of respectively 0.0010 and 0.0034 μg.ml^{-1} during uptake and 0.0004 μg.ml^{-1} during elimination. The uptake period is 25 days and the elimination period is 8 days [1].

The data in figure 3.2 are expressed as an amount of cadmium per mussel, Q_m, where:

$$Q_m \equiv c_{ww} V_{ww} \tag{3.18}$$

The change in the amount of cadmium per mussel is:

$$\frac{d}{dt} Q_m = V_{ww} \frac{d}{dt} c_{ww} + c_{ww} \frac{d}{dt} V_{ww} \tag{3.19}$$

The mussel wet weight is given in equation 3.13, so the change in mussel wet weight is:

$$\frac{d}{dt} V_{ww} = d_s (\frac{d}{dt} V + \alpha_e ((1+r) \frac{d}{dt} V + V \frac{d}{dt} r)) \tag{3.20}$$

Substitution of equation 3.20 and equation 3.12 in equation 3.19 results finally in:

$$\frac{d}{dt} Q_m = \alpha_e V^{2/3} (r_{da} c_d + r_{pa} f c_p) - Q_m \frac{\frac{r_{ad}}{\gamma}}{V^{1/3} (1 + \frac{P_{ea}}{\gamma} (e+r))} \tag{3.21}$$

The uptake and elimination from cadmium out of water and food are simultaneously estimated on these data. Regarding the complexity of the experimental system the fit is quite satisfactory. This fit is an example in which the ordinary 1-compartment models fail to predict the uptake/elimination process.

A lack of fit of the Cd-115m uptake data in a first analysis indicated the involvement of an additional process. So an instantaneous adsorption of the dissolved Cd-115m on the daily added algae was assumed. The partition coefficient of Cd-115m with the algae is taken to be 483 which is the same as derived for Cd-109 adsorption [34]. The bioavailability of the instantaneous adsorbed Cd-115m and the equilibrium adsorbed Cd-109 differ, so two uptake constants for food derived cadmium has to be used. The instantaneous adsorbed food uptake rate constant is a factor 50 larger then the equilibrium adsorbed food uptake rate constant. This fact can be explained by differences of the cadmium ad/absorption to the algae. The equilibrium adsorbed cadmium might be incorporated in the algal cell or cell walls while the instantaneous adsorbed Cd-115m is only bound to the easily degradable mucus layers on the cell walls of the algal cells.
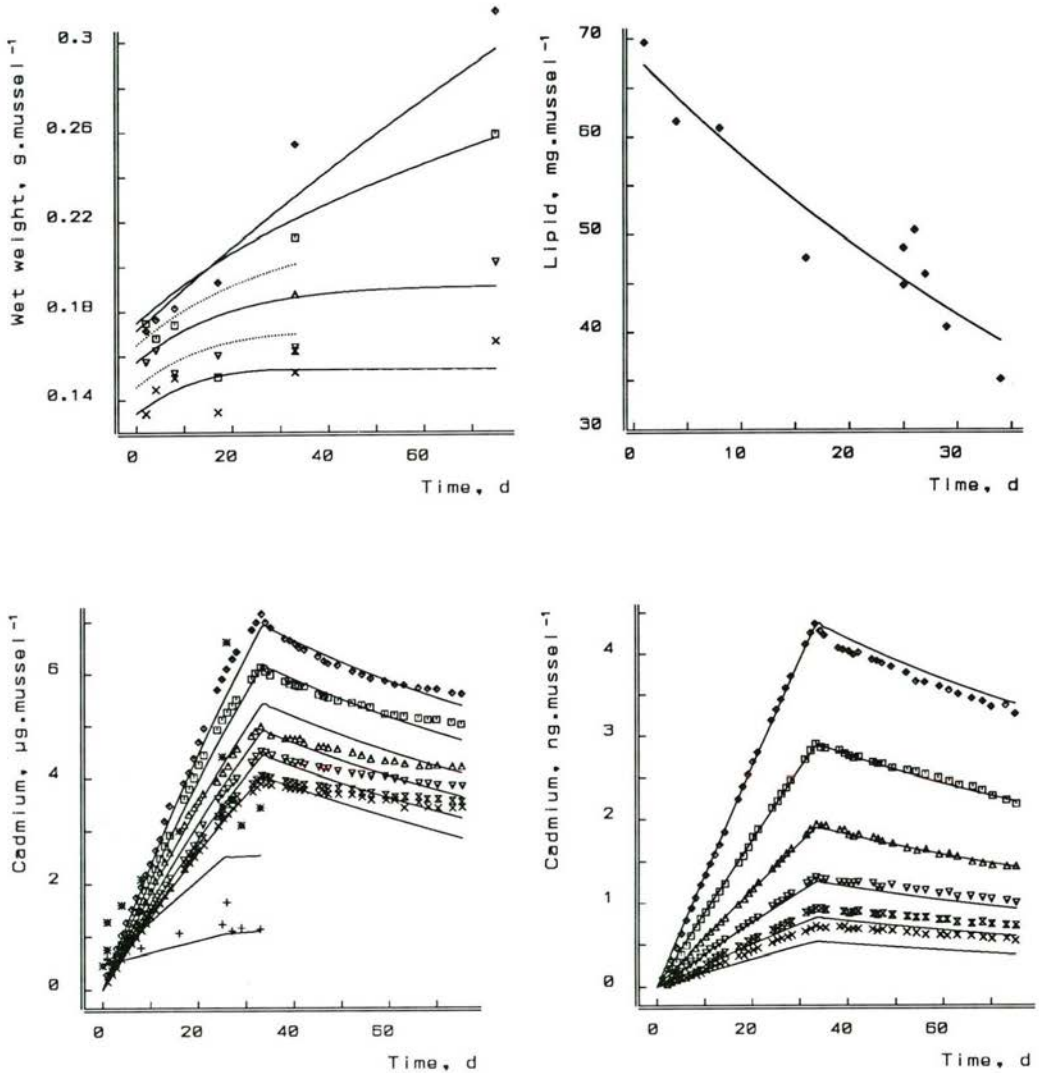
Figure 3.2: Upper left: Growth of 17-18 mm mussels at 15 °C and 6 food regimes. Estimated values are $v = 0.036$ (SD=0.0065) cm.d^{-1}, $gm = 0.0045$ (SD=0.0018) d^{-1} with a fixed value of g = 1.05 and a max. ingestion rate of 60 mg.cm^{-2}.d^{-1}. Upper right: Lipid decline of 4.5 cm mussels at 15°C. Initial lipid amount is 68.5 (SD=2.30) mg and the decline rate is 0.016 (SD=0.0017) d^{-1}. Lower left and right: Accumulation and elimination of cadmium in mussels of different size and at different ambient food levels. Cadmium, Cd-115m, is shown left and cadmium, Cd-109, is shown right. Uptake of Cd-115m is mainly via water and uptake of Cd-109 is mainly via food, see text for further explanation. The regression analysis is performed on these 14 curves simultaneously with $\alpha_e r_{da} = 12.15$ (SD=0.18) cm.d^{-1}, $\alpha_e r_{pa,Cd109} = 0.00116$ (SD=1.65 10^{-4}) cm.d^{-1}.g.cm^{-3}, $\alpha_e r_{pa,Cd115m} = 0.0536$ (SD=0.00275) cm.d^{-1}.g.cm^{-3}, $r_{ad}/\gamma = 0.0112$ (SD=0.00430) cm.d^{-1} and $P_{ea}/\gamma = 8.83$ (SD=5.25) dimensionless.

3.4.2   Cadmium kinetics in the Western Scheldt estuary

The change of cadmium concentration inside the mussel can be reconstructed from incidental measurements throughout the year on the basis of our model. Monitoring data of ambient temperature, food density and cadmium concentrations are used from location Terneuzen in the Western Scheldt estuary (Dutch Delta area) [95] [234] [271]. The data are obtained from the Ministry of Public Works and Transport, Tidal Waters Division, Netherlands (Dutch ICES contribution).

Smoothed forcing functions are obtained from incidental measurements by regression of cubic splines for particulate organic matter (POM), particulate adsorbed and dissolved cadmium see figure 3.3. The forcing function of water temperature is a cosine function, see figure 3.3. POM is calculated as difference between weight of suspended matter and ash weight of suspended matter. POM adsorbed cadmium is calculated as difference between total cadmium concentration and cadmium concentration after filtration (0.45 μm mesh size) divided by POM concentration in water.

The cadmium concentrations in the mussel are given as mean cadmium concentration in different length classes. To reconstruct the seasonal cadmium fluctuations of various length classes, we calculated the cadmium concentrations for the isoclines of the mean length of each length class, see figure 3.4. The simplifying assumptions that are appropriate for the laboratory experiments are not appropriate for the field experiments, where we have to account for reproduction and changes in lipid content prior to spawning. We here assume that the storage and reproduction compartments are allowed to vary and cumulate through the seasons depending on food and temperature. The spawning of gametes is in the first week of May. The reproduction compartment is set to zero while the cadmium concentration jump due to the clearance of the reproduction compartment is adjusted according (for $P_{ea} \gg 1$):

$$c_{ww}(t_r^+) = c_{ww}(t_r^-)\frac{1 + \alpha_e^{-1} + r(t_r^-)}{1 + \alpha_e^{-1}} \frac{1 + \frac{P_{ea}}{\gamma}e(t_r^+)}{1 + \frac{P_{ea}}{\gamma}(e(t_r^-) + r(t_r^-))} \tag{3.22}$$

in which t_r denotes the time of spawning.

The largest mussels tend to have the largest cadmium concentrations [234]. Exceptions occur several times in the presented data, see figure 3.4. The fitted isoclines show a dynamic shift during the season of this tendency. The shift depends on food history and ambient cadmium concentrations in relation to the internal partition coefficient P_{ea}. It is not possible to reconstruct this trend in an exact manner because detailed observations of available food and cadmium concentrations are lacking.

The contribution of the different uptake routes to total cadmium burden is evaluated for field conditions. Cadmium contribution from food to total body burden depends on the environmental conditions. The ratio of uptake rates from food and water varies from 0.002 − 0.005 [34], 0.0015 [190] under laboratory conditions and from 0.27 − 1.74, under field conditions (see figure 3.4. The huge difference between laboratory and field conditions are due to the limited food availabilities in the laboratory and its low cadmium load. The data reported in figures 3.2 and 3.3 relate to loadings that differ by a factor 10.

3.5 PCB's and PAH's

Uptake of organic micro contaminants (OMICO's) from the environment is either from water (bioconcentration) or from food (biomagnification). The bioavailable fraction of the OMICO's is believed to be freely dissolved [209]. Uptake via food is also considered to be significant for OMICO's, since they are extremely hydrophobic and have high food sorption coefficients [163].

The uptake mechanism is passive diffusion through the biological membranes of gill tissue [57] [97] [164] as well as the gastro-intestinal tract [80]. Extremely hydrophobic OMICO's are not accumulated in several bioconcentration experiments. Opperhuizen [164] hypothesized that these chemicals are not able to cross membranes because of their size, that exceeds a cross section of 0.95 nm or lengths of 5.3 nm [163].

Physicochemical properties of OMICO's are of relevance to toxico-kinetics. Solubility of a chemical in fat is an important property because of the partitioning processes that occur between the aquatic phases of the body and lipid rich tissues. Fat solubility is correlated with the *n*-octanol/water partition coefficient [58]. Bioconcentration factors (BCF) (concentration in (lipid) tissue divided by ambient concentration in water, see *e.g.* [251]) are often related to log K_{ow} values in order to predict bioconcentration of new chemicals [76]. Chessels [41] argues that triolein (glyceryl trioleate) is a better model compound for lipid than octanol. Different extraction methods for lipids give each different lipid fractions and lipid amounts [207] [182]. The phospholipid-free fraction of extractable lipids give the best correlation with PCB burden [207].

Pruell *et al* [181] exposed uncontaminated mussels to resuspended sediments that were contaminated with PCB's and PAH's. The exposure and depuration periods lasted both 40 days. The exposure concentrations of particulate adsorbed and dissolved PCB's and PAH's, were sampled by two step filtering of water of the exposure systems. The first filter retained the particulate adsorbed PCB and PAH, while the second filter (polyurethane foam plugs) retained dissolved PCB and PAH only. The exposed mussels, with shell length 3.0–4.6 cm, partially depleted their lipid reserves caused by poor feeding conditions during the experiments, see figure 3.5. The scaled functional response f was estimated to be about 0.17 in the experiments. The initial value of the scaled reserves was assumed to be 0.3.

Due to the large uncertainties in the measured exposure concentrations of PCB's and PAH's, only the dissolved (retained by foam plug) concentrations are used in the analysis. The dissolved PCB concentrations of the penta- and hexachlorobiphenyls are estimated as fraction of the total PCB concentration in accordance with their fractions in Aroclor 1254, see table 3.3. The dissolved total PCB concentration is 1.81 ng.l^{-1}. The dissolved 4 ring PAH concentrations (BaA, Benz(a)Anthracene and Chry + Tri, mixture of Chrysene + Triphenylene) are respectively 0.43 and 0.59 ng.l^{-1}.

To reduce the number of parameters, the uptake and elimination constants are taken to be equal for the penta- and hexachlorobiphenyls and for the 4-ring PAH's since the molar weight and steric properties are more or less equal. The internal partition coefficient P_{ea} is assumed to be different for each compound. The results of the regression analysis are shown

Table 3.3: Fractions of individual PCB congeners in commercial Aroclor mixtures.

Source: Mullin, [153] using DB-5 cappilar column.			
PCB numbers according to IUPAC			
	Aroclor 1242	Aroclor 1254	Aroclor 1260
PCB 28	0.1431	–	–
PCB 101	0.0044	0.0706	0.0264
PCB 128	–	0.0192	0.0052
PCB 153	0.0029	0.0622	0.1058

Table 3.4: Log K_{ow} values of PCB and PAH compounds.

compound	$\log K_{ow}$	source	compound	$\log K_{ow}$	source
PCB 101	7.07	[183]	BbF	6.57	[98]
PCB 128	6.96	[183]	BkF	6.84	[98]
PCB 153	7.75	[183]	BaP	6.35	[98]
BaA	5.91	[98]	IP	7.66	[98]
Chry+Tri	5.86	[98]	BgP	6.90	[98]

in figure 3.6. The model describes the system although the estimated parameter values are poorly determined due to the large standard deviations. The large standard deviations might be caused by the large size range of the mussels (3.0–4.6 cm which corresponds with a wet weight of 1–3.6 g), the large deviations in measured dissolved OMICO concentrations and unknown size of the reproductive body compartment.

The internal energy reserves/aqueous fraction partition coefficient $\log P_{ea}$ can be compared with the $\log K_{ow}$ partition coefficient, as is shown in figure 3.7. The $\log K_{ow}$ of the compounds are given in table 3.4. The relationship of log BCF with $\log K_{ow}$ is given for comparison, data are from Geyer *et al* [76]. The BCF is reached when OMICO concentrations in mussels are in equilibrium with their environment (*i.e.* non–growing, non–reproducing, non–starving) [131]. So, the exact comparison of BCF with P_{ea} holds only in equilibrium. The dashed line is based on BCF while the drawn line is based on P_{ea}. The deviation from conditions of equilibrium of the measured mussels might cause the different slopes of the two regression lines. However the different slopes of the lines might also be caused by differences in the physiological condition of the mussel and by differences in solubility in fat and octanol for extreme lipophilic compounds [41]. P_{ea} values for other xenobiotics can be derived by interpolation of the drawn line.

Predicted P_{ea} values of 5 and 6 ring PAH's based on the relation from figure 3.7 are used for estimation of the ambient PAH concentrations in the experiments performed by Pruell [181]. These PAH's could not be detected in the foam plugs. The estimated ambient

concentrations are of the same order of magnitude or smaller than measured 4 ring PAH concentrations. The estimated concentrations reflects the total bioavailable concentration of both the dissolved and sediment adsorbed fractions.

Data concerning shell length and PCB concentration in soft tissues can be used to estimate ambient PCB concentration, as can be seen in figure 3.8 from [134]. The estimated parameters of total PCB in figure 3.6 are used to reconstruct this curve and to estimate dissolved total PCB concentration. The functional response f has to be fixed on 0.7 because data on growth or food densities are lacking. The reconstruction of ambient dissolved total PCB can be improved when the food density in the environment is measured and/or when the growth is measured, possibly via annual rings on the shells. The functional response can be reconstructed from the growth curve of the mussel, [92], which makes the dissolved PCB concentration reconstruction more reliable.
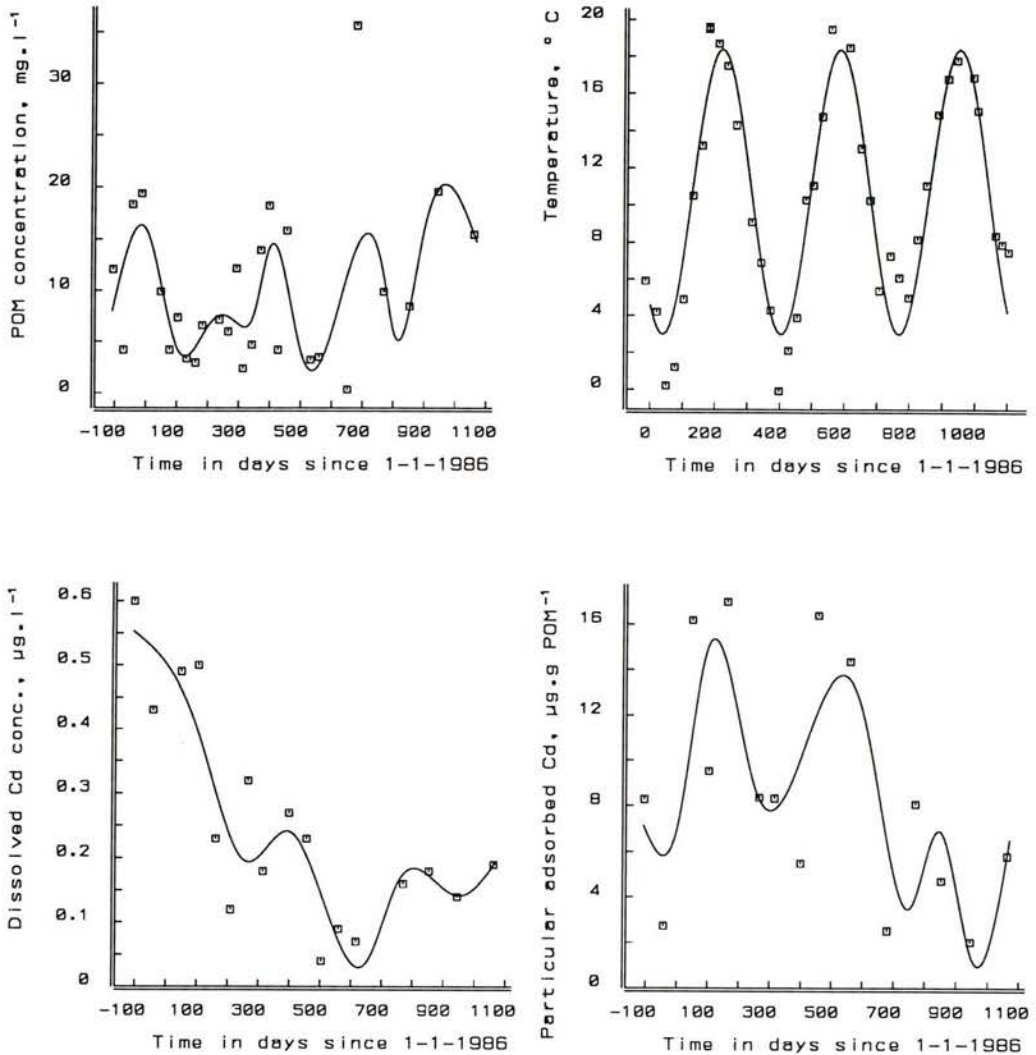
Figure 3.3: Measurements and forcing functions for input variables for reconstruction of cadmium concentrations in mussel in the Western Scheldt (Dutch Delta area) at location Terneuzen. Data are from Dutch contribution to ICES and provided by the Ministry of Public Works and Transport, tidal Water Division. Upper left: Particulate Organic Matter (POM) (location Terneuzen). Smoothed cubic spline function with knot values which are estimated at days (since 1/1/1986) -107, 0, 100, 200, 250, 300, 400, 450, 500, 770, 800, 900 and 1070. Upper right: Temperature with sinusoidal interpolation function: $T(t) = 10.7 - 7.7 \cos 2\pi \frac{t-38.3}{365}$, time in days. Lower left: Dissolved cadmium concentrations. The knot values are estimated at days (since 1/1/1986) -107, 100, 250, 400, 550, 650, 750, 850, 950 and 1070 . Lower right: Particulate (POM) adsorbed cadmium concentrations. Knot values of adsorbed cadmium are calculated at days -107, 0, 100, 250, 400, 600, 750, 850, 950 and 1070.
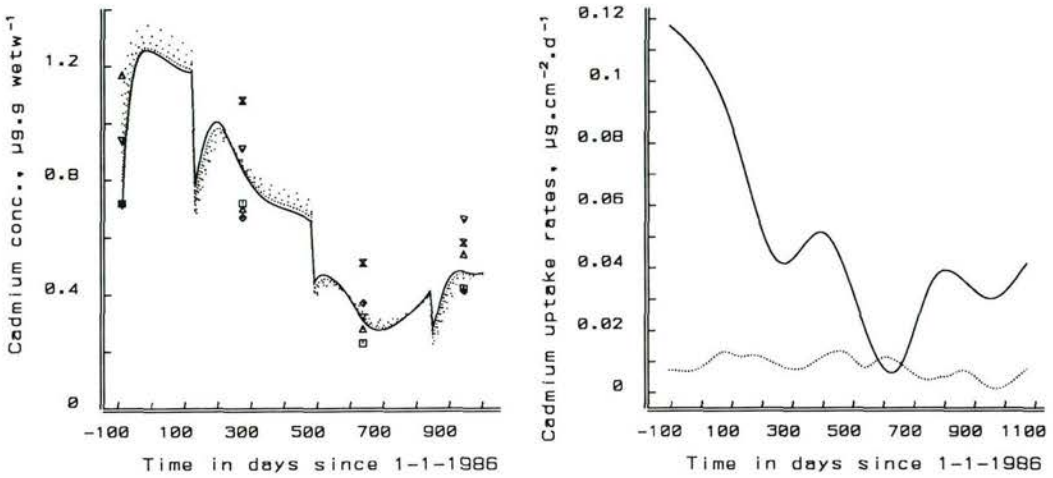
Figure 3.4: Left: Cadmium concentration for length isoclines in mussels of 2.8 ($\diamond$ and —), 3.5 ($\square$ and ...), 4.1 ($\triangle$ and ...), 5.0 ($\triangledown$ and . . .) and 5.9 ($\bowtie$ and . . .) cm respectively. Regression analysis is performed on these 5 curves simultaneously with $r_{da} = 213$ (SD=92.2) cm.d^{-1}, $r_{pa} = 1.40\ 10^{-3}$ (SD=1.53 10^{-3}) cm.gpom.d^{-1}.cm^{-3} and $r_{ad}/\gamma = 0.0964$ (SD=0.148) cm.d^{-1} with $v = 0.059$ cm.d^{-1}, $gm = 0.0045$ d^{-1} $g = 1.05$, $K = 3$ mg POM.l^{-1}, $\kappa = 0.75$ and P_{ea}/γ=8.83.
Right: Uptake rates of both uptake routes (dissolved (—) and food($\cdots$)). The mean contribution of food adsorbed cadmium to total tissue burden is a fraction of 0.278 (minimum 0.0382 and maximum 1.74).
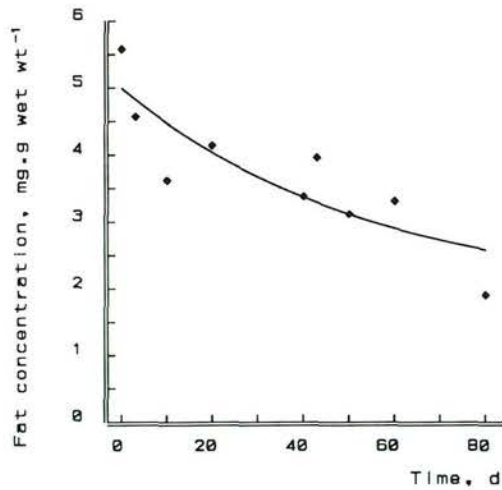

Figure 3.5: Lipid depletion during uptake and elimination of PCB and PAH in 3.0–4.6 cm mussels at 15 °C from [181]. The fitted equation is $E(t) = E_\infty + E_0 \exp -at$ with $E_0 = 3.14$ (SD=0.63) mg fat.g$_{ww}^{-1}$, $E_\infty = 1.84$ (SD=0.41) mg fat.g$_{ww}^{-1}$ and $a = vV^{-1/3}$ with $v = 0.023$ cm and $V^{1/3} = 1.27$.
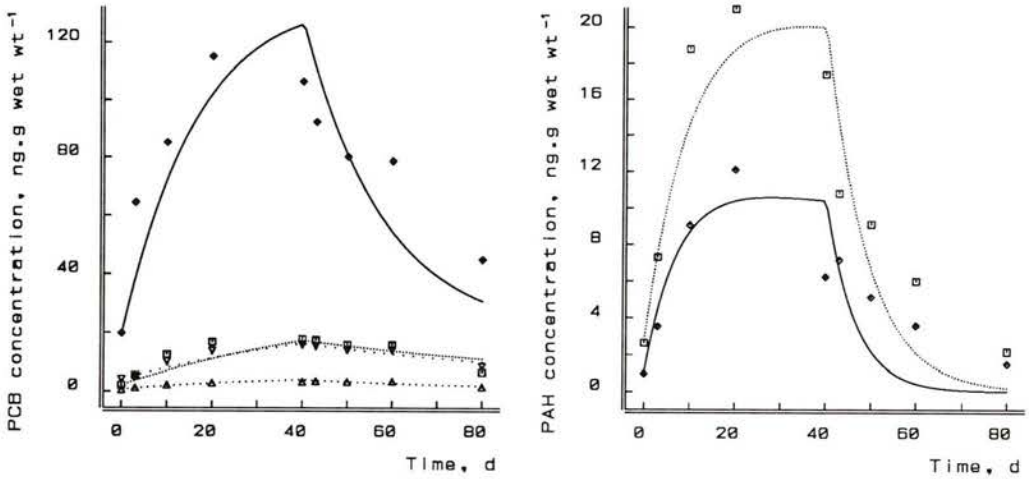
Figure 3.6: PCB (left) and 4 ring PAH (right) uptake and elimination in mussel, data from [181]. Equation 3.9 is used. The PCB congeners are: total PCB $\diamond$, PCB101 $\square$, PCB128 $\triangle$ and PCB153 $\triangledown$. The estimated parameters are: $r_{da} = 13395$ (SD=2514) cm.d^{-1}, $r_{ad} = 2713$ (SD=3E8) cm.d^{-1}, $\log P_{ea}$ is respectively 4.78, 5.29, 5.11 and 5.27 (SD for each 4.7E3). The PAH's are BaA $\diamond$ and Chry + Tri $\square$. The estimated parameters are: $r_{da} = 11336$ (SD=3772) cm.d^{-1}, $r_{ad} = 3176$ (SD=3E7) cm.d^{-1} and $\log P_{ea}$ is respectively 4.42 and 4.56 (SD for each 4.4E3) and $\gamma = 10$. The initial values for e and R are 0.3 and 0.8 respectively.

Figure 3.7: Left: Relation between $\log P_{ea}$ or BCF and $\log K_{ow}$. $\log P_{ea}$ values are estimated in figure 3.6 while BCF is given in Geyer [76]. The regression lines are $y = ax + b$ with y is $\log P_{ea}$ or $\log BCF$ and x is $\log K_{ow}$. The estimated values are: BCF: $a = 0.90$ (SD=0.096) and $b = -1.06$ (SD=0.41) ($\cdots$ and +); P_{ea}: $a = 0.48$ (SD=0.077) and $b = -1.72$ (SD=0.52) (— and □)
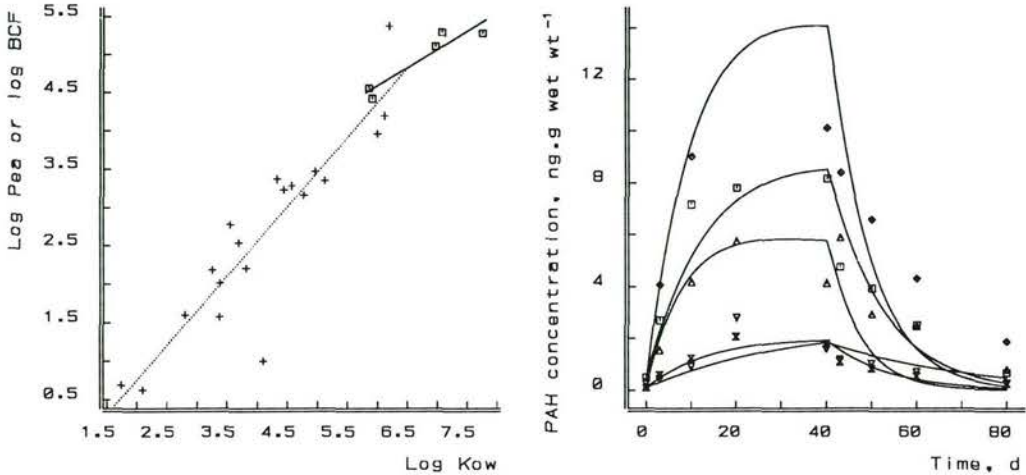Right: Accumulation and elimination curves according to equation 3.9 of 5 and 6 ring PAH's, source [181]. The following PAH's are used: BbF ◇, BkF □, BaP △ and IP ▽ BgP ⋈.
The estimated parameters are: $r_{da} = 6897$ (SD=3026) cm.d^{-1}, $r_{ad} = 6216$ (SD=744) cm.d^{-1} and the dissolved PAH concentrations are respectively: 0.66 (SD=0.29), 0.31 (SD=0.14), 0.35 (SD=0.16), 0.035 (SD=0.021) and 0.066 (fixed) $\times 10^{-3}$ ng.cm^{-3} and $\gamma = 10$. The initial values for e and R are 0.3 and 0.8 respectively.
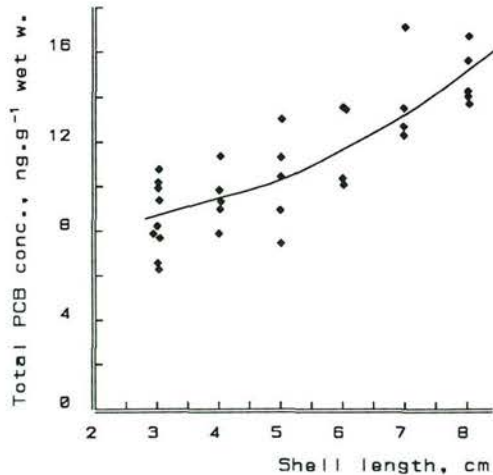
Figure 3.8: Relation between shell length and total PCB concentration in soft tissue, data from [134]. Equation 3.9 is used in this reconstruction with: $r_{da} = 13395$ cm.d^{-1}, $r_{ad} = 2713$ cm.d^{-1}. The estimated values of the partition coefficient $\log P_{ea} = 5.96$ (SD=0.13) and the dissolved total PCB concentration $c_d = 0.0080$ (SD=0.0011) ng.l^{-1}. With $f = 0.7$ and the yearly mean temperature was estimated to be 15 °C.

3.6 Discussion

The model, equation 3.9, is basically a simple one-compartment model:

$$\frac{d}{dt}c_{ww} = k_{da}c_d - k_{ad}c_{ww} \tag{3.23}$$

where k_{da} and k_{ad} are the uptake and elimination constants respectively, c_{ww} is the internal concentration and c_d the ambient xenobiotic concentration. The bioconcentration factor is thus

$$\text{BCF} = \frac{c_{ww}}{c_d} = \frac{k_{da}}{k_{ad}} \tag{3.24}$$

Equation 3.9 differs from this simple model by allowing for different uptake routes , changes in lipid contents and size of the animal.

These differences work out such that the coefficients of the one-compartment model are no longer fixed, but change in time. Figure 3.9 (left) shows the BCF of cadmium as function of scaled storage density e and shell length L. The BCF increases with increasing size and decreases with increasing storage density e. The decrease of BCF with increasing storage density is caused by growth dilution of the xenobiotic due to high growth rates at high stored energy densities. Figure 3.9 (right) shows BCF as function of scaled reproductive density r and partition coefficient P_{ea}. The dot in both plots represents the common point (the intersection point of the two planes in 5–D hyperspace). The BCF is, as can be seen, not a constant value but varies with changing physiological conditions. Xenobiotics with fast pharmaco-kinetics relative to physiological rates are likely to follow a simple one compartment model with fixed coefficients more closely.

The kinetic model presented in this paper is successfully applied to various experiments and field data sets. The estimated parameters are sometimes poorly determined, due to a lack of physiological data, especially size and reserve dynamics. The analysis can be improved when more physiological data on the mussel during the experiments are available. The physiological condition of the mussel influences the kinetics of xenobiotics significantly, especially when it is slow and if the xenobiotic is hydrophobic.

The successful reconstruction of cadmium concentration in soft tissues of mussels of different length classes encourages the application of the DEB–based model in scenario simulation studies for management purposes. Its simple structure allows the reconstruction of ambient xenobiotic concentrations. The typical shape of shell length–PCB concentration curve reveals essential information on the internal partitioning of the xenobiotic, but this analysis could be improved when the annual rings in the shell were available. Therefore we recommend the measurement of growth in monitoring programs as the 'Mussel Watch'.

The advantage of the model applied in this paper above other toxico-kinetic models, [13], [36], [95], [108], [226], [157], [251], is its tight coupling between bioenergetics and toxico-kinetics which results in a parameter sparse model. The DEB–model can be and has be tested without any connection to toxico-kinetics [92]. This facilitates interpretation of toxico-kinetic studies in which the animal changes its physiological condition. It also
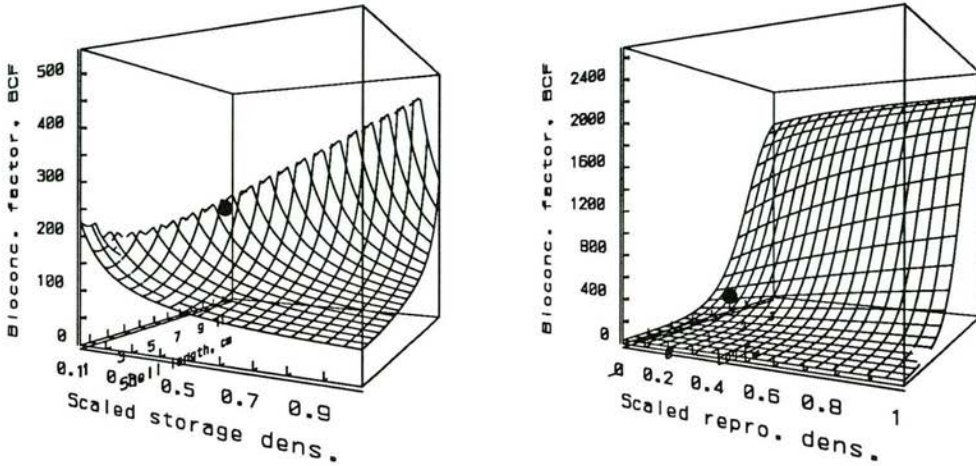
Figure 3.9: Bioconcentration factor, BCF from equation 3.23, as a function of physiological variables of the DEB model (equation 3.12). The uptake and elimination constants r_{da} and r_{ad}/γ are for cadmium, see figure 3.2.
Left: BCF as a function of scaled storage density, e, and shell length, L, for a mussel with P_{ea}/γ = 8.83 and $r = 0.1$. The dot in (right) corresponds to this parameter combination.
Right: BCF as a function of scaled reproductive density, r and partition coefficient, $\log P_{ea}/\gamma$, with $L = 5$ cm and $e = 0.4$. The dot in (left) corresponds to this parameter combination.
Physiological parameters: $v = 0.023$, $gm = 0.00533$, $a = 1.03$, $\kappa = 0.95$ and $a_e = 0.95$

opens the possibility to evaluate toxic effects of xenobiotics on growth, reproduction, respiration or feeding as function of xenobiotic tissue concentration [130].

Acknowledgements

Part II

The potato cyst nematode

Chapter 4

Growth curve analysis, I

4.1 Introduction

Sedentary plant parasitic nematodes are major pests of many world crops. For instance the need to limit economic loss from the two potato cyst nematode (PCN) species *Globodera rostochiensis* and *Globodera pallida* (Heteroderidae) impose restrictions on agricultural practices in The Netherlands and many other countries. In common with several other genera, cyst nematodes induce modified host plant cells from which the animals feed. Such feeding sites are essential for development of females which cause most of the plant damage. Large densities of the parasites present at planting cause subsequent loss of crop yield or even death of the host [55]. Restrictions on the use of nematicides to control PCN are being enforced in many countries such as the Netherlands. As a consequence changes in pest management must be made to accommodate a greater dependence on integration of rotation and resistant cultivars. This requires improvements in the scientific basis for management and this is the motive underpinning the development of the approach in this work.

The development of a nematode on a plant depends upon a number of both abiotic and biotic factors. The influence of the host plant in the absence of resistance have been examined for *Meloidogyne javanica* [29]. Here it is established that different host species support dissimilar reproductive performances by *M.javanica*. There is an influence of host nutritional status and also a density dependent relationship between the growth rate and ultimate nematode biomass [28]. Such effects probably occur for cyst nematodes but that of host species is potentially more discernible for *Heterodera schachtii* (beet cyst nematode) with a wide host range than for PCN with its comparatively narrow host range.

Host differences influence the growth and reproduction of *G.pallida* because a range of cultivars exists that vary from highly susceptible to partially resistant. Resistance is usually assayed experimentally, using test cultivars in canisters or pots and the plants are challenged by an inoculum of different nematode populations or densities [69, 132, 55, 8]. The ratio between the density of eggs present before and after parasite reproduction provides a measure of host resistance. This approach does not discriminate among effects of host finding, penetration and subsequent parasite development. Also, it does not determine directly the reproductive performance of those individuals that establish on the plant. A more direct approach can be pertinent when resistance is expressed against the established feeding nematode. This is the principal of this work. We use a standard protocol [195, 12, 11] to control unwanted sources of variation before studying growth rates of sedentary nematodes.

A thorough study of growth rates requires a basis for analysis. We decided to examine the potential of a Dynamic Energy Budget (DEB) model [125] for the analysis of growth of sedentary plant parasitic nematodes. The model considers an individual as an input-output system with size, stored energy and reproductive output as state variables. Originally, the model was developed for *Daphnia magna* Straus [129, 60] and successfully applied to *Lymnaea stagnalis* [269], *Mytilus edulis* [92] and micro-organisms [130]. It permits the description of embryo development [126, 270], growth [128] and body size scaling relations [127, 128].

The DEB model is first described and then applied to growth curves for both *Meloidogyne* on different hosts and *G.pallida* on different cultivars of potato. Our intention is to investigate the relationship between body size and reproductive output. So, if resource acquisition is coupled to growth then there are consequences at the population level that may be usefully modelled for assessing host suitability and resistance.

4.2   DEB model for individuals

We will restrict the present discussion to the feeding stages of the nematodes dividing them into two groups of non-reproductive juveniles and reproductive adults. Males are uncommon for most *Meloidogyne* species and they are very small in size in comparison to females in both this genus and other Heteroderidae. Their development has little pathological effect on plants compared with that of females. Therefore the DEB model in this work considers only the development of females.

It is assumed that growth of the structural volume and the swelling of the posterior part of the nematode body, caused by reproductive structures, is isomorphic. Due to different growth characteristics, the combined growth of structural and reproductive volume is not isomorphic. The chemical composition of the structural biomass and of stored materials are each taken to be constant, and not necessarily identical. Homeostasis is assumed for structural biomass as well as stored materials. Since the composition of stored materials will differ from that of structural biomass, and the storage density can fluctuate, homeostasis is not assumed for the combination of structural biomass and stored materials.

The symbols that are used frequently in the equations are listed in Table 1.

Three state variables, volume, V (length^3), storage, E and reproductive investment R (number eggs) are distinguished. Food uptake is assumed to follow a type II Holling functional response and is taken proportional to surface area (of the stylet and/or gut), so the ingestion rate is

$$I = \{I_m\} f V^{2/3} \text{ with } f = X/(K + X) \tag{4.1}$$

where X is the food density, K the saturation constant and $\{I_m\}$ the maximum surface area–specific ingestion rate. The food-energy conversion is taken to be constant, $\{A_m\}/\{I_m\}$, so the assimilation energy, *i.e.* the total energy input, equals $A = \{A_m\} f V^{2/3}$, where $\{A_m\}$ is the maximum surface area–specific assimilation rate. The incoming energy adds to the reserves. The reserves follow a first order process when expressed as density, $[E] = E/V$, *i.e.* energy reserve per body volume. From the assumption of homeostasis for energy reserves it follows that the energy reserves in equilibrium are independent of the length of the nematode *i.e.*

$$\frac{de}{dt} = vV^{-1/3}(f - e) \tag{4.2}$$

where $e = [E]/[E_m]$, where $[E_m]$ is the maximum storage density and $v = \{A_m\}/[E_m]$ is by definition the energy conductance (length.time^{-1}). The rate at which energy is utilized from the storage must obey the conservation law of energy:

$$\begin{aligned} C &= A - \frac{d}{dt}([E])(V) = A - V\frac{d}{dt}[E] - [E]\frac{d}{dt}V \\ &= e[E_m]\left(vV^{2/3} - \frac{dV}{dt}\right) \end{aligned} \tag{4.3}$$

A fixed fraction κ of the utilized energy is spent on growth plus maintenance. The latter quantity is taken to be proportional to volume, $[M]V$. So $\kappa C = [M]V + [G]\frac{dV}{dt}$, where $[G]$ is the volume–specific costs for growth. Substitution gives

$$\frac{dV}{dt} = \frac{V^{2/3}ev - Vgm}{e + g} \tag{4.4}$$

where the dimensionless investment ratio, $g = [G]/\kappa[E_m]$, and the maintenance rate coefficient, $m = [M]/[G]$ are compound parameters. If the food density is constant long enough, (2) states that e tends to f and remains constant as well. This turns (4) into the well known von Bertalanffy growth equation, having the solution

$$V(t) = \left(V_\infty^{1/3} - (V_\infty^{1/3} - V_0^{1/3})\exp\{-\gamma t\}\right)^3 \tag{4.5}$$

where $V_\infty^{1/3} = f\kappa\{A_m\}/[M]$ is the ultimate volume$^{1/3}$ and $\gamma = (3/m + 3V_\infty^{1/3}/v)^{-1}$, the von Bertalanffy growth rate. The maximum volume$^{1/3}$ is thus $V_m^{1/3} = \kappa\{A_m\}/[M] = v/gm$, which can only be reached at prolonged exposure to abundant food.

Back substitution of (4) into the storage utilization rate (3) gives

$$C = \frac{eg[E_m]}{e+g}\left(vV^{2/3} + mV\right) \tag{4.6}$$

So, the storage utilization rate depends only on the volume of the organism and the energy reserves and not directly on food density. The energy allocation to reproduction equals $(1 - \kappa)C - \frac{1-\kappa}{\kappa}[M]V_j$ This is a continuous energy investment. The costs for the production of an egg can be written as E_0/q, where the dimensionless factor q^{-1} between 0 and 1 relates the overhead involved in the conversion from the reserve energy from the mother initial energy available for the embryo, see [270, 125] for discussion. Substitution of equation 4.6 leads to a mean reproduction rate of:

$$\frac{dR}{dt} = \frac{q}{e_0V_m}(1 - \kappa)\left(\frac{ge}{g+e}(vV^{2/3} + mV) - gmV_j\right) \tag{4.7}$$

When growth ceases, the cumulated energy drain to reproduction in animals that continue to allocate energy to reproduction under these circumstances, becomes

$$\frac{dR}{dt} = \frac{q}{e_0V_m}gm\left(eV_m^{1/3}V^{2/3} - \kappa V - (1 - \kappa)V_j\right) \tag{4.8}$$

The energy feeding the drain to reproduction accumulates during nematode development, but it is assumed to be metabolically unavailable for other purposes so $R_c = \int_{t_j}^{t_1} R'dt$, where t_j denotes the time of maturation and t_1 the time of death of the female. So this energy pool differs from that in the storage pool in its availability. In PCN, eggs are retained within the body wall of the female, which protects eggs after death of the female.

4.3   Individual growth and reproduction

The feeding site, which functions as a nutrient conducting complex, is induced by the nematode upon a specific action which degrades cell walls or enlarges the initial feeding cell [111]. Bird [29] has measured feeding sites on different host plants and the body sizes of the nematodes grown on it. Large feeding sites result in large nematodes and small sites in small ones. The contact area of the feeding site with the vascular tissues of the plant host determines the conducting capacity of the feeding site itself. The cumulative amount of nutrients for the parasite is therefore determined by the maximum size the feeding site can reach. Host status is therefore assumed to be equal to the 'mean' scaled functional response f, which is determined by the nutrient density in the feeding site. This is preferred to other estimates such as assimilation efficiency $\{A_m\}/\{I_m\}$ or energy conductance v because the latter parameters are linked to intrinsic properties of nematodes.

Measures of size during development are the body width at the mid point of the oesophageal procorpus (oesophageal region width), length, maximum mid-body width, surface area and the volume of the nematode. The oesophageal region width is taken as a

measure of structural volume, V, while the mid-body width provides a measure of the accumulated reproductive output, R_c.

Growth of *G.pallida* on potato cultivars of different host status Multa (partial resistant) and Maritta (susceptible) is shown in Figure 4.1. Bertalanffy growth equations, equation 4.5, are fitted to measures of the oesophageal region width during development. The fit is satisfactory for both of the cultivars, implying a more or less constant food density throughout development. PCN developed on the resistant cultivar Multa are about a factor of 2.7 smaller than individuals developed on the susceptible cultivar Maritta. In addition PCN that developed on Multa failed to reproduce. This may result from insufficient energy uptake to maintain a female reproductive system.

Different host species can also have effects on growth as is shown for volume growth, $V_i(t)$, of *M.hapla* in Figure 4.2. The fitted equation is:
$$V_i(t) = (f_i V_m - (f_i V_m - V_b) \exp\{-t/(3/m + 3f_i V_m/v)\})^3$$
with f_i the scaled functional response for the i-th cultivar. *M.hapla* fail to reproduce on plants when the functional response f_i is about $2.3 - 2.7$ less than for susceptible hosts. This suggests that either maximum oesophageal region width or scaled functional response provides a measure of host ability to support fecund females.

Ingested energy is according to the DEB theory partitioned to three main processes: growth, maintenance and reproductive growth. The reproductive output is determined when the growth curve is known. Figure 4.3 shows the parallel growth of the oesophageal region width and mid-body width. Equations 4.4, 4.7 and 4.8 are integrated using a Douglas Adams fifth order predictor corrector [37] with the assumption that the food density remains constant during development. This assumption is realistic because growth is of the von Bertalanffy type, see figures 4.1 and 4.2. The parallel action of changes in width of the oesophageal and mid body region with time confirms the supposition of a direct coupling between structural volume growth and reproductive output.

4.4 Competition for space in the root system

The feeding site induced by a nematode occupies a root volume associated with the vascular cylinder in the root. It is assumed that the nematode ingests a fraction s of the available transported nutrients, X, in the vascular cylinder. The amount of available nutrients in the root system decreases progressively with increasing numbers of nematodes, as is shown for certain essential amino acids [86]. The carrying capacity of the plant for nematodes depends on the initial amount of available nutrients X and on the nutrient conducting efficiency s of the feeding site. The amount of nutrients available after the n-th feeding site is characterized by X_n which is:

$$X_n = (1 - s)^n X_0 = X_0 \exp\{-\delta n\} \quad \text{with} \quad \delta = -\ln(1 - s) \tag{4.9}$$

This function describes a density dependent individual resource partitioning which affects the scaled functional response f_n. Decreasing functional responses affects the egg production of PCN as is shown in Figure 4.4
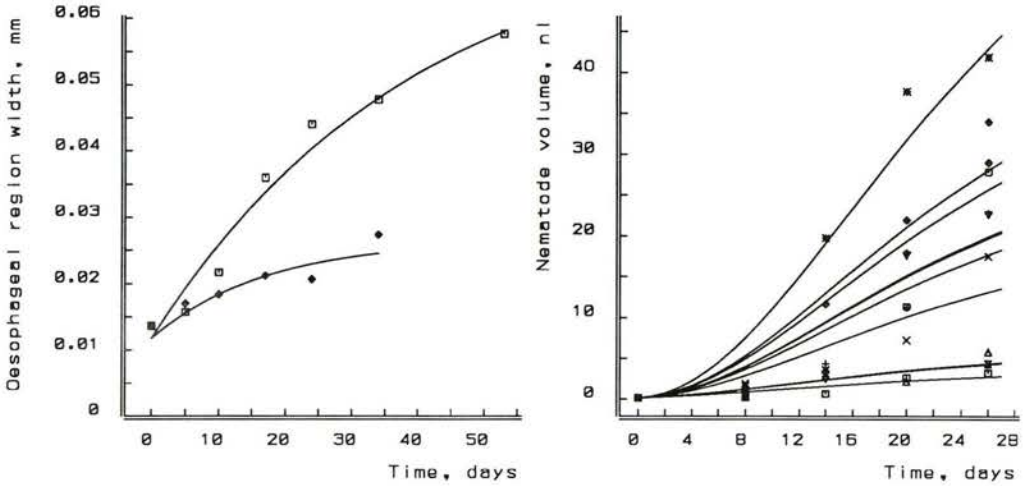
Figure 4.1: Oesophageal region width of *G.pallida* grown on 2 potato cultivars Multa (resistant) ◇ and Maritta (susceptible) □ at 20 °C. Fitted curves are $L(t) = L_\infty - (L_\infty - L_0)\exp\{-\gamma t\}$. Initial oesophageal region width L_0 is a in common estimated parameter: 0.012 (SD=6.1 10^{-4}) mm. The other estimated parameters are for the susceptible interaction: L_∞ is 0.074 (SD=3.3 10^{-3}) mm and γ is 0.026 (SD= 2.6 10^{-3}) d^{-1}. For the resistant interaction: L_∞ is 0.027 (SD=4.1 10^{-3}) mm and γ is 0.059 (SD= 0.030) d^{-1}.

Figure 4.2: Volume growth of *M.hapla* on ten host species varying in host suitability for the nematode. Fitted curves are cubed Bertalanffy growth equations, equation 4.5 with scaled food density as unique parameter per curve. No egg production was measured at values of f_i: 0.20, 0.22 and 0.23. While egg production was measured following parasitism of all eight hosts providing f_i values between 0.34 and 0.53. Data are from F.A.Al-Yayha, Centre Plant Biochem.& Biotech.Univ.Leeds.

Figure 4.3: Growth of oesophageal region width (—) and mid-body width ($\cdots$) of *G.pallida* on potato cultivar Bintje at 20 °C. The equations are 4.4, 4.7 and 4.8 for oesophageal region width and mid-body width respectively.   The estimated parameters are m=0.070 (SD=0.034) d^{-1}, g= 6.2 (SD=1.7) and κ=0.09 (SD=0.13) with the energy conductance v is fixed on 1.3 10^{-4} $m.d^{-1}$ and $f = e$ is fixed on 0.8.
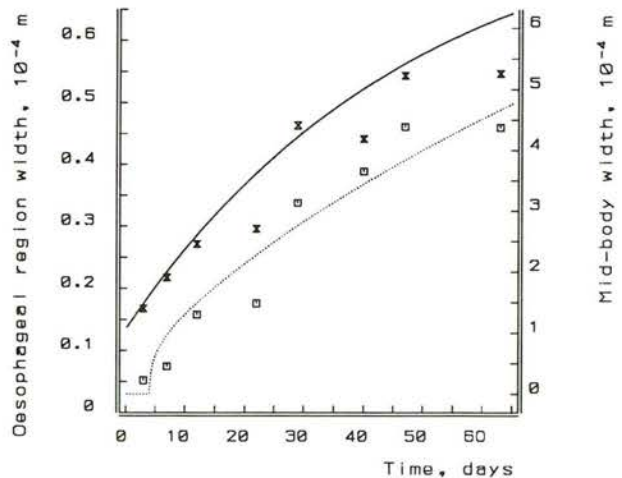
Plant yield itself is affected by large nematode burdens of the root system. The increasing damage of PCN on potato cultivar Bintje is shown in Figure 4.5. It is assumed that the damage to the plant is proportional to the amount of nutrients withdrawn by the feeding sites, so equation 4.9 can be used.

Plant tolerance to nematodes is defined as the capacity of a host to withstand a certain burden of nematodes [243]. The factor δ in equation 4.9 can be considered to indicate tolerance since it defines a 'resource extinction' for nematodes.

The interaction between sedentary plant parasitic nematodes and its host can be characterized by two parameters: the scaled functional response, f, which can be regarded as a measure for of host suitability and δ which can be regarded as measure of tolerance of the plant to a specific nematode population. Figure 4.6 shows the classification in respect of resistance and tolerance of a few potato cultivars and their properties for PCN in the $\delta - f$ plane.

The simulated population dynamical consequences of different plant properties $(\delta - f)$ and intraspecific competition of the nematodes is shown in figure 4.7. The left figure shows the effect on the egg production per female (cyst) while the right figure shows the same relation but now expressed as nematode egg production per plant. The maximum population reproduction rates are at intermediate initial population densities when the negative effects of nematodes on their resource outgrow the initial population density.

4.5 Discussion

This work establishes the potential of DEB for analyzing the individual growth curves of plant parasitic nematodes. It suggests that the energy available to the nematode from the feeding site it induces in the plant, determines its growth rate and fecundity. Apparently the animals are unable to rectify an inadequately forming feeding site by further stimulation of the plant. Consequently the growth rate of the nematode and its body size are compromised by biotic factors that influence the size of their feeding cells with the direct consequence of either a fall in fecundity or even a prevention of egg laying (Figure 4.1).

The DEB model provides a comprehensive approach that accommodates differences in host status of plants and both tolerance and resistance of different cultivars to one species of nematodes. With further development the model could have a range of uses. It could be of value within pest management schemes for *Meloidogyne* spp. to optimize cropping regimes when a number of crops of dissimilar host status are used in combination. It can also be used in a similar manner for a cyst nematode such as *H.schachtii* which may be offered different hosts such as oil seed rape and sugar beet within a rotational scheme. It has important potential for optimizing the utilization of partially resistant cultivars of crops such as potato showing at least some resistance post-establishment of PCN. A future research program could use the DEB model to provide an improved basis for ranking partially resistant cultivars or for determining the relative reproduction of different nematode populations (*i.e.* virulence) on one partially resistant cultivar.
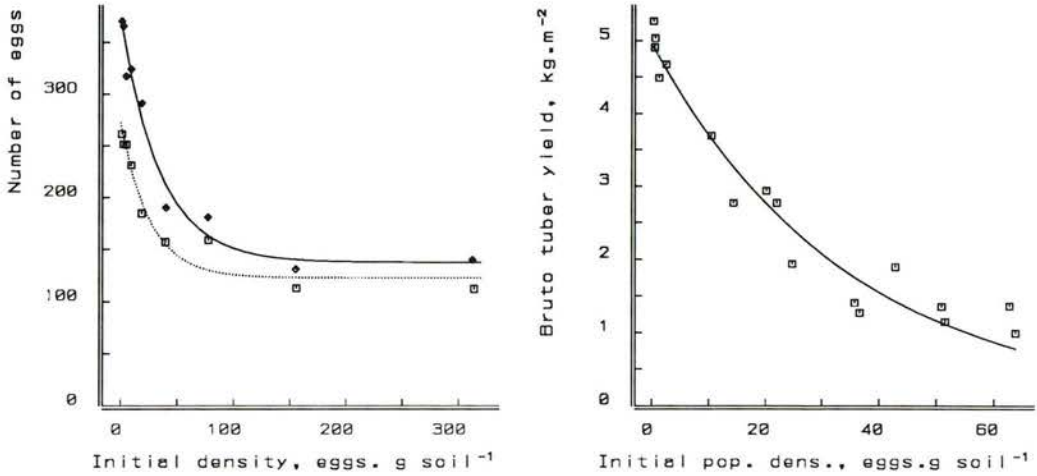
Figure 4.4: Number of eggs per cyst (female) as function of increasing population densities on different potato cultivars. The fitted curve is $Q = Q_\infty + Q_0 \exp\{-\delta N\}$. With Q the egg content per cyst and N the initial population densities. The estimates are respectively for potato cultivars Irene and Darwina: $Q_\infty = 235$ and 149 (SD= 11 and 9.7) eggs/female; $Q_0 = 138$ and 123 (SD= 8.6 and 7.6) eggs/female; δ=0.029 and 0.039 (SD= 0.0040 and 0.0068) g soil/egg. Data are from Seinhorst [218].

Figure 4.5: Yield of potato cultivar Bintje as function of initial population density. The fitted curve is $Y = Y_0 \exp\{-\delta N\}$ with Y the tuber yield per area. The estimates are respectively:Y_0=5.0 (SD=0.14) kg/m^2 and δ=0.029 (SD=0.0020) g soil/egg. Data are from L.Molendijk, Governmental Crop Research Station, PAGV, Lelystad, The Netherlands.
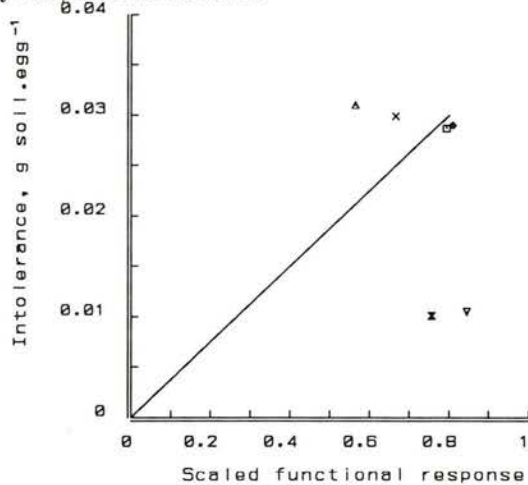
Figure 4.6: Scaled functional response f_i, defined as resistance and tolerance δ_i of different potato cultivars (1) susceptible: □, Irene; ◇, Bintje (2) partial resistant: ×, Multa; △: Darwina (3) tolerant: ▽, Ehud and ⋈, Astarte. The estimates are from figures 4.4 and 4.5. The $x - y$ plane interception is used in figure 4.7 as y-axis.
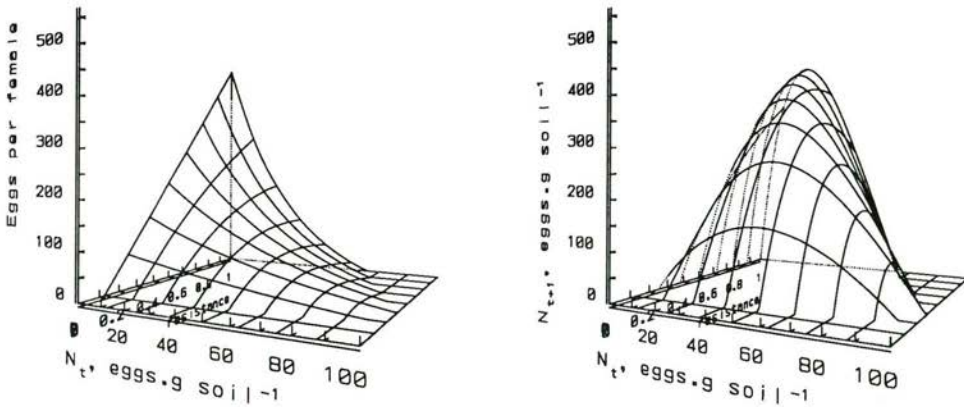
Figure 4.7: Left: egg content per female as function of initial population density, N_t, and of combined resistance and tolerance for the i-th host. The equation is: $f_i Q_0 \exp\{-\delta_i N_t\} - P$. In which P is proportional to the immature volume V_j.

Right: final population density N_{t+1} as function of initial population density, N_t, and of combined resistance and tolerance. The equation is : $\phi N_t f_i Q_0 \exp\{-\delta_i N_t\} - P$ in which ϕ is the fraction invading nematodes in the root. The properties of the plant (Y-axis) are a combined function of resistance and tolerance corresponding with the straight line in figure 4.6.

Table 4.1: Variables, primary and compound parameters

symbol	dimension	interpretation
variables		
t	time	time
X	weight.length^{-3}	food density
f	–	scaled functional response: $X/K + X$
V	length^3	body volume
E	energy	energy storage
e	energy.length^{-3}	scaled energy storage density: $E/[E_m]V$
R_c	number eggs	cumulated number of eggs
primary parameters		
V_b	length^3	volume at birth
V_j	length^3	volume at start reproductive stage
K	weight.length^3	saturation constant
$\{I_m\}$	weight.length^{-2}.time^{-1}	maximum surface area–specific ingestion rate
$\{A_m\}$	energy.length^{-2}.time^{-1}	maximum surface area–specific assimilation rate
$[E_m]$	energy.length^{-3}	maximum storage density
$[M]$	energy.length^{-3}.time^{-1}	volume–specific maintenance costs per unit of time
$[G]$	energy.length^{-3}	volume–specific costs for growth
κ	–	fraction of utilized energy spent on maintenance plus growth
q	–	mother–egg energy conversion overhead
s	–	nutrient conducting efficiency
δ	weight.ind.$^{-1}$	resource extinction for nematodes
compound parameters		
v	length.time^{-1}	energy conductance: $\{A_m\}/[E_m]$
m	time^{-1}	maintenance rate constant: $[M]/[G]$
g	–	energy investment ratio: $[G]/\kappa[E_m]$

Chapter 5

Growth curve analysis, II

submitted: R.J.F. van Haren, F.K. Arntzen and H.J. Atkinson
Growth of vermiform nematodes compared with growth and fecundity of the potato cyst nematode Globodera pallida *on different hosts, a model approach*

5.1 Introduction

Nematode growth is usually measured from changes in cross-sectional area, chemical oxygen demand, dry weight or volume. The latter may be obtained indirectly from morphometric measurements [3, 193]. Another approach is to quantify nematode development for instance by monitoring first appearance of a specific developmental stage. This approach is frequently combined with determining the effects of temperature. Temperature influences growth and development of poikilothermic animals within lower and upper limits. Usually growth and development increases from the lower threshold to an optimum before declining at the upper temperature limit. Temperature affects development of *Meloidogyne javanica, Heterodera avenae, H. cajani, Globodera pallida* and *G. rostochiensis* in this way [66, 137, 106, 149, 224]. A model can be developed that is based on the product of time and temperature above the basal minimum and time (a day-degrees concept). This allows development to be modelled in relation to environmental temperature but it assumes a linear relationship between temperature and growth below the optimal for development [106, 224]. This approach is not suited for quantifying changes in size which are important for nematode fecundity.

A second approach to study growth of nematodes is to analyze body size directly against time. When the lethargus before a moult is of significant duration, inflection points occur in the growth as for *Aphelenchus avenae* [67]. Therefore analysis has sometimes been restricted to growth for a single stage of development [31]. Discontinuous growth is particularly noticeable for *M. javanica* species because after establishment the animal moults without intermediate feeding from the second-stage juvenile to the adult female [27]. Maximum size achieved by the nematode is influenced by quantity of food available to *Caenorhabditis briggsae* [205, 206] and it is also likely to be influenced by both food

quality and intraspecific competition as occurs for *M. javanica* [28, 29] and *H. schachtii* [109]. Maximum size is also influenced by host plant species [29, 5] and by cultivars differing in levels of partial resistance [31, 179, 187, 259].

Growth over a period of continuous growth is usually modelled with a range of empirical curves including logistic, Gompertz, and Chapman-Richards [180, 205, 146]. These models envisage growth as an autonomous process without any relationship to energetic constraints. Even more complex models in which energetic constraints are incorporated still consider growth as autonomous without links to energetics [146, 179].

Atkinson [10] suggested that energetic constraints imposed by trophic form may influence the body size of plant parasitic nematodes. Recently we have begun to address energetic requirements for growth of the plant parasitic nematode, *G. pallida* by applying a Dynamic Energy Budget model [90]. This approach is based on the work of Kooijman [125] whose models have been previously applied to a range of invertebrates [92, 184, 269]. The DEB model distinguishes three main body fractions for an animal: (1) structural biovolume (somatic tissue) (2) stored energy reserves and (3) gonads and/or stored energy reserves allocated to reproduction. The contribution of these body fractions to total biovolume changes with time although homeostasis for each fraction is assumed. The proportion of incoming energy stored is proportional to the surface area of the structural biovolume. Energy utilization from these reserves is allocated to (a) growth (b) maintenance and (c) reproduction. A fixed fraction of the utilized energy is allocated to reproduction while the remainder is allocated to growth and maintenance. Energy demands for maintenance have priority over those for growth, which ceases when food densities are low. The energy costs of maintenance are proportional to structural biovolume. At constant food densities, the stored energy reserves are in equilibrium with the environment and consequently growth of structural biovolume is a weighted difference between surface area and volume. Previous application of the DEB model to sedentary cyst nematodes [90], assumed that *G. pallida* experiences constant food densities once established as a parasite. This simplifies the DEB model and in these conditions growth of the structural biovolume follows the Bertalanffy growth curve.

Within a species, size is often related to fecundity [170, 125]. This effect has been reported for *M. incognita* and correlated with the resistance status of the cultivar of alyce-clover genotypes [178] but not vines [146]. Plant resistance to nematodes is defined from parasite reproduction and may be either qualitative or quantitative in nature [43, 243]. Qualitative resistance of the potato to *G. pallida* and *G. rostochiensis* is considered to indicate a single gene for resistance whereas that of a partial nature has a polygenic basis [243]. Recently a cultivar of potato, Multa has been developed which provides monogenic resistance to certain populations of *G. pallida* [6] which correspond to Pa2 forms on the European pathotyping scheme [132]. Resistance to nematodes is usually assessed from the multiplication factor *i.e.* ratio of the initial and final population densities after growth on a host plant which for *G. pallida* is estimated from the encysted egg number [48]. Such measurements do not distinguish between resistant responses that influence the frequency of female establishment from those that act later to reduce her fecundity.

We have applied the DEB model to analyze the quantitative growth patterns of several,

vermiform nematodes to verify this approach to analysis of nematode growth. Following this, we have developed a form of the model for females of *G. pallida* beyond the position reached in our previous work [90]. In particular we have applied the model to define the influence of host status on body size and fecundity of *G. pallida* during both a compatible and incompatible interaction with potato cultivars. Our objective is to consider the value of the approach for assessing quantitative resistance.

5.2 Materials & Methods

5.2.1 Growth of *G. pallida* under experimental conditions

G. pallida (population 'Rookmaker' designated as Pa3, Research Institute for Plant Protection) were reared in a glasshouse on susceptible cultivar Irene in 10 dm^3 pots. Cysts were recovered from the soil and stored using standard procedures [225]. They were soaked for one week in tap water prior followed by potato root diffusate at 20 °C [225]. Nematodes hatched 1-3 days later were used for experiments. Explants of potato cv Bintje from tissue culture of about 3-4 cm were supplied by the NAK, Emmeloord, NL. They were added to autoclaved growth pouches (Northrup King, Vaughan's Seed Company, USA) containing 8 cm^3 Steiner feeding solution. Four pouches were placed in each autoclaved sun transparent tissue culture bag (44.0 × 20.5 cm) which was equipped with 24 mm 0.02 mm filter disc (SIGMA Chemical Company). After adding 50 cm^3 sterile water, the bags were closed and placed in a phytotron (20 °C, 80% relative humidity, 16/8 LD and 1.26 MJ.m^{-2}.h^{-1} light energy). Roots of about 5-8 cm were developed after 6-8 days. The growth pouches were opened and circular 9 mm Whatman GF/A glass microfiber filter was placed beneath the growing root tip. Thirty nematodes in about 15 mm^3 were pipetted on the root tip which was covered by a second filter and incubated as before. The filters were removed after 24 h to provide a limited infection-period. Infected roots were sampled each week and nematodes were stained in-situ by boiling them in 0.05% cotton blue lactophenol [225]. Differentiated root tissue with nematodes were transferred to 50% glycerol in water, desiccated and mounted permanently in pure glycerol [225]. Nematodes were measured using a differential interference contrast microscope (200 x magnification Zeiss Axioskop) equipped with a drawing tube and a xy-tablet digitizer (MiniMop, Kontron Bildanalyse). Surface area, length, oesophageal width and mid-body width were measured. Oesophageal (region) width was measured at the proximal base of the medium bulb of the oesophagus.

5.2.2 Growth of *G. pallida* on different cultivars

Tubers of potato cvs Bintje, Elles, Darwina, Multa and Maritta were allowed to chit in the dark. A wedge shaped region (3 cm long, 2 cm depth, 1 cm width) around one shoot of 1 cm long was excised with a sterile scalpel and allowed to dry for 1 h. It was sterilized in 1% hypochlorite solution with tween for 7 minutes, washed in running tap water for 1 h and placed in the pouch. Plants were established in the phytotron and infected with

twenty J2's of Pa3 on cvs Bintje, Elles and Darwina and thirty J2's of Pa2 populations D236 (virulent against Maritta only) or P2-22 (virulent against both Multa and Maritta) on cvs Multa and Maritta [6]. Filters were removed after 24 h and the plants were grown. Four pouches were harvested weekly, nematodes were again stained inside the root and oesophageal width of individuals was determined as before. The number of developed females per root were counted for Pa3 on cvs Bintje, Elles and Darwina after 45 and 52 days of development (harvests 7 and 8).

Excised sprouts of cvs Multa and Maritta were grown on 20 cm³ 2% bacto agar in tap water in 8.5 cm diameter petri dishes and infected as before. Petri dishes were stored in the dark. After 13 days post-infection, the roots were harvested and stained as before. The number of penetrated nematodes were counted and their developmental stage and sex were determined. The cross-sectional area of each nematode was measured using the calibrated xy-tablet.

5.2.3   Cyst size and fecundity of *G. pallida*

Cysts of the Pa3 population used above (reared on cv Irene) were sieved through a bank of 16 sieves ranging in mesh size from 0.250 mm to 0.750 mm in steps of 0.025 – 0.100 mm. Twenty full cysts from each fraction were crushed and the eggs suspended in 10 cm³ from which egg numbers were counted for two replicate samples of 1 cm³.

5.2.4   Model description

Growth of the structural biovolume follows, under conditions of constant food densities, the Bertalanffy growth curve:

$$L(t) = L_\infty - (L_\infty - L_b) \exp\{-\gamma t\} \tag{5.1}$$

In which L is a length measure of the structural biovolume, L_∞ is the ultimate length achieved, L_b is length at birth and t is time. The parameters L_∞ and γ of the Bertalanffy growth curve for *G. pallida* can be interpreted in terms of the DEB theory, see van Haren [90]. The growth rate γ (d⁻¹) can be rewritten as:

$$\gamma = \frac{gm}{3(f+g)} = \left(\frac{3}{m} + \frac{3d_m L_m}{v}\right)^{-1} \tag{5.2}$$

with f is the scaled functional response, v is the energy conductance, g is the energy investment m is the maintenance rate constant and d_m is the shape factor for a nematode, see [90] for an extensive discussion and [125] for derivation of the model.

The maximum length, $L_\infty = fL_m$ of the nematode can only be reached at optimal environmental conditions and can be written as:

$$L_m = \frac{v}{gm} \tag{5.3}$$

At sexual maturity, with size L_p, sedentary cyst nematodes cumulate the investment of energy into reproduction inside their bodies. The cumulated energy investment into reproduction between times t_1 and t_2 is given by Kooijman [125] (page 147-148):

$$e_R(t_1, t_2) = \begin{cases} 0 & \text{if } L(t) \leq L_p \\ q_R m \int_{t_1}^{t_2} \left(\frac{g+l(s)}{g+f} f l^2(s) - l_p^3 \right) ds & \text{if } L(t) > L_p \end{cases} \tag{5.4}$$

where $l = fL/L_\infty$ is the scaled length and q_R is the scaled reproduction rate.

The basic growth pattern for nematodes is isomorphic vermiform. We assume saccate nematodes do not differ from this basic growth pattern and effectively superimpose their gonads and the relative high energy reserves allocated to reproduction on the surface area of the structural biovolume. This can be idealized as a cylinder, see figure 5.3. The oesophageal width provides a measure of structural biovolume because it is hardly used for storage of energy reserves. Mid-body width $L_d(t)$ is the sum of oesophageal width $L(t)$ and twice the gonal length $L_R(0, t)$ at each site. Gonads and stored energy allocated to reproduction are deposited around the cylindric shape of the nematode so the increase in width is proportional to the energy cumulated for reproduction. On this basis gonal length $L_R(t)$ is:

$$L_R(0, t) = \begin{cases} 0 & \text{if } L(t) \leq L_p \\ \dfrac{V_R q_R m \int_0^t \left(\frac{g+l(s)}{g+f} f l^2(s) - l_p^3 \right) ds}{L^2(t)} & \text{if } L(t) > L_p \end{cases} \tag{5.5}$$

where the volume V_R is a constant which converts the scaled cumulative reproductive energy per squared oesophageal width into the contribution to the total width. Mid-body width is consequently the sum of oesophageal width and twice the gonal length:

$$L_d(t) = L(t) + 2L_R(0, t) \tag{5.6}$$

The cross sectional area of the nematode A is proportional to $L^2 + 2L_R L$:

$$\begin{aligned} A(t) &= \alpha L^2(t) + 2\beta L_R(t) L(t) \\ &= \alpha L^2(t) + 2\beta \left(\frac{L_d(t) - L(t)}{2} \right) \\ &= (\alpha - \beta) L^2(t) + \beta L(t)(L_d(t) \\ &= \alpha' L^2(t) + \beta L(t) L_d(t) \quad \text{with } \alpha' = \alpha - \beta \end{aligned} \tag{5.7}$$

The final number of produced eggs R_c at the end of the growing season at $t = t_\dagger$ is proportional to the total energy allocated to reproduction, so $R_c = V_E e_R(0, t_\dagger)$, where V_E is egg content per unit volume. The relation between mid-body width and number of produced eggs can be derived after substitution of R_c in equation 5.5 and 5.6:

$$L_d(t_\dagger) = L(t_\dagger) + 2 \frac{V_R R_c}{V_E L^2(t_\dagger)} \quad \text{if } L(t) > L_p \tag{5.8}$$

$$R_c = \frac{V_E}{2V_R} (L_d(t_\dagger) L^2(t_\dagger) - L^3(t_\dagger)) \quad \text{if } L(t) > L_p \tag{5.9}$$

It is assumed that all physiological rates are in the same way affected by temperature of the body. This implies that the rate constants γ, v and m (dimension time^{-1}) are function of temperature, T. For a specific temperature range the (non-linear) Arrhenius temperature correction is usually applied [125]:

$$k(T) = ck(T_1) \exp \left\{ \frac{T_A}{T_1} - \frac{T_A}{T} \right\} \tag{5.10}$$

where T is the absolute temperature (in Kelvin), T_1 a chosen reference temperature and k a physiological rate. The physiological rates are reduced at low and high temperatures due to inactive enzyme configurations at these temperatures. This means that the physiological (reaction) rate has to be multiplied by the fraction of the enzyme that is in its active state. According to this fraction c:

$$c = \left(1 + \exp \left\{ \frac{T_{A,L}}{T} - \frac{T_{A,L}}{T_L} \right\} + \exp \left\{ \frac{T_{A,H}}{T_H} - \frac{T_{A,H}}{T} \right\} \right)^{-1} \tag{5.11}$$

where T_L and T_H relate to the lower and upper boundaries of the temperature tolerance range and $T_{A,L}$ and $T_{A,H}$ are the Arrhenius temperatures for the rate of decrease at both boundaries.

5.2.5   Data analysis and parameter estimation

The data was collected from values or figures (using the x-y tablet) in the literature and by experimentation. The derivatives of total sum of squares (TSS) with respect to the parameters (*i.e.* the normal equations) are approximated by the forward difference method. The roots of the normal equations are solved with the Gauss-Newton method for systems of nonlinear equations [189]. Standard deviations of the parameters are estimated according to the large sample theory of maximum likelihood estimators [46], assuming a normal distribution for the scatter around the deterministic model. When data are available for more than one set of environmental conditions (food density, temperature etc.,), a simultaneous fitting procedure was applied.

5.3   Results

5.3.1   Temperature and development rates

The effect of temperature on development of *G.pallida* was re-analyzed with equations 5.10 and 5.11, using previously published data [149, 137, 204], see figure 5.1. The lower and higher temperatures of the temperature tolerance region were fixed at 3 and 33 °C. These figures are realistic since Stanton [228] found development and hatch of *G. rostochiensis* at 5 and 30 °C. Small differences in the temperature tolerance region has a minimal impact on the fitted parameters. The optimum temperature for development rates appears to be approximaly around 22 °C.

Figure 5.1: Arrhenius temperature correction for stage specific development rates of *G. pallida*. Simultaneous regression analysis with equations 5.10 and 5.11 is applied on data from [149] ($\cdots$) on maximum development rates (first nematode completing development) and from [137] ($\cdots$) and [204] (—) on median development rates. The estimated parameters are: T_A is 8033 (sd=561) K, T_H is 298.3 (sd=0.37) K. The estimated maximum development rates k are respectively for J2–J3: 4.84 (sd=0.29) days □, J2–J4: 8.96 (sd=0.21) days △, J2–male: 14.4 (sd=0.15) days ⋈ and the estimated median development rates are, embryo–J2: 7.03 (sd=0.31) days ◇, J2–J3: 8.95 (sd=0.22) days +, J2–female: 18.4 (sd=0.12) days ×. The reference temperature is 20 °C (293.15 K) and the parameters T_L, T_{AL}, T_{AH} are fixed at respectively 276.15 K, 16158 K and 37372 K.
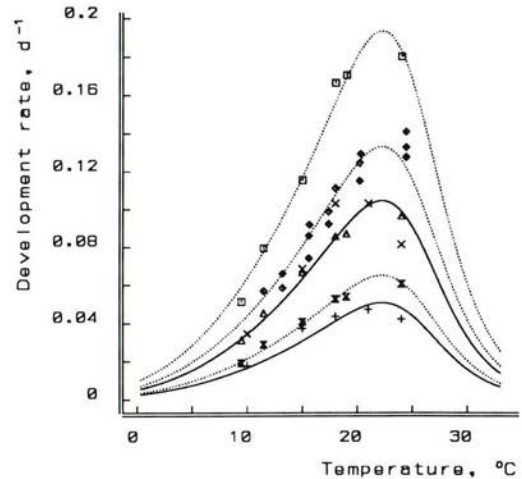
5.3.2 Growth of vermiform nematodes

The growth curve of *C. briggsae* at constant food density fits a Bertalanffy curve (figure 5.2) with differences in food density influencing the final weights of the nematode, the largest experiencing the highest food densities. A vermiform plant parasitic nematode which conserve its shape throughout development is shown in figure 5.2. *Aphelenchus avenae* grows according to a common estimated growth rate γ for both length and width. This apparent constant proportionality between the two linear measurements implies isomorphic growth.

5.3.3 Growth of *G. pallida*

Females of saccate species show a clear change in shape as they grow. We suggest mid-body width is a size measure for fecundity and oesophageal width is a measure for the structural part. The cross-sectional area, A, is composed of a both structural part and a gonal part of the biomass. In figure 5.4, the cross-sectional area is plotted against the oesophageal and mid-body width and decomposed into its discrete parts, according to equation 5.7. The estimated shape parameters α and β have been used in simultaneous regression analysis to provide figure 5.5 which indicates growth for both the parts of the body. Figure 5.5a shows a Bertalanffy curve for the oesophageal width. It is a smooth (Bertalanffy) growth indicating that oesophageal width is an isomorphic measurement throughout growth. The satisfactory

fit also implies that food density remains constant during development. Mid-body width increases with time (figure 5.5b) a few days after establishment. The oesophageal width is around 0.022 mm when mid-body growth commences and this is assumed to be the minimum size for sexual maturation: L_p. The nine parameters given in the legend of figure 5.5 describe the morphological and energetical growth of *G. pallida* on potato cultivar Bintje.

The relation between size and fecundity from equation 5.9 is given in figure 5.6. Fecundity was measured for cysts, oesophageal width and as a consequence could not be measured directly because this region is often lost during removal of cysts from plants. Therefore it is calculated using the parameter values given in figure 5.5. The minimum mid-body width (diameter cyst) for egg-bearing females is estimated to be about 0.22 mm. This corresponds with an oesophageal width of about 0.04 mm.

5.3.4   Growth of *G. pallida* on different hosts

Results for growth of Pa3 on partial resistant cultivars Darwina and Elles is shown in figure 5.7. Female development occurs with estimated final oesophageal widths smaller than of Bintje. The predicted fecundities differ considerably, as can be seen in table 5.2. The differences in fecundity are also reflected in the differences in cross-sectional area. The fractions of established and developed females relative to the initial inoculum of 20 J2's of the partial resistant cultivars are lower relative to cv Bintje, see table 5.2. The product of fraction developed females and their fecundity can be regarded as the ratio between initial and final population density *i.e.* the multiplication factor. The multiplication factors are respectively for Bintje, Elles and Darwina: 456, 112 and 107. When ranked relative to cv Bintje the values are $1\times$, $0.25\times$ and $0.23\times$ respectively.

Results for growth of Pa2 populations D236 and P2-22 on cvs Maritta and Multa are shown in figure 5.8. The susceptible cv Maritta supports a large final length of the oesophageal width for both populations of *G. pallida*. The estimated final oesophageal widths, L_∞, differ by almost a factor of three between the compatible and incompatible interactions of D236 with cv Maritta and Multa respectively. Final oesophageal width of P2-22 on Multa appeared to be smaller relative to Maritta, indicating a possible source of partial resistance, which is confirmed by pot experiments [6]. Experiments performed in petri dish, confirmed that cv Multa supports only development of males (table 5.3). The final oesophageal width of males developed on Multa are the same as for males developed on cv Darwina: about 0.027 mm.

5.3.5   Host suitability ranking

Final oesophageal width (L_∞) is plotted against both final width and the Bertalanffy growth rate γ in figure 5.9. The relation between the data points seems to be linear but this requires confirmation by further study with more nematode-host plant interactions. The predicted fecundity (from figure 5.6) is plotted against L_∞ for oesophageal width in figure 5.9. The dark grey region in figure 5.9 represents the oesophageal width range below

which only male development occurs. The light grey region represents a transition zone, due to uncertainty, between the minimum female oesophageal width below which no reproduction can occur (from figure 5.6) and the final male oesophageal width. Further study with more nematode-host plant interactions might give a better estimate for minimum female oesophageal width final male oesophageal width.

5.4 Discussion

Our analysis of previously published data for growth of vermiform nematodes suggests that Bertalanffy growth curves can be applied to the species we considered. Vermiform nematodes remained basically isomorphic during development. This implies that eggs production by mature females is constant over a period of time as is shown for *A. avenae* [68] and *C. briggsea* [205, 206].

In contrast, the saccate nematode *G. pallida* cumulates the energy allocated to reproduction and the resultant retention of eggs is associated with a change in body shape. The oesophageal region is not involved in the storage of eggs or energy reserves and so remains isomorphic during development. This body region can therefore be analyzed with the same Bertalanffy growth curves as used for the vermiform nematodes. Equation 5.1 suggests a body length for a hypothetical vermiform, female *G. pallida* of about 3.1 mm which is larger than corresponding estimates for *A. avenae* (1 mm) [67] and *D. dipsaci* (1.3 mm) [31]. The body length of vermiform *G. pallida* males derived in the same way as for the vermiform female is between 0.8 – 1.1 mm. This is in close agreement with actual data of vermiform males of 1.0 – 1.2 mm [229]. The figure for *G. pallida* provides an estimate of the extent that the trophic form of *G. pallida* via specialised feeding cells supports a larger body size than achieved by vermiform plant parasitic nematodes that do not modify plant cells.

The overall relationship between cyst size and fecundity found in this work has been suggested previously from experiments with susceptible and resistant cultivars [152]. A more comprehensive data set with cysts of various *G. pallida* populations, virulence groups and reared on various susceptible cultivars [7] supports the conclusion of this work that there is an overall relationship between these two factors. There is also an overall relationship between oesophageal width and mid-body width for nematodes grown on different cultivars, which demonstrates the direct relation between somatic tissue size and fecundity.

Our work demonstrates that host ranking for *G. pallida* suitability from oesophageal width provides a simple and reliable experimental system for comparative measurements of growth. The direct relation between size and fecundity enables estimates for fecundity based on size measurements alone. In combination with the number of established females predictions of the multiplication factor N_{t+1}/N_t can be made. Different methods for assessing the multiplication factor can be compared by scaling the multiplication factor on a reference cultivar [173]. Comparison of the scaled multiplication factors obtained by pot experiments (1, 0.24 and 0.13 for respectively Bintje, Elles and Darwina at 0.4 egg.g soil[1] [93]), are in agreement with those found in this paper (1, 0.25 and 0.23) and show the same

ranking.

The particular advantage of measuring oesophageal width is its direct relation with the energy uptake by the nematodes. The estimated parameters m, g, $V_R q_r$ and L_m can be used for establishing the energy budget of the nematode [92, 125] and in further analysis for modelling population dynamics of *G. pallida* on different hosts and different initial population densities. Furthermore the Bertalanffy growth curve can be applied to the data providing the growth conditions remain constant. This facilitates parameter estimation for comparative research on host suitability. As resistance is currently measured from egg production, we suggest that sources of resistance that do not effect nematodes as we describe affect processes other than growth. For instance, nematode population increase could also be reduced by the frequency of success in establishment rather than by influencing subsequent growth of females.

Table 5.1: Variables and parameters

| symbol	dimension	interpretation
variables		
t	time	time
T	temperature	temperature
f	–	scaled functional response
L	length	length structural biovolume
A	length^2	cross sectional area
V	length^3	structural volume
l	–	scaled length structural volume: $\frac{L}{L_m}$
L_R	length	cumulated gonal length
L_d	length	total length (mid-body width): $L + 2L_R$
R_c	#	cumulated number of eggs at $t = t_\dagger$
e	–	scaled energy density
e_R	–	scaled energy density into reproduction
parameters		
L_b	length	length at birth
L_p	length	length at start reproductive stage
L_m	length	maximal length
L_∞	length	ultimate length: fL_m
$V_R q_R$	length^3	conversion cumulative energy investment reproduction to contributed gonal length
V_E	#.length^{-3}	volume specific egg content
$t_\dagger$	time	time of end of growing season
v	length.time^{-1}	energy conductance
m	time^{-1}	maintenance rate constant
g	–	energy investment ratio
T_A	temperature	Arrhenius temperature, K
T_L	temperature	lower temperature threshold
T_H	temperature	upper temperature threshold
T_{AL}	temperature	Lower Arrhenius temperature
T_{AH}	temperature	Upper Arrhenius temperature
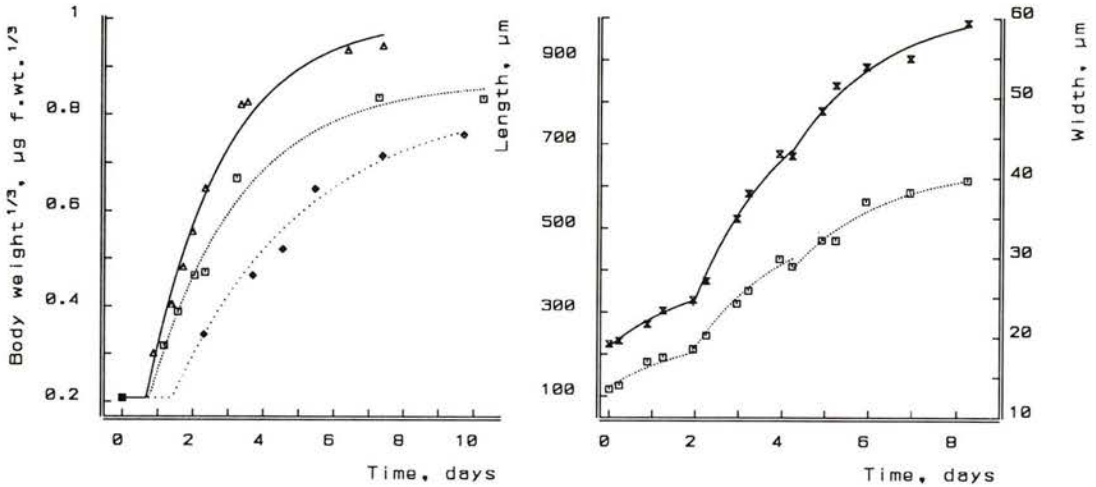
Figure 5.2: Left figure: Growth of *Caenorhabditis briggsae* at different food (bacterial *Escherichia coli*) concentrations, data are from Schiemer [205]. The fitted curves are $V_{m,i}^{1/3} - (V_{m,i}^{1/3} - V_0^{1/3}) \exp\{-\gamma_i(t - d_i)\}$ with a time delay d_i at the onset of growth and i the counter for each food density. The fitted cuberoot weights (in $\mu g^{1/3}$) are: $V_0^{1/3}$=0.207 (sd=0.0141), $V_{m,1}^{1/3}$=1.00 (sd=0.0277), $V_{m,2}^{1/3}$=0.869 (sd=0.0262), $V_{m,3}^{1/3}$=0.835 (sd=0.0593); the growth rates (in d^{-1}) are: γ_1=0.467 (sd=0.0493), γ_2=0.396 (sd=0.0592), γ_3=0.265 (sd=0.0682); the time delays (in days) until first feeding are: d_1=0.682 (sd=0.0827), d_2=0.770 (sd=0.141), d_3=1.41 (sd=0.303).

Right figure: Growth in length and width of *Aphelenchus avenae* feeding on the fungus *Rhizoctonia solani*, data are from Fisher [67]. The simultaneous fitted curves are $L_{j,k} - (L_{j,k} - L_{j-1,k}) \exp\{-\gamma(t - d_j)\}$ with j the counter for the developmental stages and k representing the counters for length and width respectively. The fitted body lengths and body width (in μm) for each developmental stage are: $L_{0,l}$=224.6 and $L_{0,w}$=14 (fresh hatched, second stage, fixed values), $L_{1,l}$=402 (sd=21.4) and $L_{1,w}$=21.0 (sd=4.81) (final length and width third stage, initial length and width fourth stage), $L_{2,l}$=881 (sd=44.5) and $L_{2,w}$=36.0 (sd=4.34) (final length and width fourth stage, initial length and width adult stage), $L_{3,l}$=1035 (sd=21.6) and $L_{3,w}$=41.7 (sd=8.45) (final length and width adult stage), the growth rate γ=0.465 (sd=0.0588) d^{-1}, the acclimatization time d_0=0.0758 (sd=0.0837) days and the development times d_1 and d_2 until the fourth larval stage and the adult stage are respectively 2.29 (sd=0.103) and 6.02 (sd=0.668) days.
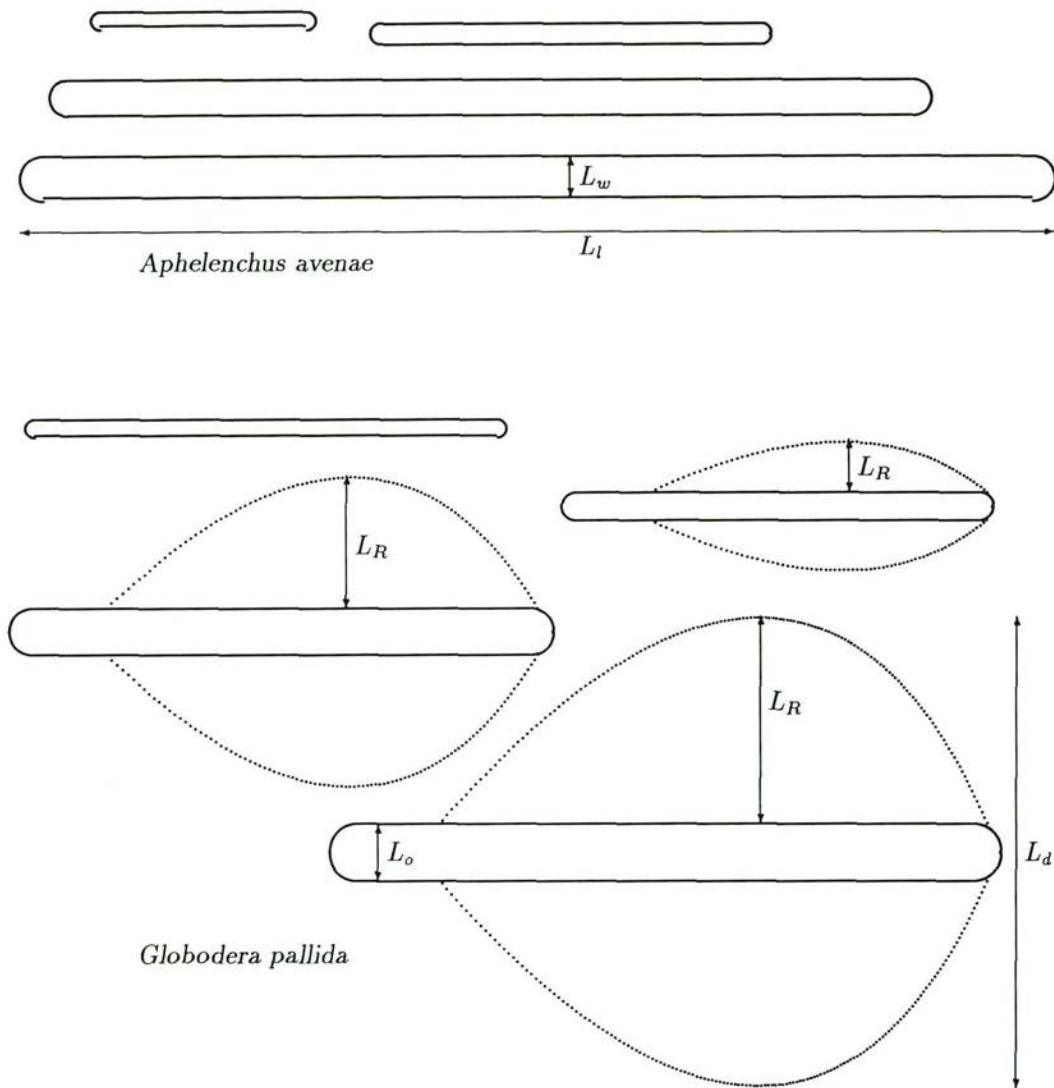
Figure 5.3: Morphometrics of *A. avenae*, see figure 5.2 and *G. pallida*, see figure 5.5, are drawn on the same scale. *A. avenae* is drawn at $t=0$, $t=2.29$, $t=6.02$ and $t=8$ days which corresponds with the length and width of the moulting periods. L_w and L_l correspond respectively with 41.7 and 1035 μm. *G. pallida* is drawn at $t=0$, $t=12$, $t=29$ and $t=63$ days. Cross-sectional area is sum of structural (αL^2) and gonal area $\beta L_R L$, see equation 5.7. L_o and L_d correspond with 60 μm and 470 μm respectively.
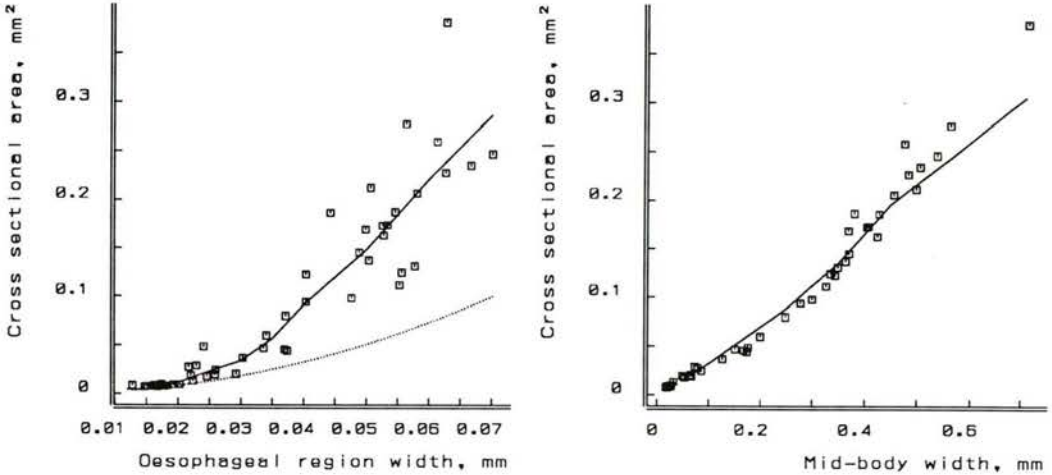
Figure 5.4: Relation of oesophageal width, L (left), and mid-body width, L_d (right), with cross sectional area A of *G.pallida* grown on the susceptible cv Bintje (experiment 1). The simultaneous (left and right) fitted curves are $A = \alpha' L^2(t) + \beta L_d(t) L(t)$ with $\alpha'=20.2$ (sd=3.97) and $\beta=5.10$ (sd=0.51). The dashed line in the left figure represents the contribution of structural area to the cross sectional area.

Table 5.2: Mean oesophageal width, mid-body width and cross sectional area of Pa3 after 52 days development on different cultivars with fraction of developed females, estimated final oesophageal width, L_∞ and maximal predicted fecundity, see also figure 5.7.

cultivar	oesoph. width	mid-body	area	fract. females	L_∞	pred. fecund.
	mm	mm	mm^2		mm	eggs.cyst^{-1}.
Bintje	0.0608	0.532	0.249	.44	0.076	1037
sem	0.00237	0.0130	0.0115			
Elles	0.0565	0.434	0.179	.18	0.069	624
sem	0.00130	0.0223	0.0147			
Darwina	0.0540	0.409	0.175	.13	0.073	830
sem	0.00156	0.0248	0.0184			
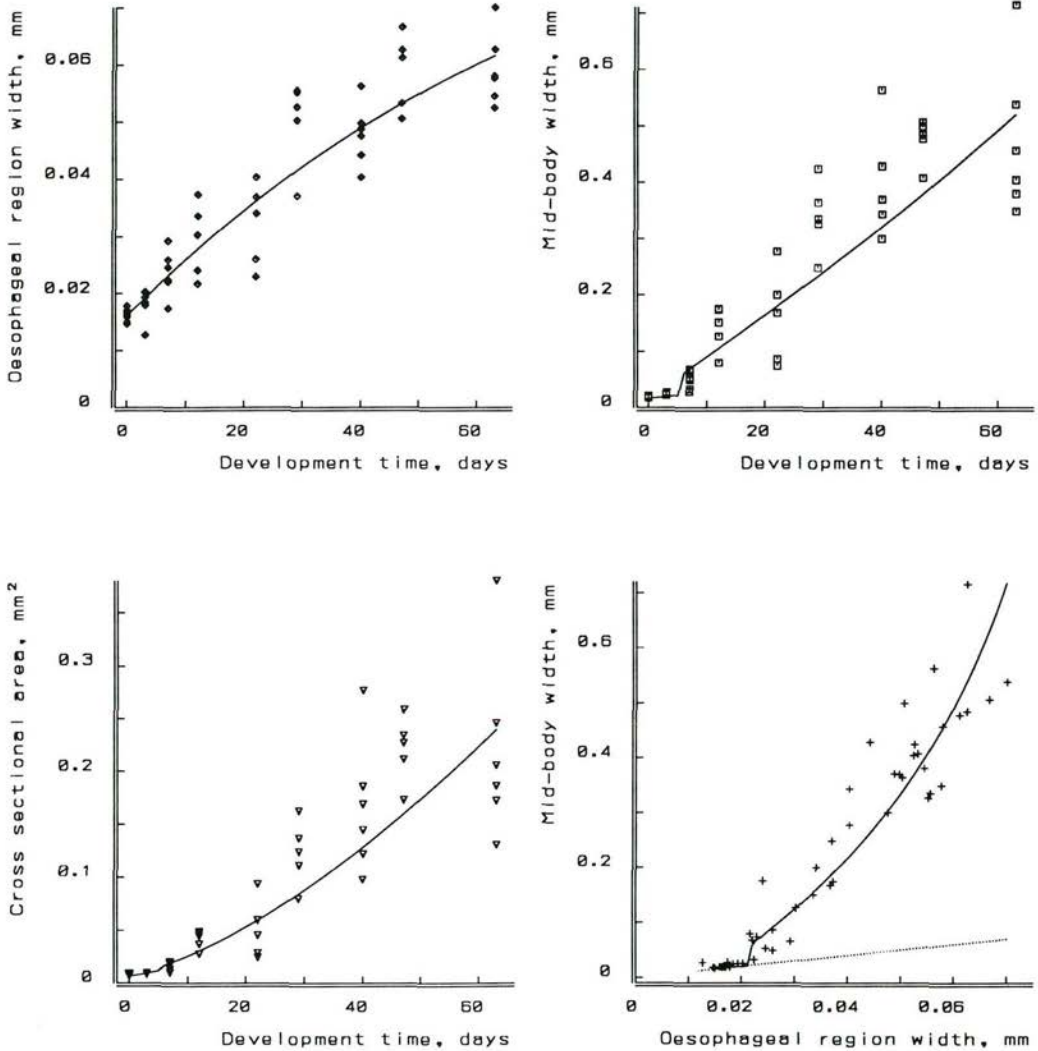
Figure 5.5: Growth of the morphometric variables oesophageal width L, mid-body width L_d, and surface area A, of *G.pallida* and the relation between oesophageal and mid body width on cultivar Bintje. Fitted equations are 5.1 and 5.6. The morphometric parameters α and β from equation 5.7 are estimated separately in figure 5.4. The estimated parameters are m=0.0624 d^{-1} (sd=0.012), g=1.26 (sd=0.616) and $V_R q_R$=.00288 (sd=3.07 10^{-4}). The next parameters are fixed: L_∞=0.0987 mm, L_p=0.022 mm, L_b=0.0161 mm, f=0.8, α=20.2 and β=5.1. The dashed line in the bottom right figure represents the contribution of oesophageal width to mid-body width.

Figure 5.6: Diameter cysts of *G.pallida* and its egg content. Cysts are classified in cohorts of 30 μm distance and the egg content of 20 cysts is determined. The fitted curve is equation 5.9 with an offset ξ corresponding with the size at start of the reproductive stage: $R_c = \delta(L_d L^2 - L^3) - \xi$. Since only mid-body width could be measured reliably, the corresponding oesophageal width L was reconstructed from calculations based on figures 5.4 and 5.5. The estimated parameters δ and ξ are respectively 2363 (sd=148) eggs$\times$100.mm^{-3} and 0.660 (sd=0.251) eggs$\times$100.
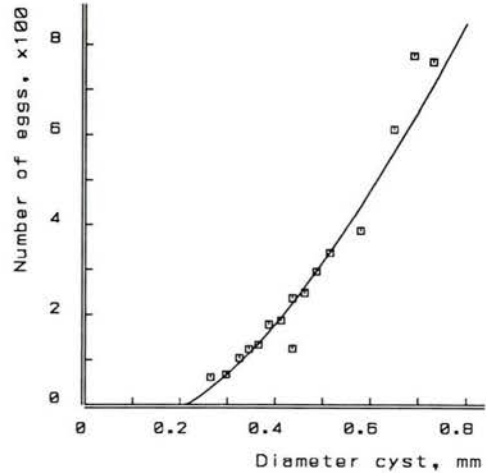
Table 5.3: Cross sectional area, sex ratio and developmental stage of populations Pa2 D236 and P2-22 grown on cultivars Maritta and Multa after 13 days at 20 °C

cultivar	population	area mm^2	$\pm$ sem	n	female	male
Maritta	D236	0.02225	4.47E-4	185	159	61
Maritta	P2-22	0.02564	5.74E-4	93	117	21
Multa	D236	0.01799	5.20E-4	28	0	33
Multa	P2-22	0.02691	4.24E-4	95	119	46

total number individuals and per developmental stage						
cultivar	population	total	J2	J3	J4	adult
Maritta	D236	342	17	78	214	33
Maritta	P2-22	238	17	56	143	22
Multa	D236	164	41	89	34	0
Multa	P2-22	330	4	107	189	30
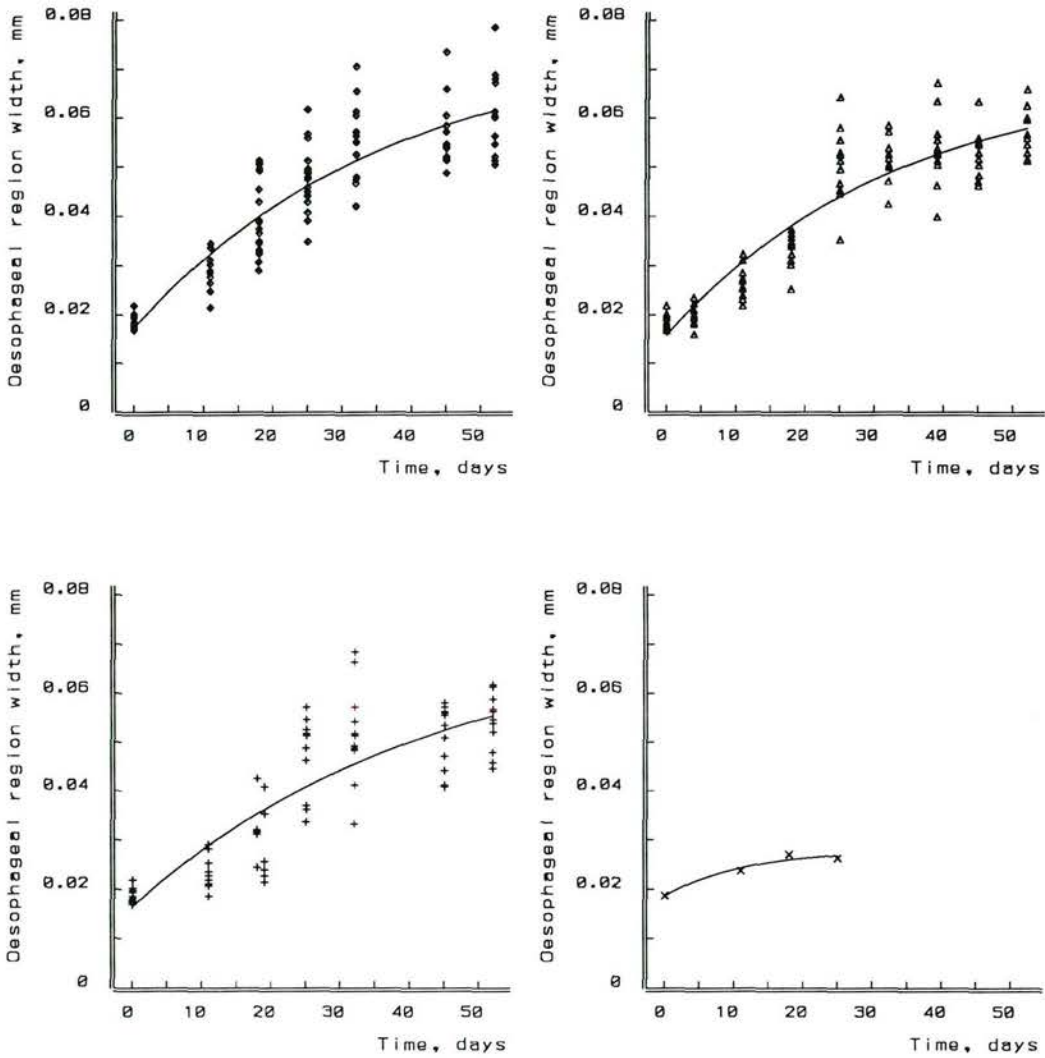
Figure 5.7: Growth of *G. pallida* Pa3 on Bintje (◇) and the partial resistant cultivars Elles (△) and Darwina (+). The lower right curve represents male development on cv Darwina (×). Fitted curves are $L(t) = L_\infty - (L_\infty - L_0)\exp\{-\gamma t\}$. The final length, L_∞, and growth rates, γ, are respectively for Bintje, Elles, Darwina and Darwina, male: L_∞=0.076 (sd=.0068) mm and γ=0.027 (sd=.0058) d^{-1}; L_∞=0.069 (sd=.0053) mm and γ=0.030 (sd=.0059) d^{-1}; L_∞=0.073 (sd=.012) mm and γ=0.023 (sd=.0082) d^{-1}; L_∞=0.028 (sd=.0017) mm and γ=0.087 (sd=.040) d^{-1}.

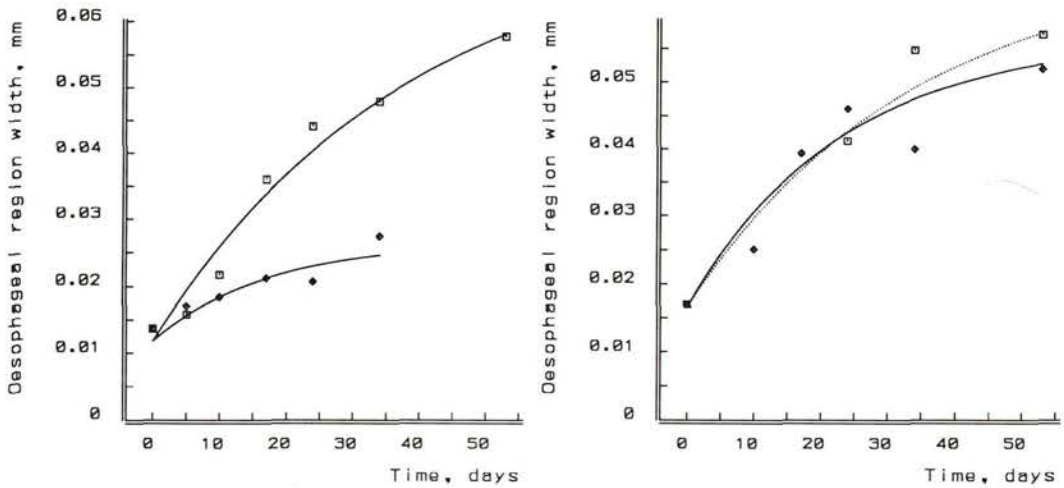Figure 5.8: Oesophageal width of *G.pallida* population D236 (left) and population P2-22 (right) grown on potato cultivars Multa ($\diamond$, —, resistant for D236) and Maritta ($\square$, $\cdots$, susceptible) at 20 °C. Fitted curves are $L(t) = L_\infty - (L_\infty - L_0)\exp\{-\gamma t\}$. Initial oesophageal width L_0 is an in common estimated parameter for population D236: 0.012 (sd=6.1 10^{-4}) mm and for population P2-22: 0.016 (sd=4.7 10^{-4}) mm. The other estimated parameters are for population D236 grown on Maritta: L_∞=0.074 (sd=3.3 10^{-3}) mm and γ=0.026 (sd=2.6 10^{-3}) d^{-1}. For population D236 grown on Multa (only male development): L_∞=0.027 (sd=4.1 10^{-3}) mm and γ=0.059 (sd=0.030) d^{-1}. The other estimates for population P2-22 grown on Multa are L_∞=0.057 (sd=1.7 10^{-3}) mm and γ=0.043 (sd=3.9 10^{-3}) d^{-1}. For population P2-22 grown on Maritta: L_∞=0.067 (sd=3.9 10^{-3}) mm and γ=0.029 (sd=4.5 10^{-3}) d^{-1}.
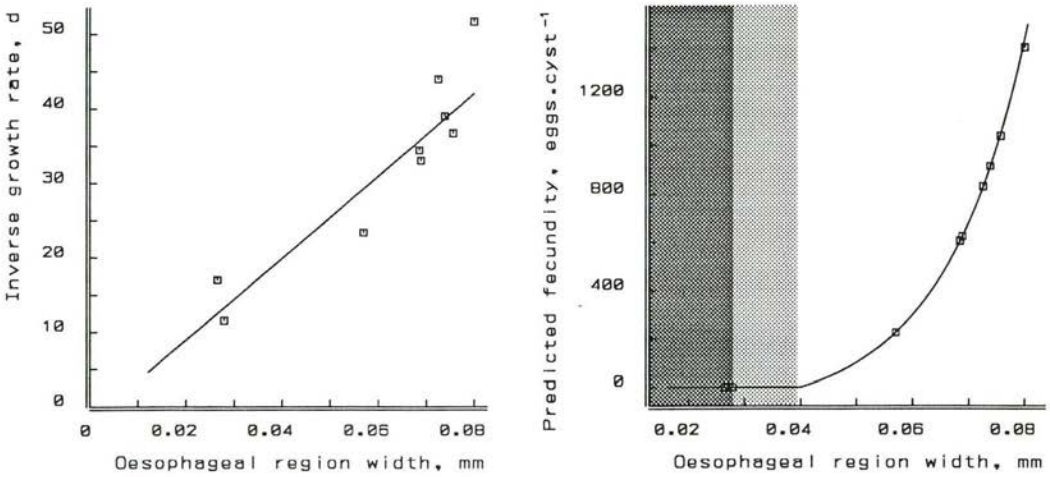
Figure 5.9: Left figure: Classification of performance of different populations of *G. pallida* on different host cultivars. The data points used, are the estimated parameters from figures 5.7 and 5.8. The relation between ultimate length of the oesophageal width L_∞ and inverse Berta-lanffy growth rates $1/\gamma$ is according to equation 5.2: $1/\gamma = a + bL_\infty$. The estimates are for a and b respectively: -2.1 (sd=5.3) d and 550 (sd=83) d.mm^{-1}. Right figure: Predicted fecundity of female *G. pallida*. The prediction is based on the estimated parameters in figure 5.5 and 5.6. The boxes (□) refer to the same estimated final oesophageal widths, L_∞, as in the left figure. No egg production occurs in the shaded areas below oesophageal widths of 0.04 mm, see figure 5.6.

Chapter 6

Measuring feeding rates

6.1 Introduction

Cyst-forming nematodes induce syncytial feeding cells in roots of their host plants. These modified plant cells function as transfer cells, providing the nutrients essential for the nematodes' sedentary parasitism. The role of the syncytium as efficient exchanger of solutes has been deduced from structural and ultra structural studies in which cell wall protuberances adjacent to conducting elements are found [114, 111]. This is predominantly adjacent to xylem vessels, but ingrowths can be found when syncytia contact sieve tubes [114]. The bulk of solutes is likely to enter the syncytium from the apoplast via the wall ingrowths because plasmodesmatal frequency of the syncytium with neighbouring cells is low [111]. Moreover it is found that the beet cyst nematode *Heterodera schachtii* does not develop normally when the syncytium fails to make contact with xylem elements as is found in resistant interactions [83, 141].

Root knot nematodes, *Meloidogyne* spp., feeding on syncytial analogue structures, giant cells, act as strong carbon sinks for $^{14}CO_2$ when exposed to leaves [30, 144], implying a transport pathway of photoassimilates via the phloem. Dorhout [54, 53, 51] has found apoplastic as well as symplastic transport pathways for selected fluorescent tracers into *Meloidogyne incognita* induced giant cells. Dorhout [54, 51] suggests large transport rates for both pathways, despite the low plasmodesmatal frequency [114, 111]. He also confirms the existence of the proton (H+) pump mediated transport in the plasma membrane at wall ingrowths adjacent to xylem elements [51]. Sijmons [220] stresses the importance of amino acid porters acting in symport with the proton pump for efficient removal of nitrogen compounds from the apoplast.

The quality and quantity of the withdrawn nutrients might affect nematode development. The nematode feeds from the syncytium in regular cycles of respectively ingestion,

resting and salivation [263]. Nutrients are withdrawn from the syncytium through feeding tubes which are established at each feeding cycle and probably act as a sieve [203, 263]. Molecules of a maximum Stokes radius between 3–4 nm are ingested, while larger molecules are excluded. This has been found by *in situ* microinjection of fluorescent dextrans differing in molecular weight [33]. Concentrations of ATP (adenosine triphospate), G-6-P (glucose-6-phosphate), glucose and free amino acids are elevated in syncytial tissue compared to growing root tips [84]. X-ray microanalysis [44] has revealed differences between mineral content of syncytium and unmodified host tissue. Syncytia induced by *Globodera rostochiensis* have less Na and S than other plant cells [44]. Single free amino acids are important for nematode development as is demonstrated by Grundler and Betka [86, 26]. Glutamine appears to have positive effects on development while methionine, phenylalanine, lysine, and tryptophan have negative effects on development.

The quantity of withdrawn nutrients is hard to detect. Attempts have been made by Müller [151] to estimate ingestion rates by means of time-lapse film analysis of defecating nematodes. Wyss [263] however states that this estimate is not reliable and should be improved by calculations of volume changes in the pump chamber (valve system) during median bulb pulsation and the frequency of bulb pulsations *cf.* Seymour [219]. Sijmons [221] has calculated in this way an ingestion rate for a J4 female *Heterodera schachtii* of 0.4–0.6 times and for an adult female of four times the syncytial volume per day.

Ingestion rates of *G. pallida* are studied in this paper with aid of the apoplastic fluorescent tracer fluorescein. It is assumed that uptake rates of the fluorescent tracer is equivalent to uptake rates of nutrients *i.e.* ingestion rates. This assumption is only valid when 1) uptake via food is the only uptake route and 2) diffusion of the fluorescent tracer via the nutrients uptake route is negligible relative to ingestion rates. Dorhout [53] has demonstrated that fluorescein is able to accumulate inside giant cells and root knot nematodes when applied apically to the xylem. In this study attempts are made to quantify the ingestion rates of adult females by image analysis with low-lux video cameras, see *e.g.* [143], when similar procedures are followed. These measurements are compared with calculated ingestion rates based on measured diameters of the pump chamber of the median bulb.

6.2 Materials & Methods

6.2.1 Plant growth

G. pallida (population 'Rookmaker' designated as Pa3, Research Institute for Plant Protection) were reared in a glasshouse on susceptible cultivar 'Irene' in 10 dm³ pots. Cysts were recovered from the soil and stored using standard procedures [225]. They were soaked for one week in tap water prior followed by potato root diffusate at 20 °C. Nematodes hatched 1-3 days later, were used for experiments. Explants of potato cv Bintje from tissue culture of about 3-4 cm were supplied by the NAK, Emmeloord, NL. They were added to autoclaved growth pouches (Northrup King, Vaughan's Seed Company, USA) containing 8

cm^3 Steiner feeding solution. Four pouches were placed in each autoclaved sun transparent tissue culture bag (44.0 × 20.5 cm) equipped with 24 mm 0.02 mm filter disc (SIGMA Chemical Company). After adding 50 cm^3 sterile water, the bags were closed and placed in a phytotron (20 °C, 80% relative humidity, 16/8 LD and 1.26 MJ.m^{-2}.h^{-1} light energy). Roots of about 5-8 cm were developed after 6-8 days. The growth pouches were opened and 9 mm Whatman GF/A glass microfiber filter was placed beneath the growing root tip. Ten to fifteen nematodes in about 15 mm^3 were pipetted on the root tip which was covered by a second filter and incubated as before. The filters were removed after 24 h to provide a limited infection-period. Plants were allowed to grow until the female nematodes appeared outside the root. They were then used for fluorescein uptake studies.

6.2.2   Calibration imaging system

Fluorescent images were made with a Leitz DM RB epifluorescence microscope equipped with a Zeiss 20× LD Achroplan objective, a 50 W mercury lamp, an I3 'blue' filter set (BP 450-490/RKP 510/LP 515) and an low-lux PLT 450 CCD camera (Adimec, Netherlands) attached with a 0.3× C-mount. Fluorescein has a green fluorescent in buffered tap water with an emission maximum at 515-520 nm [53].

Video images were digitized using the frame grabber of an image analysis system (GOP-302, Context Vision, Sweden with SUN3 host). The captured images are processed and corrected for camera deviations before analysis. The linearity of response to the fluorescent was determined by measuring the light output from solutions of sodium fluorescein in NaOH buffered tap water (pH=7.8). Known dilutions of this solution were placed in a haemocytometer (depth 0.200 mm) with the epifluorescence in place. Fluorescence values were determined in duplicate from a fixed area in the field [15] after 15 seconds of photobleaching.

The photobleaching power was determined with the same haemocytometer filled with 3 μM sodium fluorescein in buffered tap water exposed to continuous excitation. The images are integrated 23×, captured and processed each second plus the time necessary for completing the image acquisition program.

6.2.3   Dye application and uptake measurement

Plants were carefully removed from the pouch and transferred to a 9 cm diameter petridish with 5 cm^3 0.1% agarose (SeaKem, LE, FMC corporation). One healthy root with nematodes was carefully laid apart and fixed in position with plasticine. About 1–2 cm of the root tip was placed on parafilm and decapitated with a razorblade. Immediately after that a 100 mm^3 pipet tip (5 mm of top removed) filled with 0.03 mM fluorescein in tap water and sealed on one side with plasticine was connected to the root and sealed with silicone grease. Subsequently the system was transferred to the microscope. A bright field image was grabbed by the image analyzer and the shape of the nematode was outlined manually. The number of frames of the camera was adjusted to the emitted light in maximal 5 seconds excitation. Subsequently 1-2 images were taken after 20 minutes each, with

15 seconds excitation. The outlined (nematode) area was analyzed for its intensity (grey values). The plant system was then transferred to the phytotron and kept in dark for until the next measurement (24, 48 and 72 hours later).

Controls followed the same treatment, but in stead of fluorescein, tap water was used.

Volumes, V, of the nematodes were determined by dividing the IA captured images in 40–50 cross sections of 11.74 μm thickness, h. The volume was calculated according:

$$V = \sum_{i=0}^{n} \pi h r_i^2 \tag{6.1}$$

Photographs are made directly from the screen of the image analysis system with a Polaroid Freeze Frame Video recorder on Kodak Ektachrome 100 ISO colour slides film, from which black and white reproductions are made.

6.2.4   Data analysis

The mean intensity I of the outlined area is calculated by the total sum of single grey values g_i multiplied by the number of pixels p_i and subsequently divided by the total number of pixels of the area:

$$I = \frac{\sum_{i=1}^{256} g_i p_i}{\sum_{i=1}^{256} p_i} \tag{6.2}$$

The linearity and of the low-lux camera and the calibration of the imaging system is tested with the following equation:

$$I = \alpha F[C] + b \tag{6.3}$$

with I is the mean intensity, grey value.pixel^{-1}, F the number of frames, $[C]$ the concentration, mM, α the proportionately constant, grey value.(pixel.frame.mM)$^{-1}$ and b the offset, grey value.pixel^{-1}. The intensity of the outlined area (ranging between 0 and 256 grey values) was transformed according the calibration to fluorescein concentration:

$$[C] = \frac{I - b}{\alpha F} \tag{6.4}$$

Uptake of the dye is analyzed with a one compartmental model with first order kinetics of tracers [213]:

$$Q(t) = Q_0 \exp\{-k_e t\} + \frac{k_a}{k_e} c(1 - \exp\{-k_e t\}) \tag{6.5}$$

in which Q is the concentration of the dye inside the nematode pmol.mm^{-3}, Q_0 the concentration of the dye at t=0 (including autofluorescence), c the concentration of fluorescein in xylem, pmol.mm^{-3}, k_e the elimination rate d^{-1} and k_a the uptake rate, mm^3.mm^{-3}d^{-1}.

The intensity decreases during measurements due to photobleaching. It is assumed that decay of intensity due to photobleaching has a similar mathematical formulation as

the decay of an radio active isotope. Since ingestion during the 15 seconds measurement can be neglected, only decay of the tracer is of importance. So the total experiment can be represented by two equations, one for the decay only and one for the uptake/elimination:

$$Q(t) = \begin{cases} Q_0 \exp\{-k_b t\} & \text{during measurement: } k_b \gg k_e \\ Q_0 \exp\{-k_e t\} + \frac{k_a}{k_e} c(1 - \exp\{-k_e t\}) & \text{otherwise: } k_b = 0 \end{cases} \tag{6.6}$$

in which k_b is the photobleaching rate d^{-1}.

6.2.5 Measuring diameter of valves in median bulb of oesophagus

The diameter of valves in the median bulb was determined with fixed and in glycerol mounted *G. pallida* used in growth and development experiments, described in [89]. A Zeiss Axiovert 10 inverted microscope equipped with differential interference contrast (DIC) and Zeiss ACE analog contrast enhancement was used. Images were printed on a Sony UP-811 video graphic printer. Diameters of the feeding pumps were measured manually from the printed images. Magnifications up to 2950× were reached in this way. Oesophageal (region) width was measured at the proximal base of the median bulb of the oesophagus.

Photographs were made with a Contax camera attached to the Sony video graphics printer on Kodak Plus-X-Pan 125 ISO black and white film.

6.3 Results

6.3.1 Calibration

The response of the imaging system to fluorescent light emitted by solutions containing various concentrations sodium fluorescein in tap water was at least linear over the range 0.3 μM to 30 μM, as can be seen in figure 6.1. The sensitivity of the camera was adjusted by changing the number of integration frames, which could vary between 1 and 999 frames. The estimated parameters, given in figure 6.1, were used to calculate the fluorescein concentration inside the nematode.

Photobleaching of the tracer is an important process as can be seen in figure 6.1. Therefore a standard period of 15 seconds of photobleaching was taken in order to reduce small differences in opening of the aperture of the excitation light beam. The estimated parameter k_b was used in further analysis of the experiments.

6.3.2 Fluorescein uptake

Fluorescein applied apically to the root was transported rapidly upwards by xylem elements. Within 1–2 minutes the fluorescein had reached the feeding site of the nematode. Xylem transport however was not always successful probably due to disrupting the vascular
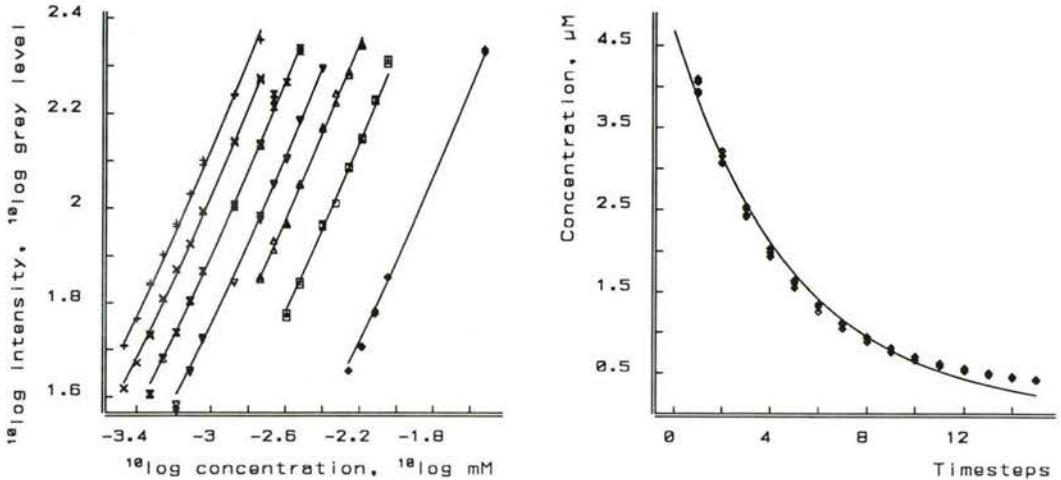
Figure 6.1: Left: Calibration of low-lux camera with fluorescein. Fitted function is: $I = \alpha F[C] +$ b. Regression analysis is performed on non-transformed data. The estimated parameters are: α is 2246 (SD=12.87) (grey level.[pixel.frame.mM]$^{-1}$) and b is 9.755 (SD=0.6428) (grey level.pixel^{-1}). The number of integration frames, F, is respectively 3 ($\diamond$) 9 ($\square$) 15 ($\triangle$) 21 ($\triangledown$) 31 ($\bowtie$) 43 ($\times$) and 55 ($+$) times.
Right: Photobleaching of fluorescein measured in standard volumes at 3 μM. Four series are measured. Time steps are 1 second with the time necessary for completing the program loop. Each time step is around 6.8 seconds. The number of integration frames is 23. An exponential decay function is fitted: $c(t) = c_0 \exp\{-k_b t\}$ with c_0 is 4.67 (SD=0.066) μM and k_b is 0.199 (SD=3.69 10^{-3}) time steps.

tissue by handling. Nineteen individuals have been followed in time, two were used as controls, nine accumulated fluorescein and the others were discarded due to lack of transport, leakage or otherwise.

Uptake of fluorescein by an adult female is shown in figure 6.2. Digitized images, in which the amount of whiteness (intensity) is proportional to the concentration of fluorescein inside the female are shown. The background intensity at t=0 was caused by autofluorescence of the nematode. The colour of the autofluorescence is yellowish. The autofluorescence was more intense on the outline of the nematode image suggesting that it was associated with the cuticula of the nematode. The intensity at t=1, 2 and 3 was located inside the nematode which implied an increase of fluorescein. The colour of the fluorescent inside the nematode was greenish, corresponding with the greenish colour of fluorescein.

Intensity of the outlined area of nematodes can be quantified as is shown in figure 6.3. Frequency distributions of pixels (area units) with a certain intensity are given. Intensity was transformed with equation 6.4 to its corresponding fluorescein concentration, in

which autofluorescence was assumed to be 'background' fluorescein concentration. The positive shift of frequency distributions in cause of time is obvious, implying an increase of fluorescein concentration.

The mean concentration inside the nematode was calculated by equations 6.2 and 6.4 and plotted in figure 6.4. Two possibilities of data analysis are shown, an overall uptake/elimination neglecting photobleaching and a detailed description of the processes during experimentation. Increase of fluorescein was apparent in the first day and reached steady state later. This overall trend could be described by equation 6.5, see figure 6.4 (left). The uptake process was closely matched when correction for photobleaching was applied according to equation 6.6, see figure 6.4 (right). The parameter k_a/k_e was increased when correction for photobleaching was applied. The latter more likely matched the uptake process.

Two more uptake patterns are shown in figure 6.5. The top figure represents a prolonged fluorescein uptake, in which the nematode reached slowly its steady state. The lower figure represents a fast uptake pattern. The fluorescein uptake rate in this figure was during the first hour larger than the photobleaching rate.

Sometimes during the experiment fluorescein was visible in the gelatinous matrix on the anterior end of the nematode. Figure 6.2 shows a bright field and an intensity image of the nematode used in the experiment shown in figure 6.5, top. The fluorescein was visible (greenish colour) after two days of fluorescein application. The intensity of the fluorescein was not diffused through the entire matrix but localized in a region near the anus/vulva. This implies that the fluorescein was complexed or bound in the matrix material and that production of matrix material lasted several days.

Concentration in root system

The concentration of fluorescein in the xylem was measured by outlining manually the vascular tissue within the pericycle. Figure 6.2 shows a bright field image and an intensity image of the root just above the nematodes' feeding site. The fluorescein concentration as function of time of two root experiments is shown in figure 6.6. Fluorescein remained constant for about 1–2 days in the xylem tissue indicating a continuous functioning of the transpiration stream. The root ceased functioning after these 1–2 days so uptake measurements were reliable only during the first two days.

Autofluorescence

G. pallida exhibits a yellowish autofluorescence when excited with 'blue' light, see figure 6.2. The highest intensities were reached on the outline of the nematode suggesting that the autofluorescence was correlated with cuticulous compounds. The intensity decreases when water was applied instead of fluorescein as can be seen in the second image of figure 6.2. The decrease in intensity is also shown in the intensity histograms in figure 6.7. The left figure shows a shift to left of the intensity at start and after one day of water uptake. This shift was probably caused by the photobleaching power of the 'blue' excitation. After
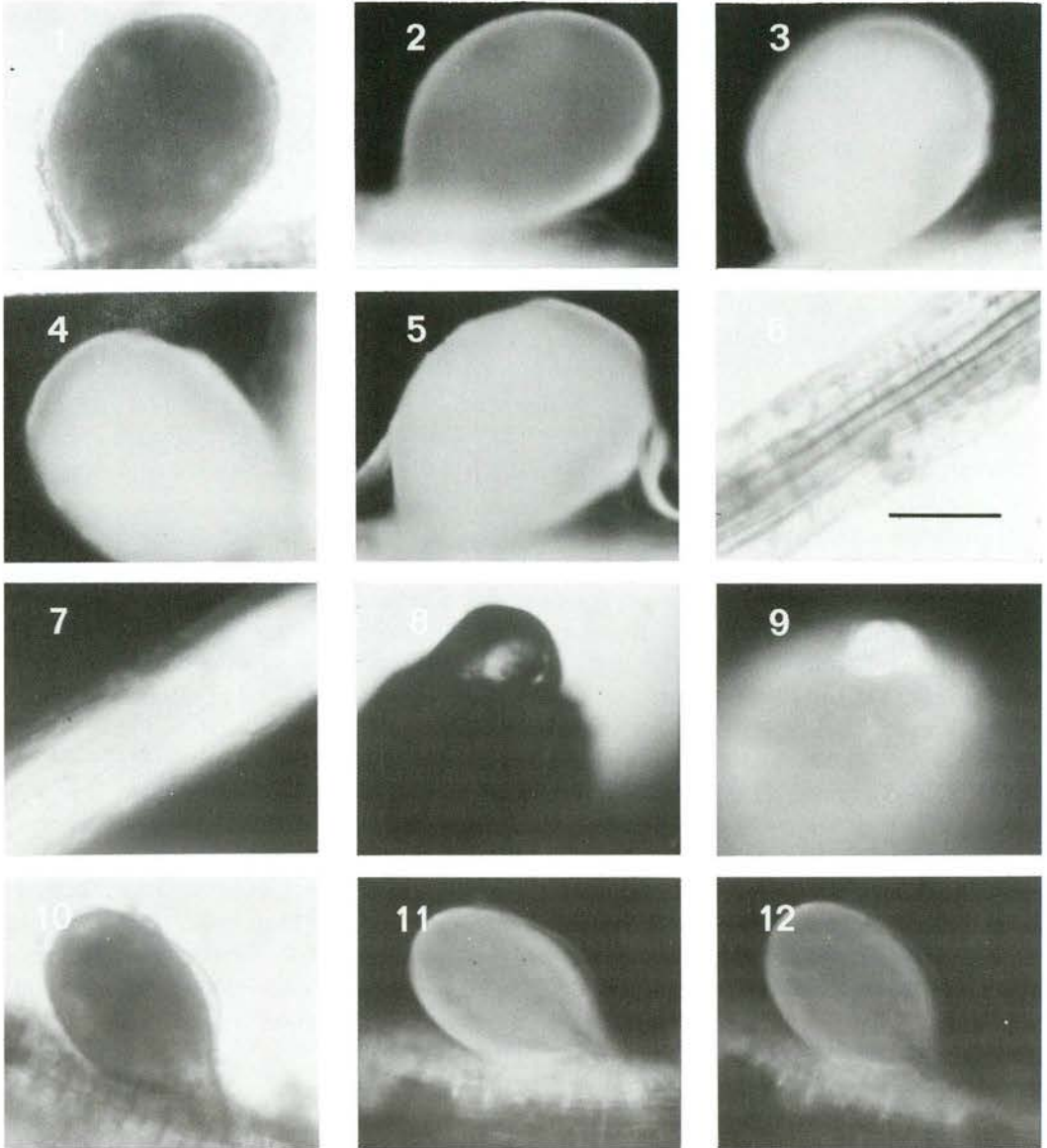
Figure 6.2: Bright field and grey value images of fluorescein intensity. Length bar in photo 6 corresponds with 200 μm. Photo (1): Bright field image at t=1, Photo (2)-(5): Accumulation of fluorescein inside *G. pallida* after t= 0, 1, 2 and 3 days of exposure, correspond with intensity histograms of figure 6.3. Photo (6) and (7): Bright field image and fluorescein intensity imaged in root. Photo (8) and (9): Bright field and fluorescein intensity (21 integration frames) imaged in gelatinous matrix on the posterior end of the nematode after two days of fluorescein application, fluorescein uptake is shown in figure 6.5, top. Photo (10)-(12): Background intensity of *G. pallida* imaged at start and after one day control (water) exposure, corresponds with figure 6.7.

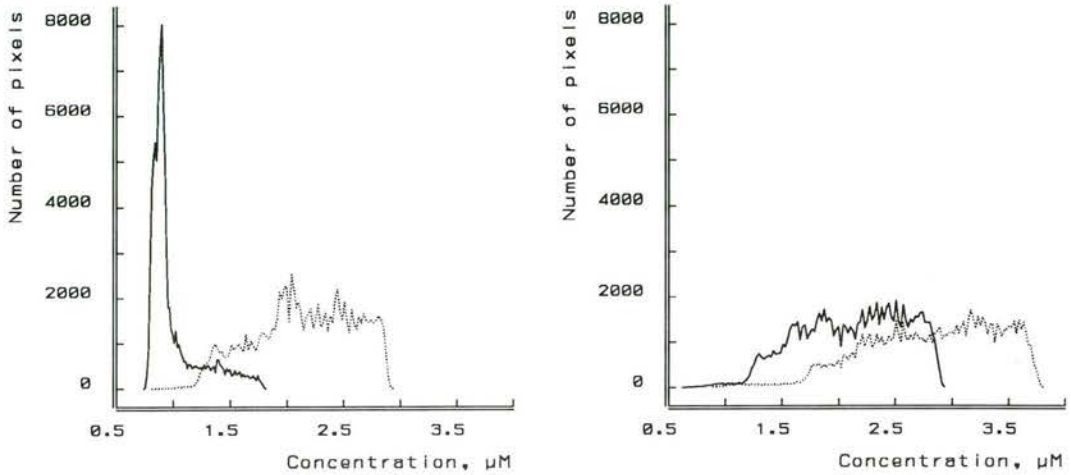Figure 6.3: Histograms of fluorescein intensity of exposure at t= 0 and 1 (left) and t= 2 and 3 days (right) in the nematode. The straight lines (—) represent t=0 and t=2, while the dotted lines ($\cdots$) represent t=1 and t=3.

one day however the autofluorescent intensity appeared to recover. The reason of this recovery is unknown but it might be related to reduced functioning of the root after one day and concomitant formation of autofluorescence substances by root tissue [9, 197]. The nematode might be able to ingest these substances.

The patterns of decrease in autofluorescence of two nematodes are shown in figure 6.8. Photobleaching of the autofluorescence was apparent over the first day. The subsequent increase in intensity is represented by dashed lines because of the unknown reason of this increase. The intensities however did not exceed the level of intensity at start of the experiment. So the intensity increase of the controls was of minor importance when compared to intensity increase due to fluorescein uptake.

A summary of rate constants and the calculated ingestion rates are given in table 6.1. The ingestion rate per individual was assumed to be the product of measured nematode volume, V, and the fluorescein uptake rate, k_a. The volumes, V, are also given in table 6.1. The mean ingestion rate for adult females was about 0.42 mm^3.d^{-1} xylem fluids per nematode. The amount of fluorescein withdrawn per day per nematode was the product of the ingestion rate and the concentration of fluorescein in xylem fluids, cVk_a. The mean amount of fluorescein withdrawn per day per nematode was 0.62 pmol.d^{-1}.

6.3.3 Diameter feeding pump and ingestion rates

The diameter of the feeding pump of *G. pallida* was determined in order to validate the uptake experiments. The diameter of the feeding pump increased with increasing size of
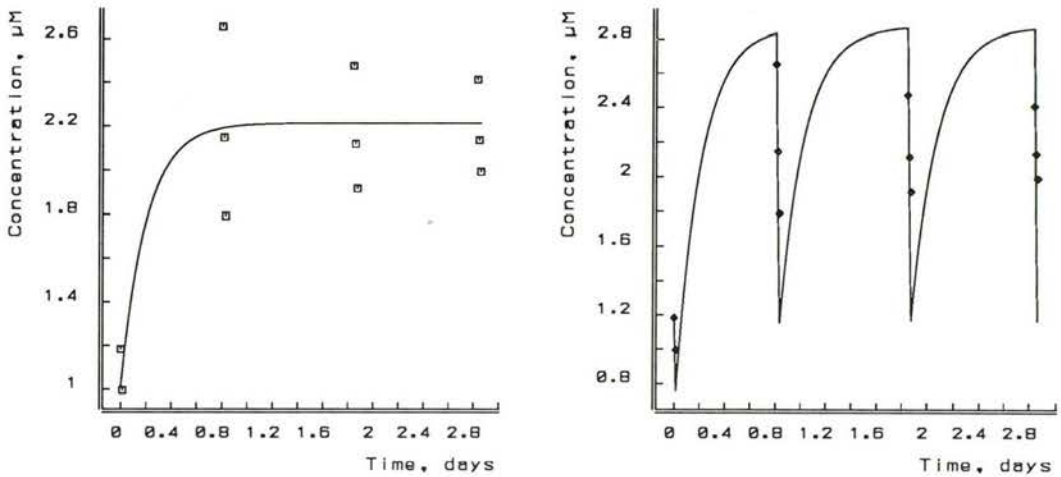
Figure 6.4: Increase of fluorescein concentration in the nematode during measurement. The left figure shows the uptake curve when no photo bleaching is assumed and only the second images of each measurement are used: equation 6.5. The estimated parameters are Q_0 is 1.01 (SD=0.186) μM k_e is 4.94 (SD=8.25) d^{-1} k_a/k_e is 0.848 (SD=0.0342) dimensionless. The measured fluorescein concentration in the root c is 2.61 μM, see figure 6.6. The right figure shows the uptake curve when photo bleaching is incorporated in the uptake process, equation 6.6. The estimated parameter k_a/k_e is 1.10 (SD=0.0646) dimensionless. The following parameters are fixed Q_0 is 1.18 μM, k_e is 4.94 d^{-1}, k_b is 32.19 d^{-1} and c is 2.61 μM.

the nematode as can be seen in figure 6.9. The feeding pump of an adult female is shown in figure 6.10. Size of the nematode was measured by determining the oesophageal width since this part of the nematode was proportional with the somatic tissue of the nematode, see van Haren [90, 89] for an extensive discussion.

Seymour [219] proposed the model $V_{pump} = (D/2)^3\sqrt{3}$ for the volume of the feeding pump of *Dytilenchus dipsaci* based on shape arguments, in which D is the diameter of the feeding pump. Depending on the pump frequency and the amount of time in the pumping phase, the ingestion rate could be calculated. *H. schachtii* exhibited 5-8 pump pulses per second and is between 60% and 70% of its time between moults in the pumping phase [263]. These estimates were used for calculations shown in the right figure of figure 6.9. The mean ingestion rate for adult females based on the diameter of the feeding pump was between 0.022–0.035 mm^3.d^{-1}.

6.4 Discussion

It is found in this paper that fluorescein applied apically to xylem vessels can be taken up by *G. pallida*. The uptake of fluorescein is a measure for ingestion of nutrients when

Table 6.1: Estimated rate constants of fluorescein accumulation and elimination and ingestion rates of adult female *G. pallida*.

	summary of rate constants					
	uptake rate	elimination rate	bleaching rate	nematode volume	ingestion rate	
figure	k_a	k_e	k_b	V	$V k_a$	$cV k_a$
	$mm^3.mm^{-3}d^{-1}$	d^{-1}	d^{-1}	mm^3	$mm^3 d^{-1}$	$pmol.d^{-1}$
6.4	5.43	4.94	32.2	0.029	0.16	0.41
6.5 (top)	5.52	0.882	32.2	0.066	0.36	0.32
6.5 (down)	25.9	14.4	32.2	0.029	0.75	1.12
6.8 (top)	–	5	1.50	0.012	–	–
6.8 (down)	–	5	2.22	0.019	–	–

Table 6.2: Relative increase/decrease of fluorescent concentration after exposure to fluorescein or water after 1 and 2 days, based on second images of each measurement.

figure	day 1	day 2
6.4	2.16	2.13
6.5 (top)	1.49	1.57
6.5 (down)	1.09	1.22
6.8 (top)	0.77	0.72
6.8 (down)	0.88	0.91

it is entering the nematode only via the stylet at a rate equivalent to the ingestion rate. Diffusion for instance of fluorescein via the stylet into the nematode alters uptake and ingestion rates. The effect of diffusion might probably be neglected because diffusion acts only when the nematodes pumping chamber is open. The pumping chamber is open only when the nematode is in the pumping phase, so uptake of fluorescein is a measure for ingestion.

The syncytium mediates between the apoplastically available fluorescein and the nematode. Therefore fluorescein has to cross the plasmolemma of the syncytium before entering the symplast from which the nematode is feeding. Fluorescein, a membrane permeable weak acid, $pK_a \approx 4.9$, remains partially undissociated at physiological pHs and passes the plasmolemma at an appreciable rate by passive diffusion [162, 53]. The passage of its dissociated anion is very slow because the octanol/water partition coefficient, $\log K_{ow}$, is 3-4 units lower than its corresponding undissociated acid [162]. Fluorescein has in its undissociated form a green fluorescent [52]. The fluorescent inside the nematode appeared

greenish, implying that the nematode ingests fluorescein in its undissociated form. It is for the mathematical analysis of ingestion rates in this paper assumed that fluorescein is only taken up in its undissociated form and that the concentration of fluorescein inside the syncytium is in (pseudo) equilibrium with the concentration inside xylem vessels.

The mean ingestion rate of 0.42 mm^{3}d^{-1} xylem fluids for adult females can now be compared with the ingestion rates calculated with the diameter of the feeding pump: the pumping ingestion rates. Pumping ingestion rates for *H.schachtii* and *G. pallida* are given in table 6.3 and are a factor 12–19 lower than the fluorescein ingestion rates measured in this paper. 'Pumping' ingestion rates neglect the passive ingestion caused by pressure differences between feeding cell and nematode. The low pressured nematode has only to open its pump lining for passive feeding as is found for the plant parasitic nematode *Hexatylus viviparus* [50]. Syncytia of *H.schachtii* have high turgor pressures (10^6Pa) [33], which also opens the possibility for sedentary nematodes to feed passively. Ingested volumes increase with increasing pressure differences. The calculations based on 'pumping' ingestion rates are therefore minimum estimates since they neglect the pressure differences between syncytium and nematode. The estimate of ingestion rate by means of fluorescent probes matches therefore more likely the actual ingestion rate.

An adult *G. pallida* female ingests 16–114 times the syncytial volume per day when estimates of syncytial volumes of *H. schachtii* are used (see table 6.4). The syncytial volume does not decrease during ingestion, so the transport rate into the syncytium matches the nematode ingestion rate. The transport rate or the solute diffusion rate across the syncytium can be calculated using the estimate of 10 times surface area increase by cell wall protuberances [113, 112]. The surface area of a 0.026 mm^3 syncytium is than 0.00878 cm^2, while the thickness of the syncytium is proportional to its cubed root. A mean transport rate of 0.42 mm^{3}d^{-1}, see table 6.1, results in a solute diffusion rate $D=1.6 \ 10^{-8}$ cm^2.s^{-1} which is about 300 times slower than free diffusion in water ($D=5 \ 10^{-6}$ cm^2.s^{-1}) [245]. For example the average diffusion coefficient of carboxy-fluorescein through the annular pore of plasmodesmata is about $D=5.4 \ 10^{-8}$ cm^2.s^{-1} [244] and the apoplastic solute diffusion of sulphorhodamine in nanopaths of wheat leaves is between $D=8$–$9.5 \ 10^{-8}$ cm^2.s^{-1} [38]. The in this paper measured solute diffusion rates are of the same order of magnitude as the other diffusion rates.

The function of the connection of syncytium with xylem elements is uptake of selected nutrients. Nitrogen rich compounds as amino-acids, amides and ureides are of importance for protein synthesis inside the syncytium. Plant species vary in their xylem fluid composition. The nitrogenous fraction can be transported either as nitrate or as organic nitrogen compounds [169]. The site of reduction of nitrate is essential for the feeding nematode to establish its feeding site. Considerable levels of nitrate reductase activity (NRA) are found in potato roots [168], comparable to the high NRA levels of field pea [169]. It is therefore likely to assume that the feeding nematode has access to organic nitrogen compounds.

The possibilities for application specific fluorescent probes for quantifying apoplastic and symplastic transport to the developing syncytium are promising, since many specific fluorescent probes exist. The technique developed by Dorhout [51] and further extended in this paper should be combined with the micro-injection experiments of Bockenhoff [33] in

order to reveal the nutrient uptake dynamics of both the nematode and its syncytium. This powerful combination is in principle capable of gaining inside in this intriguing parasite-host interaction.

Table 6.3: Calculated ingestion rates (pumping ingestion rates) based on diameter of feeding pump in median bulb and 5 or 8 pulses per second of *H. schachtii* and *G. pallida*

	Ingestion rates					
stage	*H. schachtii*				*G. pallida*	
	Wyss [263]				this paper	
	ϕ pump μm	ingestion rate mm^3.d^{-1}		n	ϕ pump μm	ingestion rate mm^3.d^{-1}
J2	2.3	0.00069	0.0011	5	2.3	0.00074 0.0012
J3	3.6	0.0031	0.0050	2	3.9	0.0036 0.0058
J4	5.2	0.0091	0.015	1	4.9	0.0072 0.011
A female	7.8	0.031	0.050	10	7.1	0.022 0.035

Table 6.4: Estimates of syncytial volumes of *H. schachtii* during development

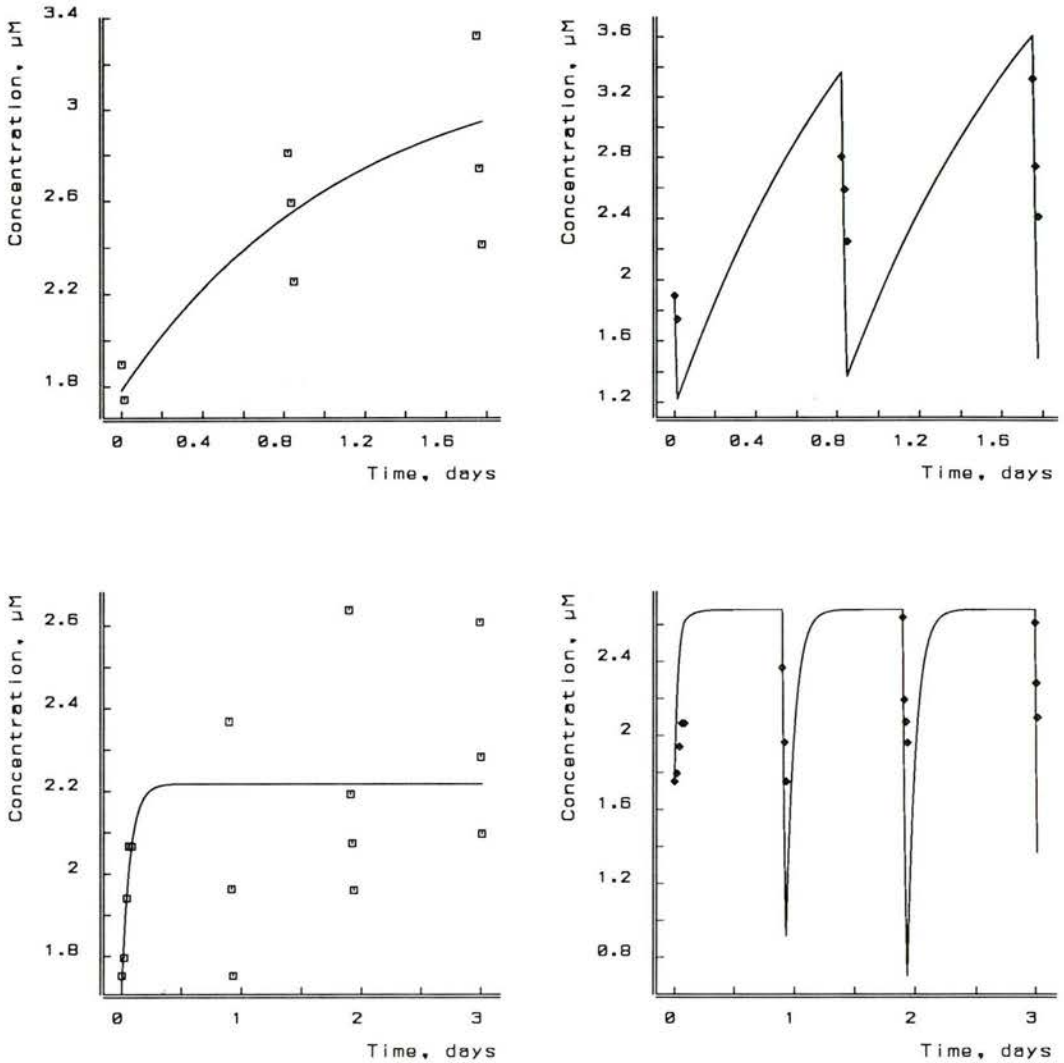|	Estimates syncytial volume *H. schachtii*		
stage	Kerstan [121] mm^3	Caswell [40] mm^3	Golinowski [83] mm^3
J2		0.0021	
J3		0.014	
J4		0.026	0.0038
A female	0.0037	0.026	

Figure 6.5: Two other fluorescein uptake patterns are shown. The left figures are fitted with equation 6.5 without photo bleaching, while the right curves are fitted with equation 6.6 with photo bleaching. The estimated parameters from the upper left figure are Q_0 is 1.78 (SD=0.168) μM k_e is 0.882 (SD=0.751) d^{-1} k_a/k_e is 3.74 (SD=0.721) dimensionless. The measured fluorescein concentration in the root c is 0.871 μM. The estimated parameter k_a/k_e from the upper right figure is 6.26 (SD=0.507) dimensionless. while the next parameters are fixed Q_0 is 1.78 μM, k_e is 0.882 d^{-1}, k_b is 32.19 d^{-1} and c is 0.871 μM. The estimated parameters from the lower left figure are Q_0 is 1.72 (SD=0.227) μM k_e is 14.4 (SD=13.6) d^{-1} k_a/k_e is 1.49 (SD=0.0443) dimensionless. The measured fluorescein concentration in the root c is 1.49 μM. The estimated parameter k_a/k_e from the lower right figure is 1.80 (SD=0.125) dimensionless. while the next parameters are fixed Q_0 is 1.75 μM, k_e is 14.4 d^{-1}, k_b is 32.19 d^{-1} and c is 1.49 μM.
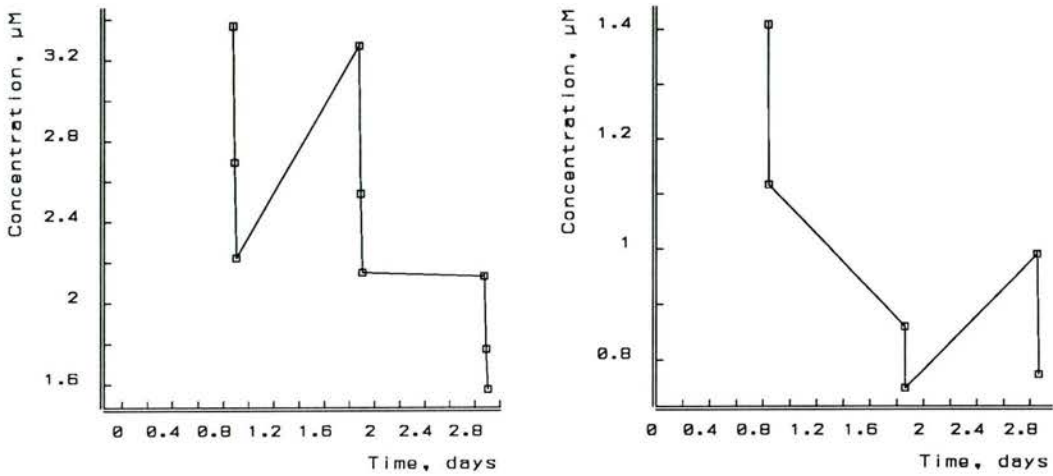
Figure 6.6: Concentration of fluorescein measured in the root after 24, 48 and 72 hours of exposure. The measured concentrations of the second images of the first and second day of the left figure are used in the data analysis of figure 6.4. The mean concentration is 2.61 μM.
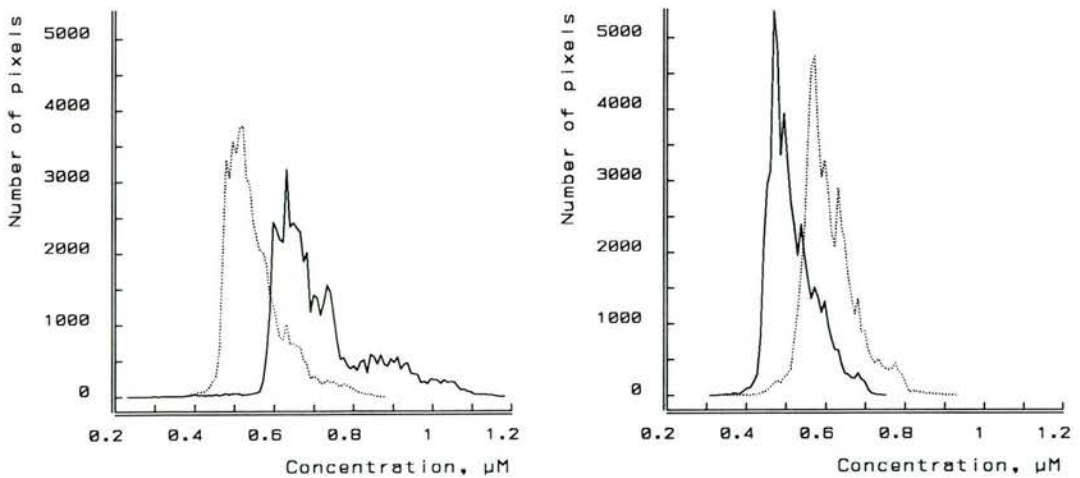
Figure 6.7: Histograms of autofluorescence of the control exposure at t= 0 and 1 (left) and t= 2 and 3 days (right) in the nematode. The straight lines (—) represent t=0 and t=2, while the dotted lines ($\cdots$) represent t=1 and t=3.
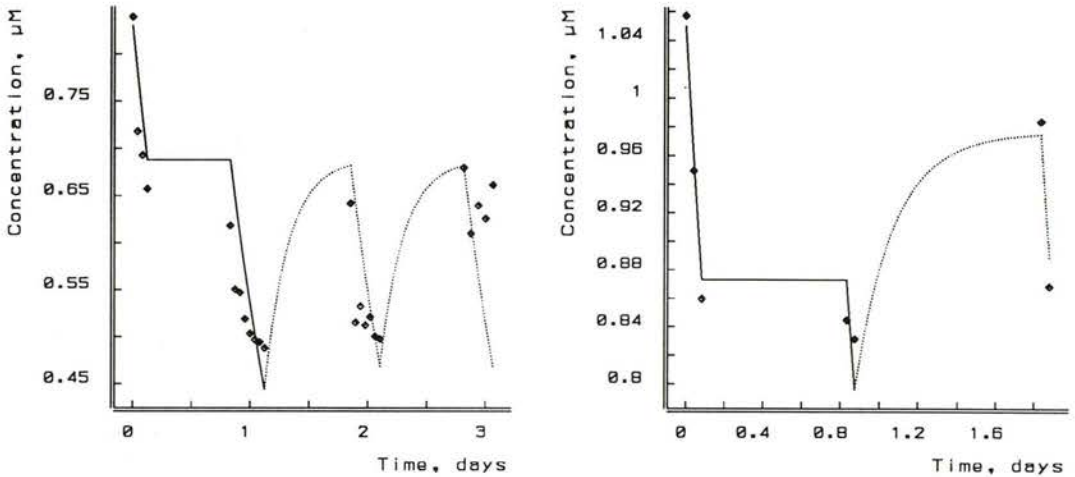
Figure 6.8: The autofluorescence of nematodes exposed to tap water instead of fluorescein. The constant photo bleaching over the first days is fitted with equation 6.6, (—). After one day an unknown autofluorescence component is taken up which process is fitted with equation 6.6, ($\cdots$).
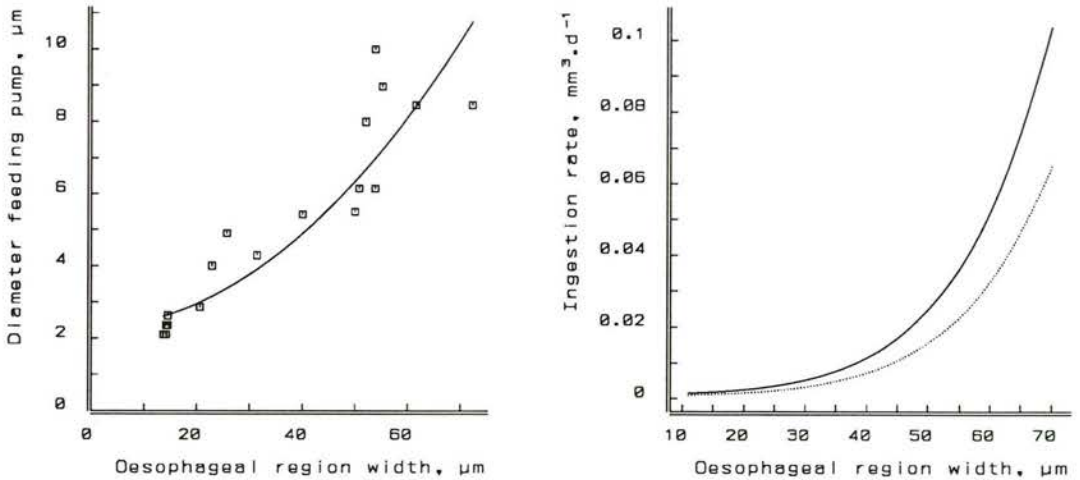
Figure 6.9: Diameter of feeding pump, D, in relation with oesophageal width, L (left) and the calculated ingestion rate (right). The regression line in the left figure is given by $D = a + \rho L^2$ with ρ is $1.6 \ 10^{-3}$ (SD=$1.9 \ 10^{-4}$) $\mu\mathrm{m}^{-1}$ and a is 2.3 (SD=0.42) μm. The right figure shows the calculated feeding rate based on 5 or 8 pump pulses per second. The pumped volume $V_{pump} = (D/2)^3\sqrt{3}$, see text for further explanation.
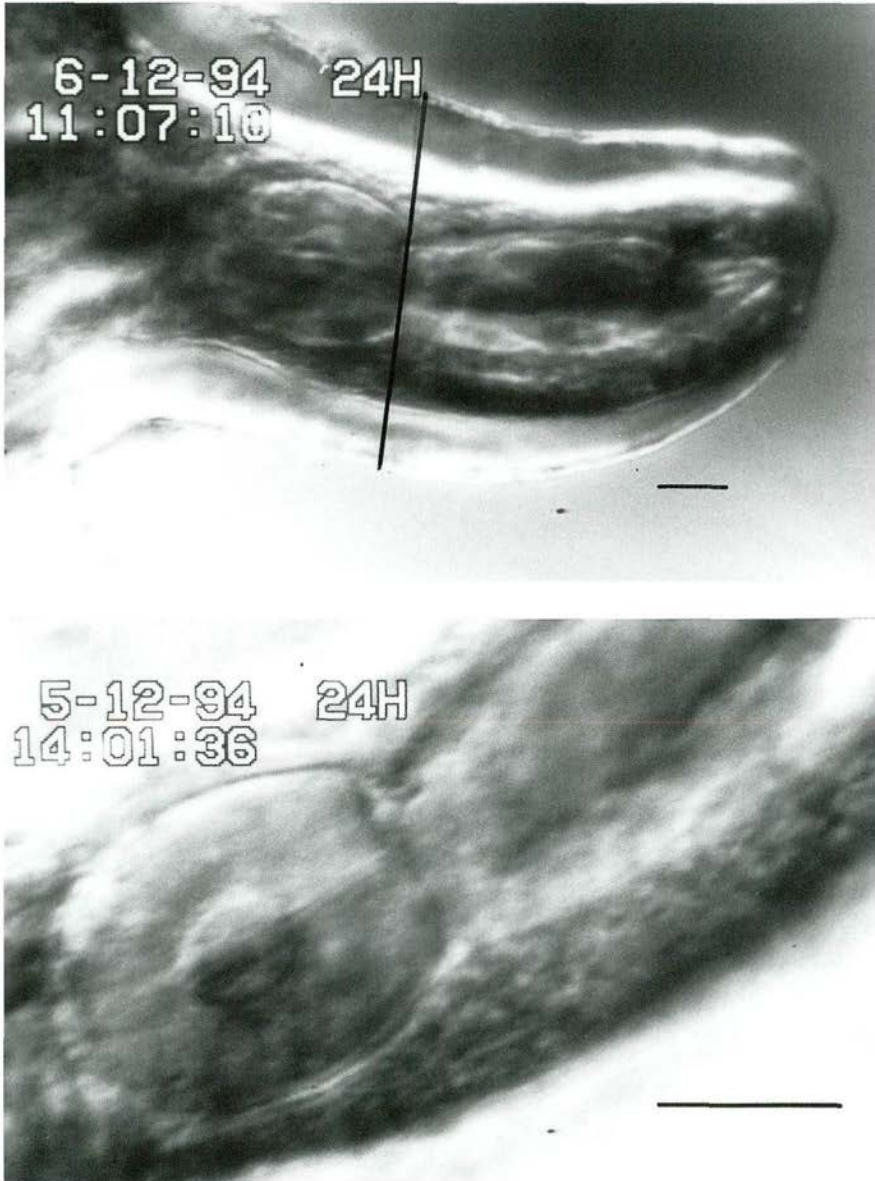
Figure 6.10: Oesophageal regions with median bulb and feeding pump of an adult female of *G. pallida* photographed with ACE-DIC contrast enhancement. Bars are 10μm. The upper photograph shows the measured oesophageal width at the proximal base of the median bulb.

Chapter 7

Population dynamics

in preparation: R.J.F. van Haren, H. Regeer and M. van Oijen
Modelling population dynamics of potato cyst nematodes based on individual energy budgets and potato root dynamics: a study into intraspecific competition

7.1 Introduction

The logistic growth model for intraspecific competition between individuals in single populations originates from Verhulst in 1838 [208]. This model and its derived versions treat individuals as identical objects. However individuals within a single population are known to differ in size and weight. Bioenergetic processes as ingestion of nutrients, growth, maintenance and reproduction are strongly size-dependent [170, 139, 125] and cause differences in allocation of nutrients between individuals.

Differences in size on the other hand are caused by different amounts of ingested nutrients [125]. Unequal resource partitioning, an aspect of intraspecific competition, leads to size differences between individuals. Determination of the degree of intraspecific competition by determination of the amount of nutrients ingested by an individual in a group is technically very difficult [139]. However, reconstructions of the amount of ingested nutrients of individuals, can be made when individual size measures are known [92, 125]. Analysis of size frequency distributions of individuals for determination of the population resource partitioning is not feasible since similar distribution functions may result from different underlying processes [138]. Therefore size distributions can only be used for testing predictions based on processes which are determined separately at the individual level.

An individual based model [49, 117] is, for these reasons, suited for studying resource partitioning between individuals. The main processes at the individual level determining individual growth and reproduction are related to energy acquisition, its storage and its use in an individual [125]. Resource partitioning in a population can be reconstructed by bookkeeping the resource utilization for individuals.

Sedentary organisms are relatively easy to study especially when these organisms are distributed along a resource gradient. An example of such a system is the interaction

of sedentary plant parasitic nematodes of the family Heteroderidae (order Tylenchida) with their host and each other. The root knot nematodes *Meloidogyne* spp. and potato cyst nematodes *Globodera* spp. are well known plant pathogenic species and are therefore studied extensively [55]. These species locate a growing root tip in soil, penetrate root tissue and establish themselves around the vascular tissue of the plant root which provides them with nourishment. Females remain sedentary and protrude the root cortex when they mature. Females of cyst nematodes retain eggs inside their cuticula which hardens after death. These species have usually one generation a year in temperate regions. Nematodes moult four times before reaching the adult stage. The four juvenile stages are numbered J1–J4 in which the second juvenile stage (J2) is the infective stage.

Population dynamics of *Meloidogyne* and *Globodera* have been studied extensively in the past and the importance of intraspecific competition for population regulation has been stressed several times [161, 216, 110, 63, 40, 217]. The models which are developed hitherto can be roughly separated into the logistic equations [161, 215, 216, 110] and the simulation models [61, 62, 64, 252, 39, 204]. Some individual based models are developed hitherto [10, 146, 179, 90, 89]. The majority of these models for population growth describes only highly aggregate population level variables such as population size, and as result can account for intraspecific competition due to increased population density in a strictly qualitative manner [47].

The dynamics of nematode populations resemble the incomplete contest competition *sensu* Lomnicki [139]. This mode of competition is characterized by unequal relations between larger individuals which can limit the resource intake of smaller individuals and smaller individuals which are unable to limit the resource intake of the former [139]. This in contrast to the scramble mode of competition in which smaller sized individuals can limit the resource intake of larger ones.

The aim of this paper is to evaluate the population consequences of the individual dynamic energy budget for growth and fecundity of individual potato cyst nematodes *Globodera pallida* [90, 89, 88]. A model for the plant-nematode interaction is developed. This model describes the resource partitioning for *G. pallida* which is based on nematode establishment, root growth dynamics and the adverse reactions of the nematode on the plant. The resource partitioning model in combination with the DEB model is used to predict population dynamics and its associated size distributions at different initial population densities. The results are tested against experimental data which are for this purpose performed in field and mesocosm at different initial population densities. Size distributions and final population densities are determined after the growing season. In addition, experiments from literature are analyzed to estimate parameters.

7.2 Materials & Methods

7.2.1 Field experiments

Field experiments were performed in the NE area of the Netherlands during the growing seasons of 1991 and 1992. The fields were infected with *G. pallida*. These experiments were described in detail elsewhere [160, 159, 91]: a summary follows of relevant details.

Potato cultivars Darwina, partially resistant to *G. pallida* and Elles, tolerant to *G. pallida*, were planted on the 15th of May, 1991 in disinfected and non-disinfected soils with severe *G. pallida* infestations. Soil was sampled by taking 6-7 kg soil per plot of 1.5 m² in about 35 soil probes. The air dried soil was processed and cysts were collected after flotation in water on a 250 μm mesh filter. Viable eggs were determined in a hatch test by putting cysts in potato root diffusate and counting the number of emerged second stage juveniles (J2's) after the test was finished. The test ended when the controls with weekly counted emerged J2's yielded relative few J2's. The number of nematodes was determined in the root system during the growing season by differential staining with lactophenol cotton blue of root tissue [225]. The size of the root system was measured by minirhizotron observation tubes in soil and by core sampling. Further details are given in van Oijen [160, 159] and van Haren [91].

7.2.2 Mesocosm (pot) experiments

Shoots of cultivars Darwina and Elles were planted in pots of 5 dm³ with 10 kg (dry weight) of standard soil, a mix of yellow sand, 50 g lavalite (2-4 mm diameter) 30 g fertilizer (NPK with trace elements, Nutriflora, Rijnvallei Netherlands) and 70 g sterilized dried cow manure (Asef) on the 14th of May 1993. Plants were grown outdoors in a herbivore protected area. *G. pallida* designated as Pa3 population 'Rookmaker' was inoculated in nylon filter bags (mesh size 25μm) with 3-375 cysts per bag. The viable egg densities were 0.4, 2, 10, 50 and 100 eggs.g soil^{-1}. Five bags were used in the mesocosms with 0.4 egg.g^{-1}, while the other densities had 10 bags per mesocosm. Darwina was grown in respectively 3, 11, 3, 3 and 11 pots for each density and Elles in respectively 3, 7, 3, 3 and 7 pots. Egg viability was assessed by crushing cysts and counting visually its viable egg content. Plants were watered daily when necessary during the growing season. After 106 days the potato plants were cut off above ground and left dry for several weeks. The air dried soil was processed and cysts were collected after flotation in water on a 250 μm mesh filter. New cysts were counted and its egg content was assessed by crushing all the cysts the mesocosm yielded with a maximum of 300 cysts.

Size distributions were determined by automated Image Analysis of all the new cysts present in a mesocosm. One mesocosm per density of 0.4 and 100 egg.g^{-1} were analyzed. About 20-50 cysts were put in counting chambers of 1 cm² with transmitted light and their images were digitized using the frame grabber of an image analysis system (GOP-302, Context Vision, Sweden with SUN3 host). The captured images were processed and corrected for camera deviations before analysis in order to obtain square pixels. Cysts

were distinguished from non-cyst particles on shape and size. Neighbouring cysts were separated digitally by a 'watershed' operation which identifies maximum intensity values between closely connected objects and makes a division at this intensity maximum.

7.2.3 Pouch experiments

Potato shoots of the cultivars Bintje, Elles and Darwina of about 1 cm in length with a wedge shaped region around the shoot were placed in autoclaved growth pouches (Northrup King, Vaughans's Seed Company USA) and established in a phytotron, as described before [90]. After 6-8 days 20 hatched juveniles in 15 mm^3 were inoculated on the root tip on glass fibre filter which was removed after 24 hours as described before [90]. Series were made with respectively 1, 2 and 3 inoculations per growing root resulting in roots with varying nematode number. Controls were made with 1 inoculation of 15 mm^3 in tap water. Roots with more then 1 inoculation were allowed to grow for 1 day before the next inoculation occurred. Root length growth was measured at each inoculation and at 4 days after the last inoculation. The inoculated roots were drawn on the transparent polyethylene of the growth pouch and measured afterwards with a xy-tablet digitizer.

7.3 Model development

7.3.1 Nematodes in soil

The population dynamic model of the nematodes is derived with the aim to link it with crop growth models of potato developed by van Oijen [158, 160, 159]. For this reason, root growth is assumed to be logistic, since root growth is usually found to obey a sigmoid relation with time:

$$\frac{d}{dt}Y = rY(1 - \frac{Y}{Z}) - D \qquad (7.1)$$

Here is Y total root length (length.plant^{-1}), r root growth rate (time^{-1}) and Z the maximum length the plant can achieve at optimal environmental conditions (length.plant^{-1}). D is assumed to be the inhibitional effect of nematodes on the root growth of the plant (length.time^{-1}.plant^{-1}). Main variables and parameters are summarized in tables 7.1 and 7.2. There is no definitive identification of a damage mechanism by nematodes; see Schans and van Oijen for an extensive discussion on this topic [204, 160, 159].

Three possible kinetic damage measures, D, can be formulated, which can be related to specific mechanisms.

1. The most straight forward damage measure is to take it proportional to the number of nematodes in the root system $D = s_1 N_e$, with s_1 is root length reduction rate per nematode (length.time^{-1}.nematode^{-1}) and N_e the number of root established nematodes (number.plant^{-1}). Each nematode has in this case a detrimental effect on root growth by either nutrient uptake, physical damaging of the plant vascular system, or both.

2. The second measure is based on the assumption that damage is proportional to number of penetrating nematodes, $D = s_2 \frac{d}{dt} N_e$ with s_2 is root length reduction per nematode (length.nematode^{-1}). This hypothesis corresponds with the induction of abscisic acid (ABA) upon each nematode establishment and subsequent photosynthesis reduction.

3. The third measure is based on the assumption that damage is proportional to the total biovolume of the nematodes inside the root system: $D = s_3 \int_0^t N_e(a)V(a)da$ in which s_3 is the root length reduction rate per nematode biovolume (length.time^{-1} length^{-3}).

Dormant nematode eggs, N_d, in the soil are activated by root exudates from the plant [253]. Root exudates are mainly produced by growing root parts [185] and are broken down due to microbial activity or otherwise [136, 204]. The soil volume in which root exudates are active, is assumed to be proportional with the explored soil volume of the root system (defined here as the rhizosphere): so all dormant eggs within the rhizosphere, N_r, can be activated and hatch proportional to root growth rate dY/dt. Growing roots increase the volume of the root system and incorporate dormant eggs inside. The change in the number of eggs in the rhizosphere, N_r is:

$$\frac{d}{dt}N_r = \left(\frac{n_d}{\rho} - kN_r\right)\frac{d}{dt}Y = \left(\frac{n_d}{\rho} - \frac{kn_rY}{\rho}\right)\frac{d}{dt}Y \tag{7.2}$$

where n_d is the dormant egg density in the soil outside the explored soil volume (number. length^{-3}), k the hatch stimulation activity per root length (length^{-1}) and ρ is the specific root density in soil (length.length^{-3}). The density of eggs within the rhizosphere is by definition: $n_r = \rho N_r/Y$. Differentiation and substitution in equation 7.2, leads to:

$$\frac{d}{dt}n_r = \left\{\frac{n_d}{Y} - n_r\left(k + \frac{1}{Y}\right)\right\}\frac{d}{dt}Y \tag{7.3}$$

The same procedure can be followed for the number of hatched, J2, nematodes N_a inside the rhizosphere. The number of hatched J2's increase by hatching and decrease due to either inactivation by starvation [195] or establishment inside the root. Hatched J2's deplete their lipid reserves and loose their motility. Motility is also affected by environmental conditions, such as soil pore size, soil moisture and temperature [231, 232, 194, 195, 196]. The effects of environmental variables other than temperature are not considered in this paper. The infective capacity of J2's decreases concomitantly with decreasing lipid reserves as is found by Robinson [195]. For reasons of simplicity it is assumed that decrease of infective capacity (inactivation rate) is proportional with the number of hatched J2's and their lipid content. Nematodes invade root tissue just behind the growing root tip in the region of elongation, close to the meristematic zone [265, 264]. So the number of invading nematodes is also proportional to the root growth rate $\frac{d}{dt}Y$ and the density of hatched nematodes n_a in the soil. The change in the number N_a of hatched J2's is consequently:

$$\frac{d}{dt}N_a = kN_r\frac{d}{dt}Y - uN_a - \frac{pn_a}{\rho}\frac{d}{dt}Y = \frac{1}{\rho}\left(kn_rY\frac{d}{dt}Y - un_aY - pn_a\frac{d}{dt}Y\right) \tag{7.4}$$

with u is the inactivation rate (time^{-1}), and p is the fraction of nematodes which succeed in root finding and subsequent establishment. The density of active J2's in the rhizosphere is by definition: $n_a = \rho N_a / Y$ and its change is:

$$\frac{d}{dt} n_a = \left\{ k n_r - n_a \left(\frac{u}{\frac{d}{dt} Y} + \frac{1+p}{Y} \right) \right\} \frac{d}{dt} Y \tag{7.5}$$

The change in number of established nematodes is:

$$\frac{d}{dt} N_e = \frac{p n_a}{\rho} \frac{d}{dt} Y \tag{7.6}$$

The nematode density n_e (nematode.length^{-1}) inside the root is by definition: $n_e = N_e / Y$ and its change is:

$$\frac{d}{dt} n_e = \left(\frac{p n_a}{\rho} - n_e \right) \frac{dY}{Y dt} \tag{7.7}$$

7.3.2 Resource partitioning amongst individuals

Invaded nematodes initiate a feeding cell close or attached to the vascular system. The feeding cell develops to a multicellular syncytium which functions as a transfer cell, providing nutrients essential for nematode development. Apoplastic and symplastic transport pathways of solutes into the syncytium are identified [30, 54, 51, 88]. Nutrients transported by the vascular system are therefore likely the main nutrient sources for the nematodes. Since root growth rate is proportional to the amount of nutrients provided by the plant, it can be assumed that nutrient availability at the site of nematode establishment is proportional to root growth rate, $\frac{d}{dt} Y$.

Upon feeding cell initiation, J2's loose their mobility and become sedentary. It is frequently found that the initial feeding cell may be destroyed by other migrating J2 in the root tissue [263]. Whenever this occurred the J2 has to find another initial cell in the vicinity of its cell or in case of failure starve to death [263]. The probability of this kind of interference increases with increasing nematode densities. The amount of nutrients X is therefore proportional to the ratio of root growth rate and the number of invaded juveniles: $X(t) \propto \frac{d}{dt} Y / \frac{d}{dt} N_e$.

It is assumed that nematodes inside the root system compete with each other and/or their host for nutrients. Intraspecific competition and host suitability are affecting sex ratio of the invaded second stage juveniles [242, 202, 241, 150, 86]. The decision about future sex of the juveniles is made in the second juvenile stage of root established nematodes (at least 3 days of feeding after invasion) [26, 86]. Food quantity and/or food quality are identified as the main causes of future sex determination [26, 86].

There are thus three density dependent processes identified, which affect resource partitioning: (1) damage and/or nutrient withdrawal to the plant, (2) interference upon feeding cell establishment and (3) density dependent sex ratio shift.

Food quality (biochemical composition of phloem and/or xylem fluids) is assumed to be constant over the entire root system but might differ between host cultivars. The amount of ingested nutrients per nematode is assumed to be proportional to the scaled Holling type II functional response, $f(t) = X(t)/(K + X(t))$ [88], in which K is the saturation constant of the functional response where nutrient intake of the nematode is half its maximum value. The probability of an invaded juvenile for becoming a female ϕ_f, can be assumed to be equivalent to the functional response of the nematode, so:

$$\phi_f(t) = f(t) = \frac{\frac{d}{dt}Y/\frac{d}{dt}N_e}{K + \frac{d}{dt}Y/\frac{d}{dt}N_e} = \frac{\frac{\rho}{pn_a(t)}}{K + \frac{\rho}{pn_a(t)}} \tag{7.8}$$

where K has the dimension (length.nematode^{-1}). Equation 7.8 implies that with increasing density of hatched nematodes the functional response decreases. The number of developing females is now:

$$\frac{d}{dt}N_{e,f} = \phi_f \frac{d}{dt}N_e = \frac{\frac{d}{dt}Y}{K + \frac{\rho}{pn_a}} \tag{7.9}$$

Let ϕ_m be the fraction of developed males: $\phi_m = 1 - \phi_f$, then:

$$\phi_m = \frac{K}{K + \frac{\rho}{pn_a(t)}} \tag{7.10}$$

The sex ratio ϕ_f/ϕ_m is then:

$$\frac{\phi_f}{\phi_m} = \frac{\frac{d}{dt}Y}{K\frac{d}{dt}N} = \frac{1}{K\frac{pn_a(t)}{\rho}} = \frac{\rho}{Kpn_a(t)} \tag{7.11}$$

See Thornley [241] for an equivalent derivation of a saturation kinetics based sex ratio model.

7.3.3 Dynamic Energy Budget (DEB) model for individuals

Determination of sex ratio based on nutrient availability connects intraspecific competition with individual energetics of established nematodes. Energetic requirements for growth of the nematode has been modelled before [90, 89, 88] on the basis of the theory of Dynamic Energy Budgets (DEB) [125]. The DEB model distinguishes three body fractions of the animal: (1) structural biovolume V, (2) stored energy reserves, e and (3) gonads and/or energy reserves allocated to reproduction, R. The ingested energy is proportional to the surface area of the structural biovolume. Energy that is utilized from these reserves is allocated to (a) growth (b) maintenance and (c) reproduction. A fixed fraction of the utilized energy is allocated to reproduction and development while the remainder is allocated to growth and maintenance. Maintenance has priority over growth, so growth ceases when

food density is low. The energy costs of maintenance is proportional to structural biovolume. The incoming energy adds to the reserves, which follow a first order dynamics when expressed as density:

$$\frac{d}{dt}e = vV^{-1/3}(f - e) \tag{7.12}$$

where e is the scaled energy density, v is the energy conductance (length.time^{-1}), f the functional response and V the structural biovolume.

The above leads to the growth of the structural biovolume:

$$\frac{d}{dt}V = \frac{evV^{2/3} - gmV}{e + g} \tag{7.13}$$

where m is the maintenance rate constant (time^{-1}) and g the energy investment ratio (dimensionless), see [125] for an extensive discussion and development of this model, including tests against experimental data.

The infective J2 stage in the soil does not feed, consequently the J2 depletes its energy reserves. The functional response is in this case $f = 0$. The energy reserves drop exponentially as:

$$E(t) = E_0 \exp\{-vtV^{-1/3}\} \tag{7.14}$$

Previous application of the DEB model to sedentary cyst nematodes [90, 89, 88], revealed that *G. pallida* experiences constant food densities once established as a parasite, so we take $e = f$. This simplifies the DEB model and under these conditions growth of the structural biovolume (equation 7.13) follows the Bertalanffy growth curve. The structural biovolume can be measured as length according to: $V = (d_m L)^3$ in which L is a length measure for the structural biovolume and d_m is a shape constant that is specific for the species under consideration and the choice of the length measure. Oesophageal (region) width is used as length measure for the biovolume, see van Haren [89] for the underpinning of this choice. Equation 7.13 can now be solved and written as:

$$L(t) = L_\infty - (L_\infty - L_b) \exp\{-\gamma t\} \tag{7.15}$$

In which L is a length measure, L_∞ is the ultimate length achieved and L_b is length at birth and t is time. The parameters L_∞ and γ of the Bertalanffy growth curve for *G. pallida* can be interpreted in terms of the DEB theory, see van Haren [90, 89] and Kooijman [125]. The growth rate γ (d^{-1}) can be rewritten as:

$$\gamma = \frac{gm}{3(f + g)} = \left(\frac{3}{m} + \frac{3d_m L_m}{v}\right)^{-1} \tag{7.16}$$

At sexual maturity, with size L_p, sedentary cyst nematodes cumulate the investment of energy into reproduction inside their bodies. The cumulative energy investment into

reproduction between times t_1 and t_2 is given by Kooijman [125] (page 147-148), see also [89]:

$$e_R(t_1, t_2) = \begin{cases} 0 & \text{if } L(t) \leq L_p \\ q_R m \int_{t_1}^{t_2} \left(\frac{g+l(s)}{g+f} fl^2(s) - l_p^3 \right) ds & \text{if } L(t) > L_p \end{cases} \qquad (7.17)$$

where $l = fL/L_\infty$ is the scaled length and q_R is the scaled reproduction rate.

Females retain their eggs at the posterior end inside the body, so fecundity is proportional to the diameter of the posterior end of the body *i.e.* mid-body width L_d. Mid-body width is the sum of oesophageal width and twice the gonal width: $L_d(t) = L(t) + 2L_R(t)$ in which $L_R(t)$ is:

$$L_R(0, t) = \begin{cases} 0 & \text{if } L(t) \leq L_p \\ \frac{V_R q_R m \int_0^t \left(\frac{g+l(s)}{g+f} fl^2(s) - l_p^3 \right) ds}{L^2(t)} & \text{if } L(t) > L_p \end{cases} \qquad (7.18)$$

where $l = fL/L_\infty$ is the scaled length q_R is the scaled reproduction rate and V_R is proportionately constant.

The final number of eggs produced per female R_c at the end of the growing season at $t = t_\dagger$ is proportional to the total energy allocated to reproduction; so $R_c = V_E e_R(0, t_\dagger)$, where V_E is egg content per unit volume. The relation between mid-body width and number of produced eggs is, see also [89]:

$$R_c = \frac{V_E}{2V_R} (L_d(t_\dagger) L^2(t_\dagger) - L^3(t_\dagger)) \quad \text{if } L(t) > L_p \qquad (7.19)$$

which can be rewritten as: $R_c = \delta \{ L_d(t_\dagger) L^2(t_\dagger) - L^3(t_\dagger) \} - \zeta$ with δ is the amount of egg per unit volume (egg.length^{-3}) and ζ (eggs) a measure corresponding with the minimum size for female maturation.

The cross sectional surface area A is a function of both oesophageal width and mid-body width: $A(t) = \alpha L^2(t) + \beta L(t) L_d(t)$ with α and β the proportionality constants, see also [89].

Temperature is an important variable in determining physiological rates of ectothermic organisms. Temperature correction functions are applied for studying individual growth and population dynamics in field or mesocosm experiments. The Arrhenius temperature correction is chosen because of its direct relation with enzyme kinetics [125, 89]. It is assumed that all physiological rates are in the same way affected by temperature of the body. This implies that the rate constants (dimension time^{-1}) are a function of temperature, T:

$$k(T) = ck(T_1) \exp \left\{ \frac{T_A}{T_1} - \frac{T_A}{T} \right\} \qquad (7.20)$$

where T_A is the Arrhenius temperature (Kelvin), T is the absolute temperature (in Kelvin), T_1 a chosen reference temperature and k a physiological rate. Reconstruction of temperature time series can be done with sinusoidal interpolation functions [94]

7.3.4   Nematode population dynamics in the root system

The host of the potato cyst nematode is an annual crop. The growing roots activate dormant eggs which hatch subsequently and establish themselves in root tissue. Age of the established nematodes increases thus with the time elapsed since establishment in the root tissue concomitantly with the age of the root tissue at the site of establishment itself. Let $N_{e,f}(a)da$ denote the number of females with an age after invasion somewhere between $(a, a+da)$ where da is an infinitesimally small time increment. The total number of females $\mathcal{N}_{e,f}$ is thus $\mathcal{N}_{e,f} = \int_0^{t_\dagger} N_{e,f}(a)\,da$. where $t_\dagger$ is the time at the end of the growing season which also marks the end of the invasion and development of the nematodes.

The total number of eggs produced per plant (root system) $\mathcal{R}$ (eggs) is :

$$\mathcal{R} = \int_0^{t_\dagger} N_{e,f}(a)R_c(a)\,da \tag{7.21}$$

where R_c is defined in equation 7.19. From equation 7.21 the mean number of eggs per female $\overline{R_c}$ can be derived: $\overline{R_c} = \mathcal{R}/\mathcal{N}_{e,f}$. The egg density of the newly formed eggs $n_d(t_\dagger)$ in the rhizosphere is: $n_d(t_\dagger) = \rho\mathcal{R}/\mathcal{Y}$, in which $\mathcal{Y}$ is the final root length at $t = t_\dagger$.

The size frequency distribution $\mathcal{F}$ based on cross sectional surface area A is now

$$\mathcal{F} = \int_0^{t_\dagger} N_{e,f}(a)A(a)\,da \tag{7.22}$$

7.4   Results and discussion

The individual based population dynamic model has many parameters. The parameters describing individual growth, development and reproduction were estimated on the basis of experiments described elsewhere [89]. These parameter values were used in this study for population dynamics. The parameter values of the individual model are given in table 7.3. The remaining parameters are given below.

7.4.1   Temperature reconstruction

Soil temperatures which have been measured weekly at 10 cm depth are shown in figure 7.1 for the field experiment in 1991 and the mesocosm experiment in 1993. The maximum estimated soil temperature was 18.7 °C in 1991 and 16.2 °C in 1993. The estimated parameters of the sinusoidal interpolation function were used in analysis of the measurements in the field and in a mesocosm with an Arrhenius temperature of 8033 [89].

7.4.2   Infectivity, damage and sex ratio

Analysis of literature data, provided parameter estimates of infectivity, damage and density dependent sex ratio. Robinson [195] found a decreasing infectivity of J2 juveniles together with a decrease of juvenile lipid content. His data are shown in figure 7.2 with a curve

Table 7.1: Variables of soil, resource partitioning and individual model

symbol	dimension	interpretation
t	time	time
Y	root length.plant^{-1}	root length per plant
N_r	number	number eggs in rhizosphere
N_a	number	number (active) hatched juveniles
N_e	number.plant^{-1}	number established nematodes in root
n_r	number.length^{-3}	density eggs in rhizosphere: $\rho N_r/Y$
n_a	number.length^{-3}	density hatched juveniles: $\rho N_a/Y$
n_e	number.length^{-1}	density established nematodes in root: N_e/Y
f	–	scaled functional response
X	length.nematode^{-1}	root length available for feeding
ϕ_f	–	fraction juveniles becoming female
ϕ_m	–	fraction juveniles becoming male
V	length^3	biovolume individual nematode
L	length	oesophageal width
L_d	length	mid-body width
e	–	scaled energy density
l	–	scaled length
R_c	number.nematode^{-1}	cumulated number of eggs per female
A	length^2	cross sectional surface area
T	temperature	temperature
$\mathcal{N}_{e,f}$	number	number females per plant
$\mathcal{R}$	number	number of eggs produced per plant
$\mathcal{F}$	number.length^2	size frequency distribution

fitted according to equation 7.14. The estimated inactivation rate of 0.11 d^{-1} was used in the population model as inactivation rate of the active juveniles, n_a in soil.

Upon invasion plants had a reduced root growth. The results of growth pouch experiments on growing root tips are shown in figure 7.3. The variation between different series has been large; so for reasons of consistency only the series with three subsequent inoculations are shown. The variation might be caused by size differences of the shoots between series. The data were analyzed with damage curves according to hypothesis (1) and (2). Both of the damage curves could be fitted on these data, therefore the simplest hypothesis, *i.e.* the linear one was chosen for parameter estimation.

From these data it appeared that cultivar Bintje was the least reduced in root growth per inoculated J2 compared to cultivars Darwina and Elles. Cultivars Elles and Darwina had the highest initial root growth rates with few inoculated J2's. The controls of the
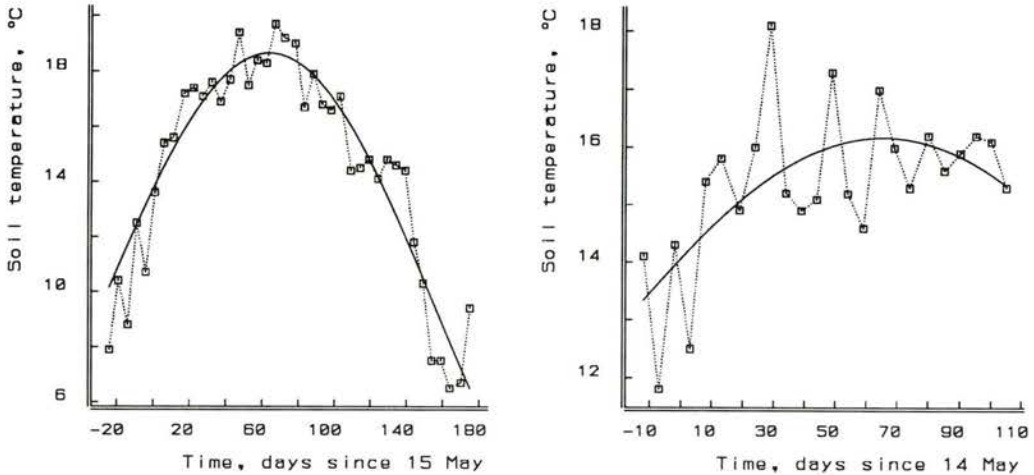
Figure 7.1: Soil temperatures measured at 10 cm depth of the field experiment in 1991 (left) and the mesocosm experiment in 1993 (right). The sinusoidal interpolation function $T(t) = \mu + \sigma \cos 2\pi \frac{t-t_r}{365}$ is applied for both time series. The estimated values for μ, σ and t_r are in 1991 respectively: 9.59 and 9.07 °C and 63.6 days and for 1993 respectively: 12.44 and 3.73 °C and 65.2 days.

cultivars, not shown here, had the highest root growth rates, with Elles the fastest growing and Bintje the slowest growing cultivars.

Density dependent sex-ratio of *G. pallida* and *G. rostochiensis* on respectively cultivars Bintje and Aran Banner is shown in figure 7.4. Equation 7.11 described fairly well the data obtained from Mugniery [150] and Trudgill [242]. The saturation constant K of the functional response could be calculated from the estimated parameter φ and the specific root densities ρ.

7.4.3   Root growth and nematode establishment in field

Root growth and nematode establishment were monitored simultaneously during the field experiments in 1991, see [160, 159] for further details. Root growth curves of cultivars Elles and Darwina in nematicide treated soil and untreated soils together with nematode densities in roots are shown in figure 7.5. This kind of nematode dynamics in root systems was observed before [59, 230], where maximal nematode densities occurred between 30 and 70 days after potato planting. The parameters of equations 7.1 through 7.3 were estimated by simultaneous regression analysis per cultivar of the data.

Root growth was suppressed in soils with an initial egg density n_d of 13.4 egg.cm^{-3}. This corroborates the measured root growth reduction in the growth pouches, see figure 7.3. The root growth curve was described by the logistic growth curve, equation 7.1 with

Figure 7.2: Decrease of lipid content ($\diamond$, —) and penetration capacity ($+,\cdots$) of infective juveniles of *G. rostochiensis* in moist soil (pF=1.66). Data are from Robinson [195] The curves are: $Q(t) = Q(0)\exp\{-\omega t\}$ with $Q(0)$ is respectively 66.4 (SD=4.73) lipid units and a fraction of 0.57 (SD=0.052) and ω is 0.113 (SD=0.014) day^{-1}. The estimated rate parameters ω when each curve is treated separately are respectively for lipid decrease and penetration 0.108 (SD=0.020) and 0.116 (SD=0.021).
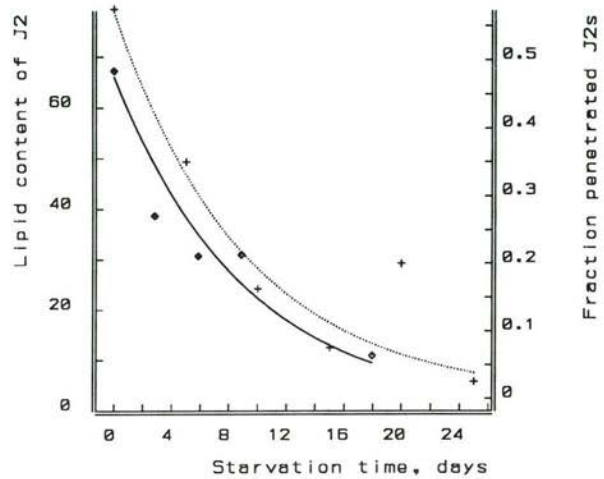
temperature correction and the linear damage hypothesis (hypothesis 1). The estimated parameters are given in table 7.4. The damage induced by nematodes on cultivar Darwina was not described properly by the logistic growth curve and the linear damage hypothesis. Therefore two separate estimates of the logistic growth curve were made for Darwina one without nematodes and one with nematodes, the estimates are given in table 7.4.

The nematode density in the root increased first, reaching its maximum close to the inflection point of the logistic growth and decreased subsequently. The decrease was caused by adult males leaving the root and by root protruded females which were lost during sampling. Therefore an additional loss term has been added to equations 7.6 and 7.7, in which the nematode loss rate is proportional to its density, this leads to:

$$\frac{d}{dt}n_e = \left\{\frac{n_d}{Y} - n_e\left(k + \frac{1}{Y}\right)\right\}\frac{d}{dt}Y - \eta n_r \tag{7.23}$$

with η the loss rate (d^{-1}).

7.4.4 Nematode population dynamics

The establishment of nematodes was studied together with root growth in the previous section. Now the population dynamics of *G. pallida* is considered in mesocosm experiments with several initial egg densities. The number of females per plant, number of eggs per female and the size frequency distribution of the females were determined in these mesocosms.

The individual growth model, equations 7.15 and 7.19, was combined with the equations describing nematode establishment, as discussed in the previous section. The results are shown in figure 7.6 and 7.9. The upper graphs of each figure show density dependent female establishment and fecundity for the cultivars Darwina and Elles. The parameter

Figure 7.3: Root growth rates of potato cultivars Bintje (—), Darwina (···) and Elles (...) with different number of applied nematodes. Root growth reduction is assumed to be proportional to established number of nematodes (hypothesis 1): $\frac{d}{dt}Y = \frac{d}{dt}Y_0 - s_1 N_e$. The estimated root growth reduction per nematode s_1 is 0.19 (SD=0.012), 0.38 (SD=0.052) and 0.39 (SD=0.0066) mm.d^{-1}.nematode^{-1} for Bintje, Darwina and Elles respectively.
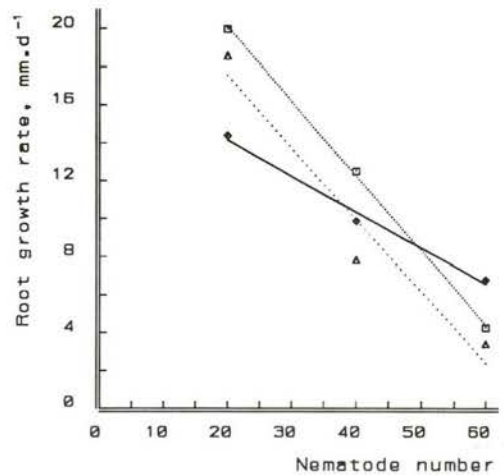
estimates of these curves are given in table 7.4. These curves show that the overall population dynamic aspects can be explained by the individual growth model with intraspecific competition.

The size frequency distribution at low initial densities (0.4 egg.g^{-1}) could not be predicted properly because of the stochastic nature of nematode invasion at very low densities, which was not modelled. At high initial densities (100 egg.g^{-1}) the frequency distribution for cv. Darwina was predicted satisfactory. The positively skewed distribution might therefore be caused by unequal resource partitioning which provides the first established females with the largest proportion of the resources relative to later established females. The latter is clearly demonstrated in figure 7.7 where cross sectional surface areas are given for female nematodes which are established at respectively day 1, 25, 55 and 90 in the root system of cultivar Darwina. The final cross sectional surface area of the females decreased due to intraspecific competition and due to differences in moment of establishment where differences in moment of establishment had the largest impact.

The final cross sectional surface area of 0.28 mm^2 of the female established at day 25 corresponded with the maximum cross sectional surface area found in the mesocosm experiment at an density of 0.4 eggs.g^{-1}. The cross sectional surface area of 0.35 mm^2 of the female established at day 1, corresponded with the largest female found at 100 eggs.g^{-1}, see figure 7.6. The probability for an early female establishment increased with increasing initial egg densities. The correspondence of these predicted cross sectional areas with the measured areas confirmed the parameter estimates of the individual growth model.

The reconstructed scaled functional response f, a nutrient measure, decreased with increasing number of active nematodes in soil which were competing for establishment in the root. After about sixty days the functional response increased again because the number of active J2 in soil decreased. The number of active J2 dropped after sixty days

Figure 7.4: Density dependent sex-ratio of *G. pallida* (□) and *G. rostochiensis* (◇) on susceptible cvs. Bintje and Aran Banner respectively. Data are from Mugniery [150] and Trudgill [242]. Curve is according to equation 7.11: sex ratio $= \varphi/N$ with $\varphi = 2.00$ (sd=0.099) (number.cm^{-1}).
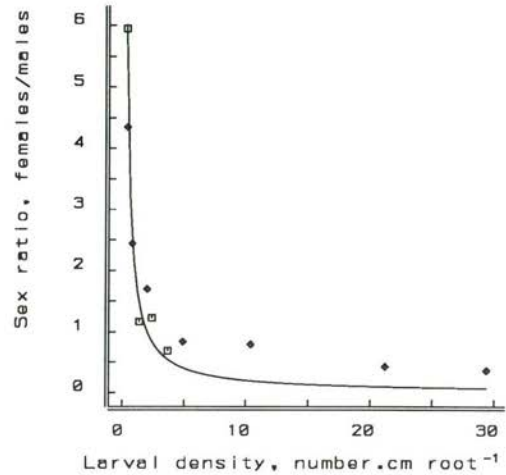
since less J2 hatched and active J2 lost their infective capacity due to starvation. The hatch of J2 decreased after sixty days because root growth diminished. This caused reduction in the root exudate production which reduced the hatch rate of J2's. These interconnected sequences are shown in figure 7.8. Only 20 % of the encysted eggs in the rhizosphere appeared to hatch in the model. Reports in literature gave values between 60-90 % [59]. The dynamics of decrease of eggs in the rhizosphere corresponded with the dynamics found in fields where the main hatch occurred within a month [166].

Although the number of females per plant and the number of eggs per female were predicted properly, the size frequency distributions of *G. pallida* grown on cultivar Elles did not agree with the observed data, see figure 7.9. The observed data resembled approximately an homogeneous distribution while the predicted distribution resembled approximately a normal distribution. The homogeneous size distribution pointed to less competition and/or interference between individuals then was assumed in the model. Potato cultivar Elles is tolerant to *G. pallida* so its crop yield is not severely affected by nematodes. This corroborates the homogeneous size distribution.

The predicted final population density $n_d(t_f)$ as function of initial population density $n_d(t)$ is shown in figure 7.10. The curve for cv. Elles closely matched the observed data. The curve for cv. Darwina deviated at higher initial densities from the observed data. This was caused by the high egg content per female found in the mesocosm relative to low initial densities.

The final length of the total root system as a function of initial density is also shown in figure 7.10. These damage curves correspond with damage curves found by Elston for yield reduction of potato crops in field [56]. The estimate of the explored soil volume by

the roots in the mesocosm was, at an initial egg density of 0.4 egg.g^{-1}, close to the 5000 cm^3 of the mesocosm itself. The estimate of the explored soil volume at 100 egg.g^{-1} was 2023 and 2400 cm^3 for Elles and Darwina respectively, which implied that only half of the soil of the mesocosm was occupied by the root system.

Size was demonstrated to depend on the cumulative amount of nutrients withdrawn by the established nematodes. Consequently, resource partitioning between individuals could be represented by ranking individuals according to size, where the largest individual was ranked as number one. The upper two graphs of figure 7.11 show the measured size rankings at respectively 0.4 and 100 eggs.g^{-1} of females developed on Darwina and Elles. The predicted size rankings for females at 100 egg.g^{-1} are shown in the lower graphs for Darwina and Elles respectively. The correspondence of the predicted and measured curves for Darwina was evident while the curves for Elles did not agree. The resource partitioning between females at 0.4 eggs.g^{-1} appeared to be similar for both of the cultivars since the negative slopes of the measured curves were similar. The resource partitioning at 100 eggs.g^{-1} differed for females grown on cv. Elles compared to cv. Darwina. The amount of available resources of high ranked (low rank number) individuals at 100 eggs.g^{-1} was comparable to the amount of resource of high ranked individuals at 0.4 eggs.g^{-1} because the initial slopes correspond with the slopes at 0.4 egg.g^{-1}. Higher ranked individuals appear not to be affected by lower ranked individuals for each cultivar.

7.5   Conclusion

Population dynamics of potato cyst nematodes can be directly derived from individual properties as shown in this paper. The size distributions are *a posteriori* results from detailed description of resource partitioning of a population of nematodes in one root system. The predicted size distributions reflect therefore the unequal resource partitioning amongst individuals as described by the model.

The approach presented here is one of the possibilities of analyzing resource partitioning as given by Lomnicki [138]. Lomnicki gives two possibilities for deriving population dynamics from resource partitioning. The first approach is based on *a priori* resource partitioning distributions, the second approach, which is applied in this paper is based on *a posteriori* resource partitioning distributions. The second approach is biologically more meaningful since hypotheses concerning sub-processes can be tested against observed data for these subprocesses.

The different distributions found for the two potato cultivars reflect differences in nematode-host interactions. The resource partitioning model derived in this paper explains partially the observed size distributions. The size distribution at 100 egg.g^{-1} for cv. Darwina is predicted properly by the resource partitioning model. Unequal resource partitioning is mainly caused by differences in time of establishment which protects earlier established females from later established females. The rank of the individual is determined by the moment at which the individual has invaded the root tissue and becomes established. This corresponds with the definition of contest competition given by Lomnicki

[139, 138].

The model derived in this paper, does not describe the homogeneous size distribution and the size ranking for cv. Elles properly. In contrast to the individual level variables [89] and the aggregated population level variables as mean number of eggs per female and number of females per plant which are described well. The biological information incorporated in the individual-based model allowed interpretation of more phenomena and testing of hypotheses. This illustrates the more powerful approach of individual-based modelling.

Three possible causes for this deviation are conceivable. First, root growth appears to be a dominating factor in resource partitioning, therefore alternative root growth models and/or nematode damage models (*e.g.* the three damage hypotheses) should be evaluated for their effect on resource partitioning curves and finally nematode size rankings. The impact of root growth on population dynamics of other soil borne pathogens has been recognized before [103, 107]. The second cause of deviation might be the interference between individuals which is here modelled only as the destruction of feeding sites by other migrating nematodes. Improvement can possibly be obtained by neglecting this type of interference since it is only observed in very thin translucent root tissue [263], whereas roots found in the field or mesocosms are much thicker. The third cause of deviation might be the assumption of constant food quality over the entire root system. The biochemical composition of xylem and/or phloem fluids might change by effects induced by invaded or established nematodes. Specific single amino-acids are identified either to improve nematode development (glutamine) or inhibit development (methionine, phenylalanine, lysine and tryptophan) [26]. The concentration of the beneficial amino acid glutamine tends to be higher distal to the syncytium then proximal to the syncytium (with reference to the root tip) whereas concentrations of the harmful amino acids are either higher or lower [26] suggesting selective removal of specific compounds from the plants vascular system by the nematode. This invalidates the assumption of constant food quality. Reduction of food quality over the root system induced by nematodes leads to an additional density dependent process. This additional density dependent process might differ between cultivars, since cultivars differing in resistance are known to differ in chemical composition [77, 79, 78].

Simplification of the model developed in this paper is possible by working out the formulations in section 7.3.4. The final potato root lengths which are reached at the end of the growing season at the different initial population densities can be used as a basis for further simplification. The total number of established females and the total number of eggs produced per plant can be regarded as a function of total root length. The simplified model can be used in potato cyst management programs where the parameters underlying the population dynamics can be estimated under controlled laboratory conditions.

Table 7.2: Parameters of soil, resource partitioning and individual model

symbol	dimension	interpretation
r	time^{-1}	root growth rate
Z	length.plant^{-1}	maximal root length
D	$\text{length.time}^{-1}.\text{plant}^{-1}$	root growth rate
s_1	$\text{length.time}^{-1}.\text{nemat}^{-1}$	root length reduction per nematode
n_d	$\text{number.length}^{-3}$	dormant egg density outside rhizosphere
ρ	$\text{length.length}^{-3}$	specific root density in soil
k	length^{-1}	hatch stimulation per root length
u	time^{-1}	nematode inactivation rate
p	–	fraction nematodes which become established
K	$\text{length.nematode}^{-1}$	saturation constant functional response
r	time^{-1}	root growth rate
L_m	length	maximal oesophageal width
L_∞	length	final oesophageal width
L_j	length	oesophageal width at maturation
L_b	length	oesophageal width at birth
v	length.time^{-1}	energy conductance
m	length.time^{-1}	maintenance rate constant
g	–	energy investment ratio
γ	time^{-1}	Bertalanffy growth rate
$V_R q_r$	length^3	conv. cum. repro. energy to gonal volume
α	–	morphometric biovolume coefficient
β	–	morphometric gonal volume coefficient
δ	egg.length^{-3}	number eggs per total volume
ζ	egg	trade off
η	time^{-1}	nematode loss rate
T_a	temperature	Arrhenius temperature

Table 7.3: Parameter values at reference temperature of 20 °C of the individual growth model estimated by van Haren [89]

parameter	dimension	Darwina	Elles
L_m	mm	0.0908	0.0860
L_b	mm	0.0161	0.0161
L_p	mm	0.0220	0.0220
m	d^{-1}	0.0624	0.0624
g	-	1.26	1.26
$V_R q_R$	mm^3	$2.88\ 10^{-3}$	$2.88\ 10^{-3}$
α	-	20.2	20.2
β	-	5.1	5.1
δ	$egg.mm^{-3}$	$2.36\ 10^5$	$2.36\ 10^5$
ζ	egg	66	66
T_A	Kelvin	8033	8033

Table 7.4: Estimated parameter values, with reference temperature 20 °C, of the model equations based on field and mesocosm data shown in figures 7.5, 7.6 and 7.9

		Field				Mesocosm			
		Darwina		Elles		Darwina		Elles	
par.	dim.	value	SD	value	SD	value	SD	value	SD
r	d^{-1}	0.21^1		0.37	0.008	0.22	0.014	0.34	0.020
r	d^{-1}	0.27^2	0.018						
Z	m	1099^1		1995	32	150		431	
Z	m	395^2	39						
s	d^{-1}			0.079	0.0075				
s_1	$m.d^{-1}.nem^{-1}$					0.0071	6.3E-4	0.045	0.0026
p	-	1	-	1	-	0.039	0.0041	0.019	0.0020
ρ	$m.cm^{-3}$	0.030	0.28	0.086	0.79	0.030	0.014	0.086	
η	d^{-1}	0.067	0.35	0.057	0.49				
n_d	$nr.cm^{-3}$	13.4		13.4					
K	$m.nem^{-1}$					0.012	0.0063	0.016	0.010
k	m^{-1}	0.0079	0.092	0.0060	0.080	0.0079		0.0060	
u	d^{-1}	0.11		0.11		0.11		0.11	

(1) without nematodes and not corrected for ambient temperatures
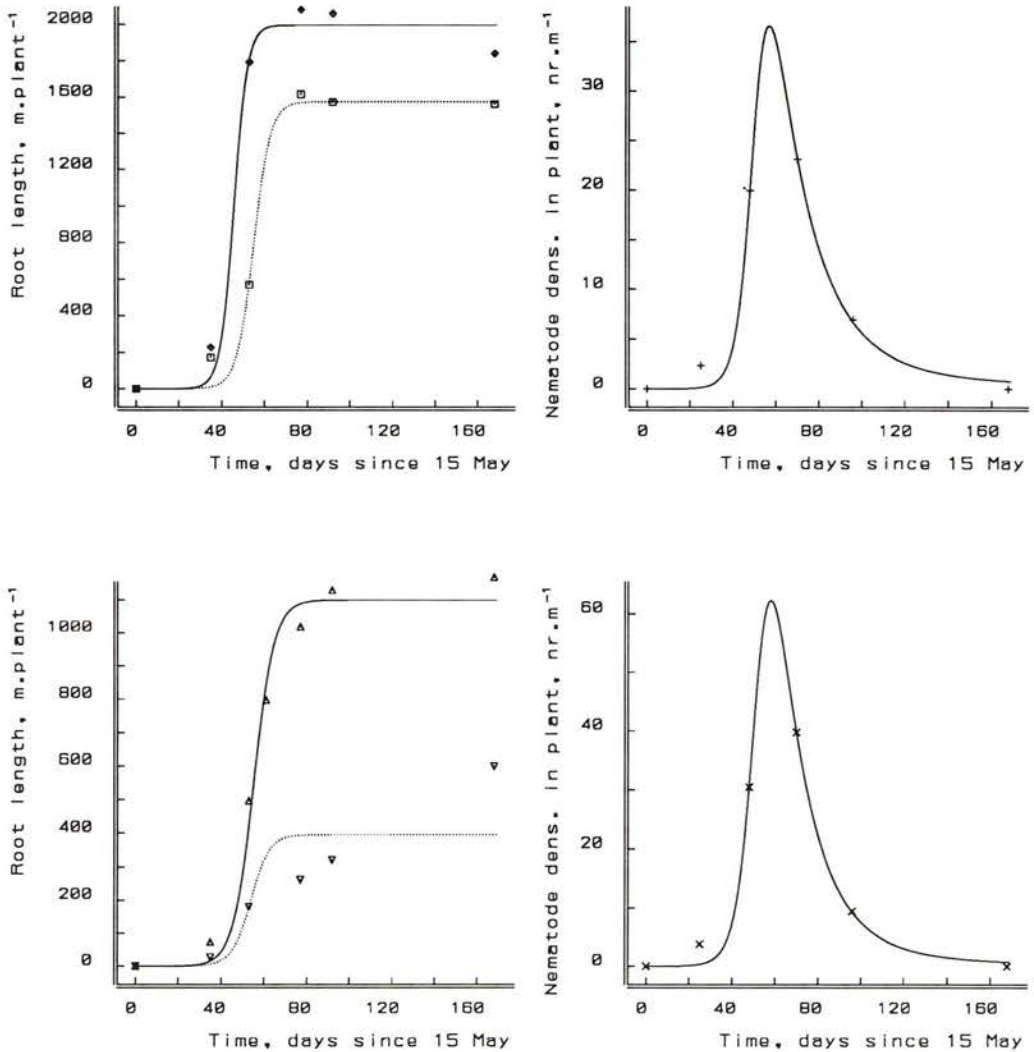(2) with nematodes, reference temperature 20 ° C

Figure 7.5: Root length and nematode density in root in the field experiment of 1991 of cultivars Elles (top) and Darwina (bottom). Equations 7.1, 7.3, 7.5 and 7.23 are used together with the interpolated temperatures and the Arrhenius temperature correction. See the text for further details. Root lengths are given in the left figures in which roots without nematodes are represented by straight (—) lines while roots suffering from nematodes are represented by dashed lines ($\cdots$).
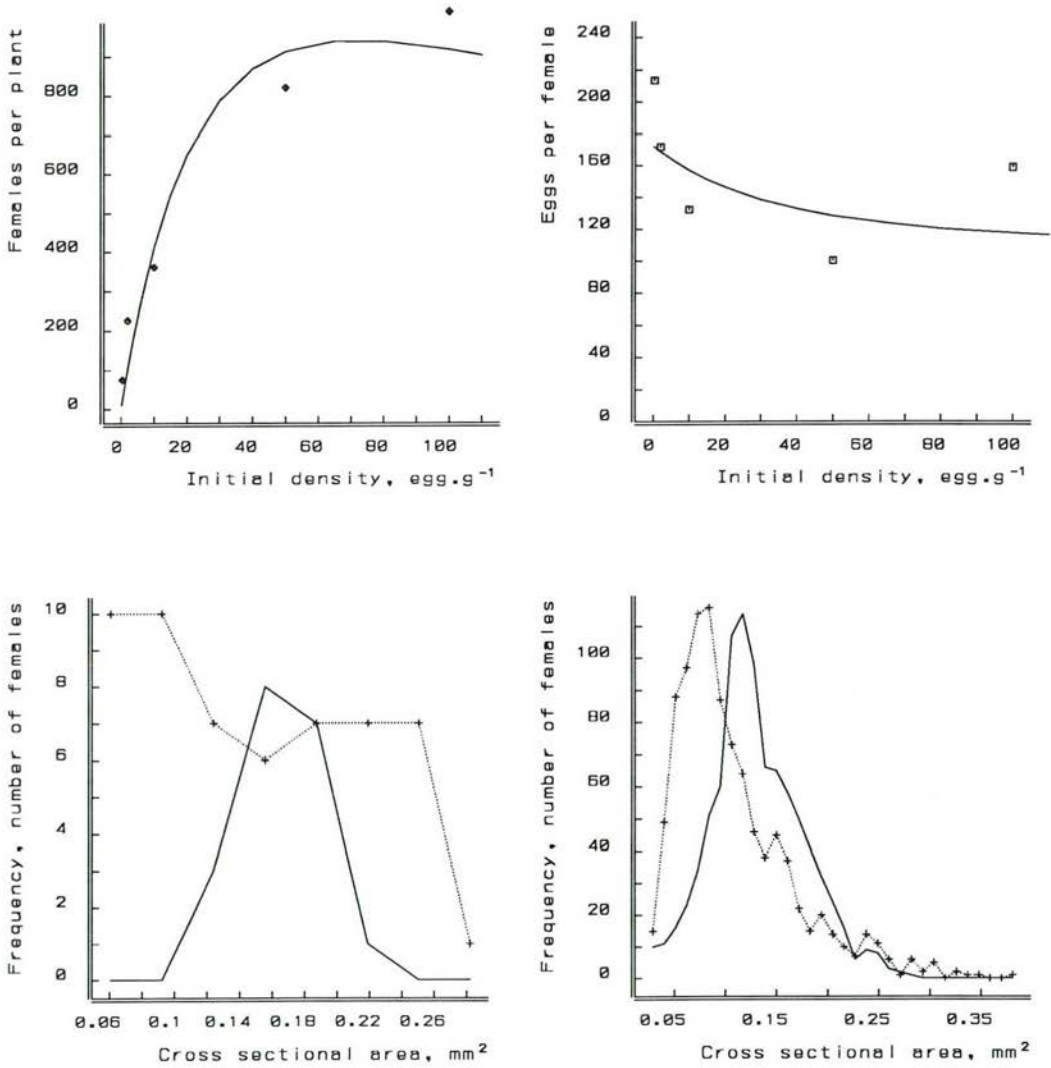
Figure 7.6: The number of developed females per plant and mean number of eggs per female as function of initial egg density on cultivar Darwina. Predicted and measured size distributions at 0.4 and 100 egg/g soil.
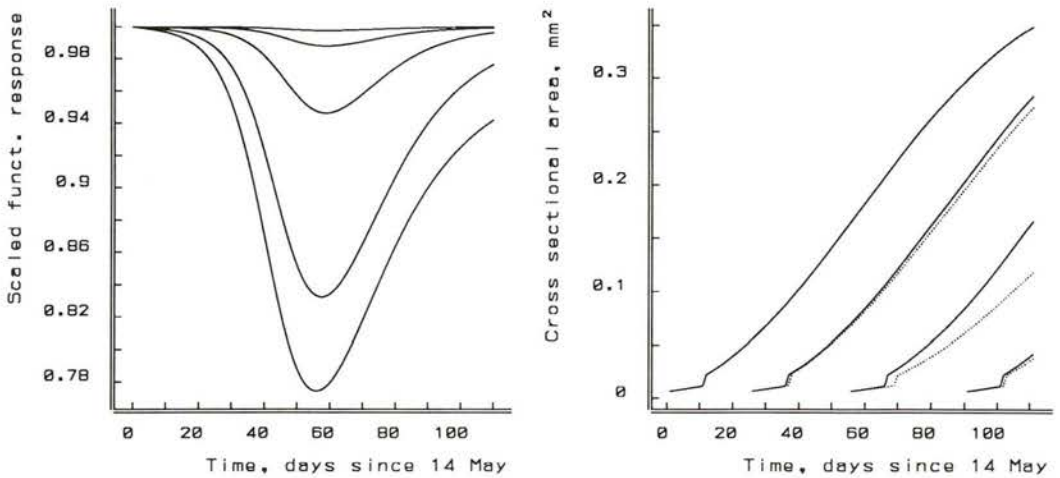
Figure 7.7: Scaled functional response f of female *G. pallida* grown on cultivar Darwina at the five initial egg densities imposed in figure 7.6. Cross sectional areas of females established at 4 different times, after 1, 25, 55 and 90 days, at two initial densities , the straight (—) lines in the right figure refer to an initial density of 0.4 eggs.g^{-1} and the dashed lines ($\cdots$) to an density of 100 eggs.g^{-1}.
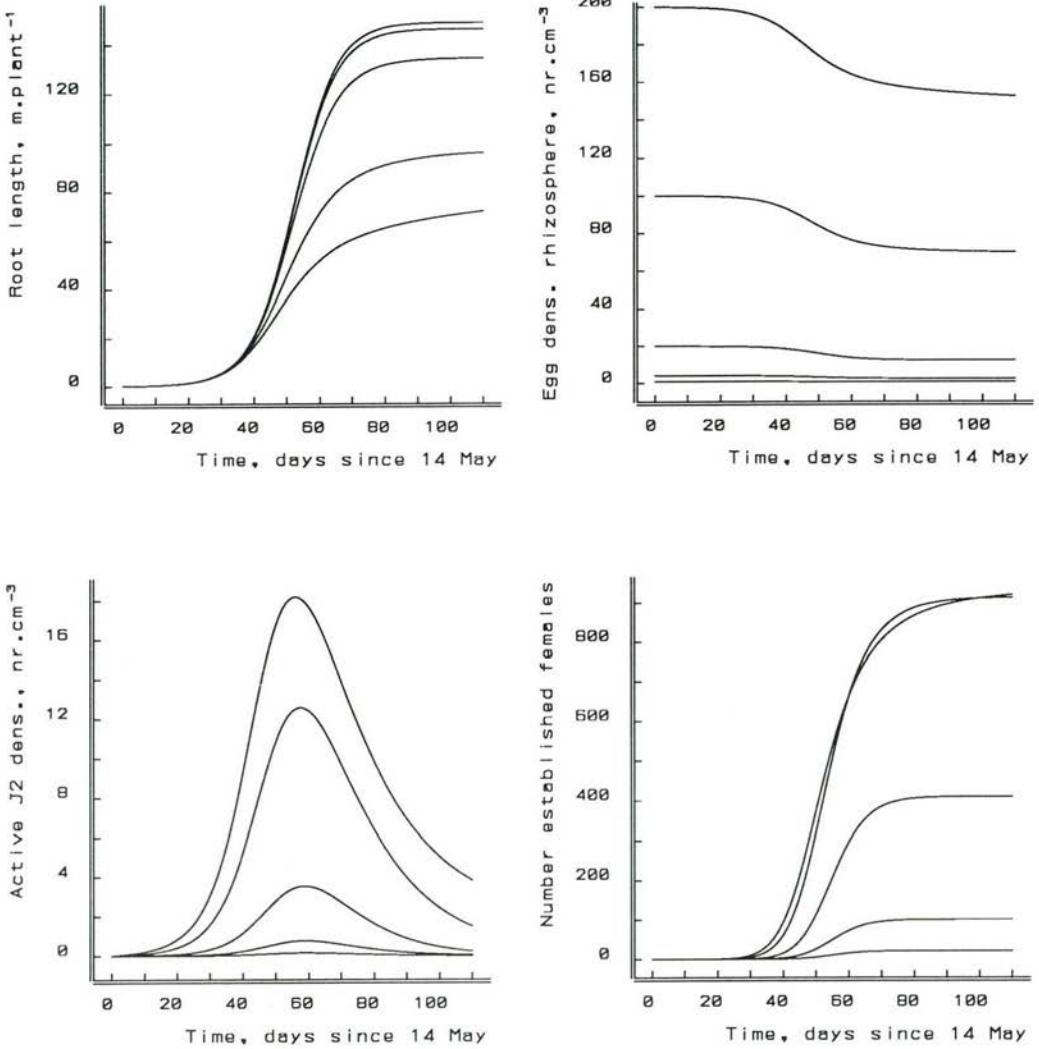
Figure 7.8: Time causes of root length Y, egg density in rhizosphere n_r, density active J2 n_a and number of established females in root N_{ef} predicted at the five initial egg densities in mesocosm with cultivar Darwina, corresponding with figure 7.6.
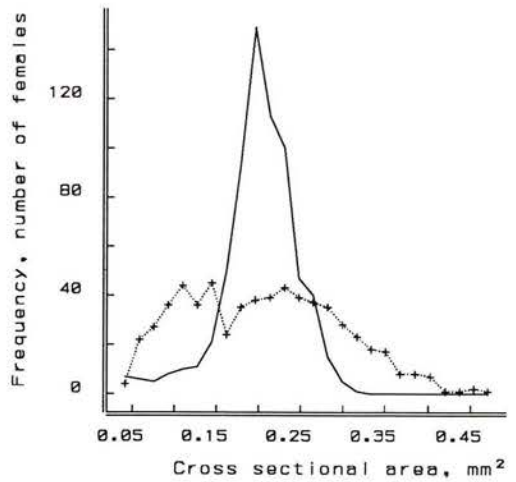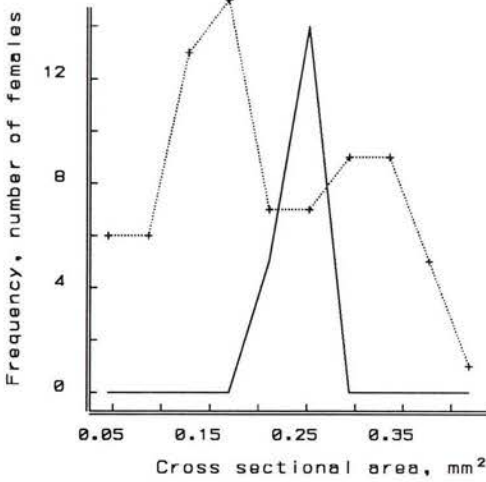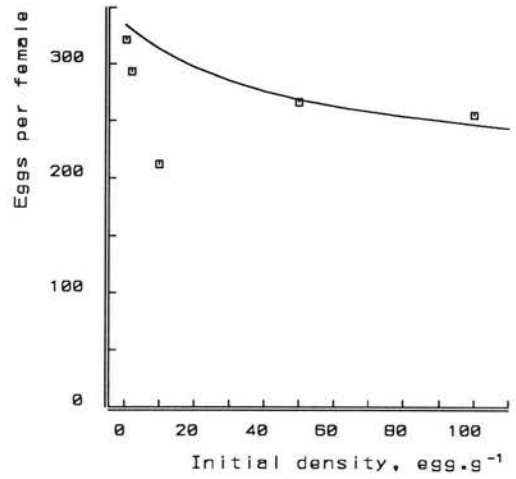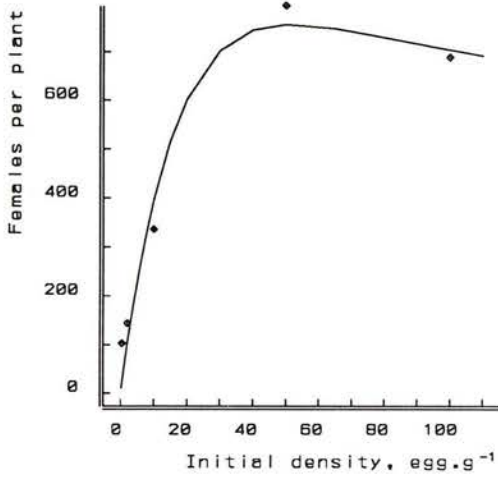
Figure 7.9: The number of developed females per plant and mean number of eggs per female as function of initial egg density on cultivar Elles. Predicted and measured size distributions at 0.4 and 100 egg/g soil.
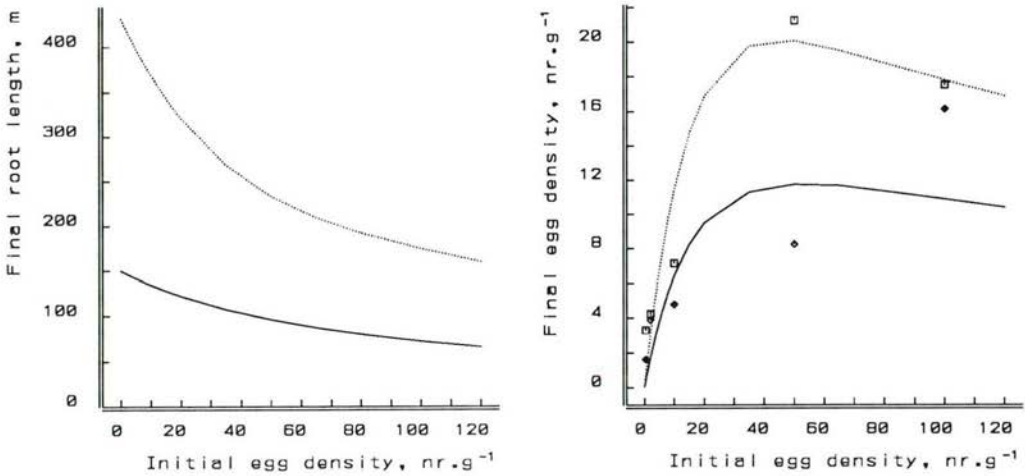
Figure 7.10: Predicted final root length y of Darwina (—) and Elles ($\cdots$) in mesocosm as function of initial density is shown left. Predicted final egg density $n_d(t_\dagger)$ of Darwina ($\diamond$) and Elles ($\square$) as function of initial egg density n_d together with measurements from mesocosm is shown right.
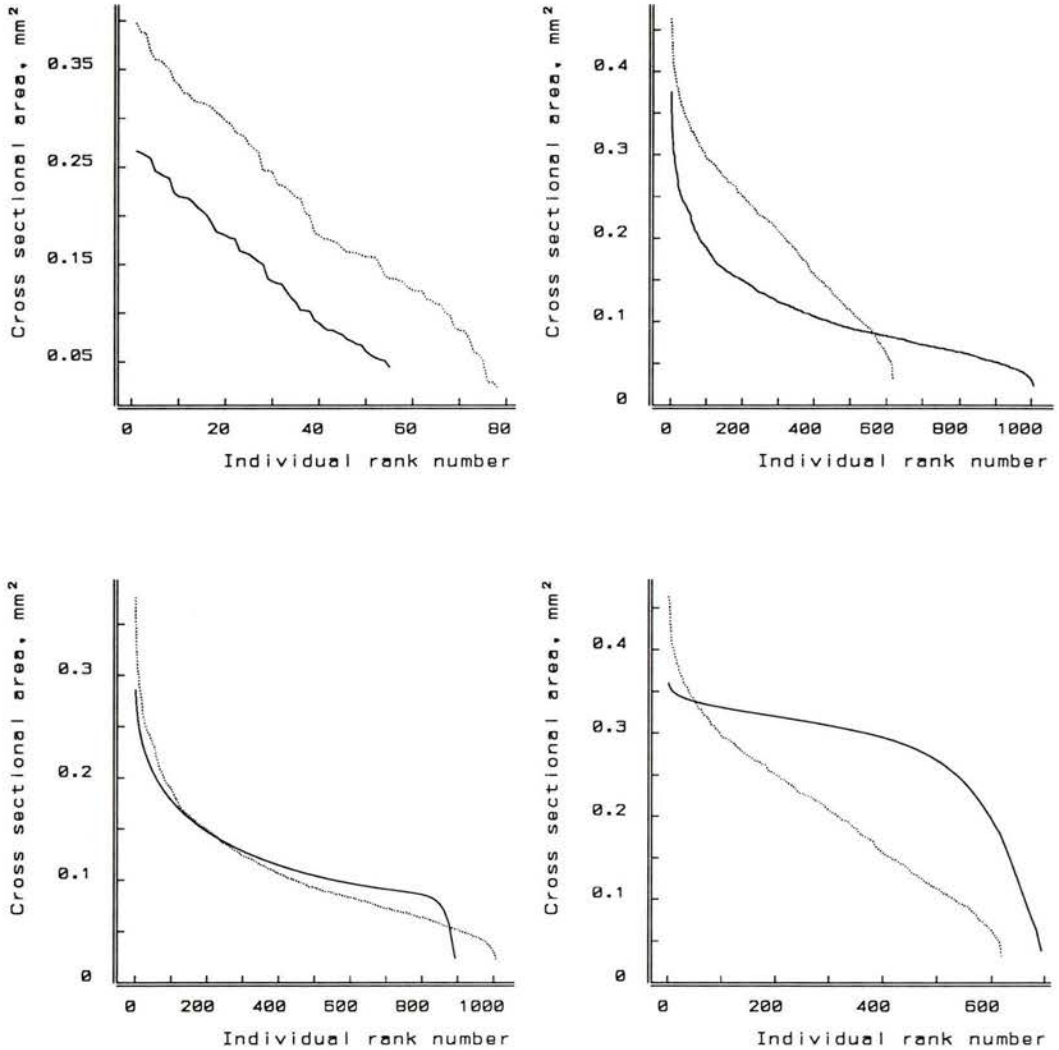
Figure 7.11: Individual ranking according to size. The upper two figures show the measured cross sectional areas at initial densities of 0.4 (left) and 100 (right) egg.g^{-1} for Darwina (—) and Elles ($\cdots$). The lower two figures show the measured ($\cdots$) and predicted (—) individual ranking for Darwina (left) and Elles (right) at initial density of 100 egg.g^{-1}. The lower two graphs correspond with the size distributions of figures 7.6 and 7.9.

Bibliography

[1] D.M.M. Adema. Accumulatie en eliminatie van enkele metalen door de mossel *Mytilus edulis*, volgens laboratorium onderzoek (in dutch). *Report MT-TNO, MD-N&E 81/3, 1-32.*, 1981.

[2] J.C. Amiard, C. Amiard-Triquet, B. Berthet, and C. Metayer. Contribution to the eco-toxicological study of cadmium, lead, copper and zinc in the mussel *Mytilus edulis*. I. field study. *Marine Biology*, 90:425–431, 1986.

[3] I. Andrássy. The determination of volume and weight of nematodes. In B.M. Zuckerman, M.W. Brezski, and K.H. Deubert, editors, *English translation of selected East-European papers in nematology*, pages 73–84, University of Massachusetts, 1967.

[4] Anonymus. *Multi-Year crop protection plan: essentials.* Ministry of Agriculture, Nature Management and Fisheries, The Hague, The Netherlands, 1990.

[5] S.A. Anwar, D.L. Trudgill, and M.S. Phillips. The contribution of variation in invasion and development rates of *Meloidogyne incognita* to host status differences. *Nematologica*, 40:579–586, 1994.

[6] F.K. Arntzen, Vinke J.H., and J. Hoogendoorn. Inheritance, level and origin of resistance to *Globodera pallida* in the potato cultivar multa derived from *Solanum tuburosum* spp. *andigena* cpc 1673. *Fundamental and Applied Nematology*, 16:155–163, 1993.

[7] F.K. Arntzen, J.C. Mulder, and H.M. Visser. Rapid and non-destructive assessment of the number of eggs in cysts of potato nematodes by weighing. *Fundamental and Applied Nematology*, 17:299–303, 1994.

[8] F.K. Arntzen and F.A. van Eeuwijk. Variation in resistance level of potato genotypes and virulence level of potato cyst nematode populations. *Euphytica*, 62:135–143, 1992.

[9] M. Arya and B. Tiagi. Autofluorescent substances in root-knots induced by *Meloidogyne incognita* on *Daucus carota* L. *Indian Journal of Nematology*, 15:14–17, 1985.

[10] H.J. Atkinson. The energetics of plant parasitic nematodes – a review. *Nematologica*, 31:62–71, 1985.

[11] H.J. Atkinson. Nematodes. In S.J. S.J. Gurr, McPherson M.J., and D.J. Bowles, editors, *Molecular Plant Pathology, A practical approach, Volume I*, page , IRL Press, Oxford, 1992.

[12] H.J. Atkinson, S.J. Gurr, M.J. McPherson, A.N. Macgregor, and D.J. Bowles. Molecular events at nematode-induced feeding sites. *Netherlands Journal of Plant Pathology*, 98 Supplement 2:175–181, 1992.

[13] M.G. Barber, L.A. Suarez, and R.R. Lassiter. Modeling bioconcentration of nonpolar organic pollutants by fish. *Environmental Toxicology and Chemistry*, 7:545–558, 1988.

[14] J.W. Baretta and P. Ruardij. *Tidal flat estuaries: simulation and analysis of the Ems estuary.* Springer Verlag, Berlin, 1988.

[15] G.H. Barrows, J.E. Sisken, J.C. Allegra, and S.D. Grasch. Measurement of fluorescence using digital integration of video frames. *The Journal of Histochemistry and Cytochemistry,* 32:741–746, 1984.

[16] B.L. Bayne. *Marine mussels: their ecology and physiology. International Biological Programme 10.* Cambridge University Press, Cambridge, 1976.

[17] B.L. Bayne. Measuring the biological effects of pollution: the mussel watch approach. *Water Science and Technology,* 21:1089–1100, 1989.

[18] B.L. Bayne, A. Bubel, P.A. Gabbott, D.R. Livingstone, D.M. Lowe, and M.N. Moore. Glycogen utilisation and gametogenesis in *Mytilus edulis* l. *Marine Biology Letters,* 3:89–105, 1982.

[19] B.L. Bayne, P.A. Gabbott, and J. Widdows. Some effects of stress in the adult on the eggs and larvae of *Mytilus edulis* l. *Journal of the Marine Biological Association U.K.,* 55:675–689, 1975.

[20] B.L. Bayne, A.J.S. Hawkins, and R. Navarro. Feeding and digestion by the mussel *Mytilus edulis* l. (bivalvia, mollusca) in mixtures of silt and algal cells at low concentrations. *Journal of Experimental Marine Biology and Ecology,* 111:1–22, 1987.

[21] B.L. Bayne, A.J.S. Hawkins, R. Navarro, and I.P. Iglesias. Effects of seston concentration on feeding, digestion and growth in the mussel *Mytilus edulis. Marine Biology Progress Series,* 55:47–54, 1989.

[22] B.L. Bayne, D.L. Holland, M.N. Moore, D.M. Lowe, and J. Widdows. Further studies on the effect of stress in the adult on the eggs of *Mytilus edulis. Journal of the Marine Biological Association U.K.,* 58:825–841, 1978.

[23] B.L. Bayne and R.C. Newell. Physiological energetics of marine molluscs. In A.S.M. Saleuddin and M. Wilbur, editors, *The mollusca, vol. 4, Physiology, part 1,* Academic Press, New York, 1983.

[24] B.L. Bayne and R.J. Thompson. Some physiological consequences of keeping *Mytilus edulis* in the laboratory. *Helgolander Wissenschaftlicher Meeresuntersuchungen,* 20:526–552, 1970.

[25] B.L. Bayne and C.M. Worrall. Growth and production of mussels *Mytilus edulis* from two populations. *Marine Biology,* 3:317–328, 1980.

[26] M. Betka, F. Grundler, and U. Wyss. Influence of changes in the nurse cell system (syncytium) on the development of the cyst nematode *Heterodera schachtii*: single amino acids. *Phytopathology,* 81:75–79, 1991.

[27] A.F. Bird. Development of the root knot nematodes *Meloidogyne javanica* (treub) and *Meloidogyne hapla* chitwood in the tomato. *Nematologica,* 4:31–42, 1959.

[28] A.F. Bird. The effect of nitrogen deficiency on the growth of *Meloidogyne javanica* at different population levels. *Nematologica,* 16:13–21, 1970.

[29] A.F. Bird. Quantitative studies on the growth of syncytia induced in plants by root knot nematodes. *International Journal for Parasitology,* 2:157–170, 1972.

[30] A.F. Bird and B.R. Loveys. The incorporation of photosynthates by *Meloidogyne javanica. Journal of Nematology,* 7:111–113, 1975.

[31] C.D. Blake. The etiology of tulip-root disease in susceptible and in resistant varieties of oats infested by the stem nematode, *Ditylenchus dipsaci* (kühn) filipjev, 2. histopathology of tulip-root and development of the nematode. *Annals of Applied Biology*, 50:713–722, 1962.

[32] R. Boalch, S. Chan, and D. Taylor. Seasonal variation in the trace metal content of *Mytilus edulis*. *Marine Pollution Bulletin*, 12/8, 1981.

[33] A. Böckenhoff and F.M.W. Grundler. Studies on the nutrient uptake by the beet cyst nematode *Heterodera schachtii* by *in situ* microinjection of fluorescent probes into the feeding structures in *Arabidopsis thaliana*. *Parasitology*, 109:249–254, 1994.

[34] T. Borchardt. Influence of food quantity on the kinetics of cadmium uptake and loss via food and sea water in *Mytilus edulis*. *Marine Biology*, 76:67–76, 1983.

[35] T. Borchardt. Relationships between carbon and cadmium uptake in *Mytilus edulis*. *Marine Biology*, 85:233–244, 1985.

[36] U. Borgmann and D.M. Whittle. Bioenergetics and pcb, dde and mercury dynamics in lake ontario lake trout (*Salvelinus Namaycush*): a model based on surveillance data. *Canadian Journal of Fisheries and Aquatic Sciences*, 49:1086–1096, 1992.

[37] R.L. Burden and J.D. Faires. *Numerical Analysis*. PWS-Kent Publishing Company, Boston, fourth edition edition, 1989.

[38] M.J. Canny. Tansley review no. 22, what becomes of the transpiration stream ? *New Phytologist*, 114:341–368, 1990.

[39] E.P. Caswell-Chen, A.E. MacGuidwin, K.T. Milne, I.J. Nelsen, C.E. Thomason, and G.W. Bird. A simulation model of *Heterodera schachtii* infecting *Beta vulgaris*. *Journal of Nematology*, 18:512–519, 1986.

[40] E.P. Caswell-Chen and I.J. Thomason. Root volumes occupied by different stages of *Heterodera schachtii* in sugar beet, *Beta vulgaris*. *Fundamental and Applied Nematology*, 16:39–42, 1993.

[41] M. Chessels, D.W. Hawker, and Connell D.W. Influence of solubility on bioconcentration of hydrophobic compounds. *Ecotoxicology and Environmental Safety*, 23:260–273, 1992.

[42] R.J. Conover. Assimilation of organic matter by zooplankton. *Limnology and Oceanography*, 11:338–345, 1966.

[43] R. Cook. Resistance in plants to cyst and root-knot nematodes. *Agricultural Zoology Reviews*, 4:213–241, 1991.

[44] R. Cook, J. Thomas, and K.A. Mizen. X-ray microanalysis of feeding syncytia induced in plants by cyst nematodes. *Nematologica*, 38:36–49, 1992.

[45] D. Cossa, E. Bourget, and J. Piuze. Geographical and seasonal variations in the relationship between trace metal content and body weight in *Mytilus edulis*. *Marine Biology*, 58:7–14, 1980.

[46] D.R. Cox and Hinkley D.V. *Theoretical Statistics*. Chapman and Hall, 1974.

[47] J.M. Cushing and J. Li. The dynamics of a size-structured intraspecific competition model with density dependent juvenile growth rates. In D.L. DeAngelis and L.J. Gross, editors, *Individual-based models and approaches in ecology, Populations, communities and ecosystems*, pages 112–125, Chapman & Hall, 1992.

[48] M.F.B. Dale. Field performance of potato cultivars resistant and partially resistant to *Globodera pallida*. *Bulletin OEPP/EPPO Bulletin*, 15:175–178, 1985.

[49] D.L. DeAngelis and L.J. Gross, editors. *Individual-based models and approaches in ecology, Populations, communities and ecosystems*. Chapman & Hall, 1992.

[50] C.C. Doncaster and Seymour M.K. Passive ingestion in a plant parasitic nematode *Hexatylus viviparus* NEOTYLENCHIDAE: TYLENCHIDA. *Nematologica*, 20:297–307, 1974.

[51] R. Dorhout, F.J. Gommers, and C. Kollöffel. Phloem transport of carboxyfluorescein through tomato roots infected with *Meloidogyne incognita*. *Physiological and Molecular Plant Pathology*, submitted, 1993.

[52] R. Dorhout and C. Kollöffel. Determining apoplastic ph differences in pea roots by use the fluorescent dye fluorescine. *Journal of Experimental Botany*, 43:479–486, 1992.

[53] R. Dorhout, C. Kollöffel, and F.J. Gommers. Alteration of regions with high net proton extrusion in tomato roots infected with *Meloidogyne incognita*. *Physiological and Molecular Plant Pathology*, 40:153–162, 1992.

[54] R. Dorhout, C. Kollöffel, and F.J. Gommers. Transport of an apoplastic fluorescent dye to feeding sites induced in tomato roots by *Meloidogyne incognita*. *Phytopathology*, 78:1421–1424, 1988.

[55] V.H. Dropkin. *Introduction to plant nematology*. John Wiley & Sons, second edition edition, 1989.

[56] D.A. Elston, M.S. Phillips, and D.L. Trudgill. The relationship between initial population density of potato cyst nematode *Globodera pallida* and the yield of partially resistant potatoes. *Revue de Nematologie*, 14:221–229, 1991.

[57] R.J. Erickson and J.M. McKim. A simple flow-limited model for exchange of organic chemicals at fish gills. *Environmental Toxicology and Chemistry*, 9:159–165, 1990.

[58] H.O. Esser. A review of the correlation between physicochemical properties and bioaccumulation. *Pesticide Science*, 17:265–276, 1986.

[59] K. Evans. Changes in a *Heterodera rostochiensis* population through the growing season. *Annals of Applied Biology*, 64:31–41, 1969.

[60] E.G. Evers and S.A.L.M. Kooijman. Feeding, digestion and oxygen consumption in *Daphnia magna* a study in energy budgets. *Netherlands Journal Zoology*, 39:56–78, 1989.

[61] H. Ferris. Development of a computer-simulation model for a plant nematode system. *Journal of Nematology*, 8:255–263, 1976.

[62] H. Ferris. Modification of a computer-simulation model for a plant nematode system. *Journal of Nematology*, 10:198–201, 1978.

[63] H. Ferris. Nematode population dynamics and management. In K.J. Leonard and W.E. Fry, editors, *Plant disease epidemiology*, pages 180–204, MacMillan, 1986.

[64] H. Ferris, S.M. Schneider, and M.C. Semenoff. Distributed egg production functions for *Meloidogyne arenaria* in grape varieties and consideration of the mechanistic relationship between plant and parasite. *Journal of Nematology*, 16:178–183, 1984.

[65] H. Fisher. *Mytilus edulis* as a quantitative indicator of dissolved cadmium. final study and synthesis. *Marine Ecology Progress Series*, 48:163–174, 1988.

[66] J.M. Fisher. Further observations on the effect of temperature on *Heterodera avenae* WOLL. *Nematologica*, 27:228–234, 1981.

[67] J.M. Fisher. Growth and development of *Aphelenchus avenae* bastian. *Australian Journal of Biological Sciences*, 23:411–419, 1970.

[68] J.M. Fisher. Investigations on fecundity of *Aphelenchus avenae*. *Nematologica*, 15:22–28, 1969.

[69] M.A. Foot. Laboratory rearing of potato cyst nematodes; a method suitable for pathotyping and biological studies. *New Zealand Journal of Zoology*, 4:183–186, 1977.

[70] B.L. Foster Smith. The effect of concentration of suspension and inert material on the assimilation of algae by three bivalves. *Journal of the Marine Biological Association U.K.*, 55:411–418, 1975.

[71] B.L. Foster Smith. The effect of concentration of suspension on the filtration rates and pseudofaecal production for *Mytilus edulis* l., cerastoderma edule l. and venerupsis pullastra (montagu). *Journal of Experimental Marine Biology and Ecology*, 17:1–22, 1975.

[72] J.P.A. Gardner and D.O.F. Skibinsky. Genotype-dependent fecundity and temporal variation of spawning hybrid mussel (mytilus) populations. *Marine Biology*, 105:153–162, 1990.

[73] S.G. George. Correlation of metal accumulation in mussels with the mechanisms of uptake, metabolism and detoxification: a review. *Thallasia Jugoslavica*, 16:347–365, 1980.

[74] S.G. George. Heavy metal detoxification in *Mytilus* kidney, an in vitro study of cd and zn binding isolated tertiary lysosomes. *Comparative Biochemistry and Physiology*, 76C:59–65, 1983.

[75] S.G. George. Heavy metal detoxification in the mussel *Mytilus edulis*, composition of cd-containing kidney granules (tertiary lysosomes). *Comparative Biochemistry and Physiology*, 76C:53–57, 1983.

[76] H. Geyer, D. Sheehan, Kotziasm D., D. Freitag, and F. Korte. Prediction of ecotoxicological behaviour of chemicals: relationship between physico-chemical properties and bioaccumulation of organic chemicals in the mussel *Mytilus edulis*. *Chemosphere*, 11:1121–1134, 1982.

[77] J. Giebel. Biochemical mechanisms of plant resistance to nematodes: a review. *Journal of Nematology*, 6:175–184, 1974.

[78] J. Giebel. Mechanism of resistance to plant nematodes. *Annual Review of Phytopathology*, 20:257–279, 1982.

[79] J. Giebel and M. Stobiecka. Role of amino acids in plant tissue response to *Heterodera rostochiensis*, 1 protein-proline and hydroxyproline content in roots of susceptible and resistant solanaceous plants. *Nematologica*, 20:407–414, 1974.

[80] F.A.P.C. Gobas, J.R. McCorquodale, and G.D. Haffner. Intestinal absorption and biomagnification of organochlorines. *Environmental Toxicology and Chemistry*, 12:567–576, 1993.

[81] E.D. Goldberg. The mussel watch - a first step in global marine monitoring. *Marine Pollution Bulletin*, 6:111, 1975.

[82] E.D. Goldberg. The mussel watch concept. *Environmental Monitoring Assessment*, 7:91–103, 1986.

[83] W. Golinowsky and C. Magnusson. Tissue response induced by *Heterodera schachtii* (NEMATODA) in susceptible and resistant white mustard cultivars. *Canadian Journal of Botany*, 69:53–62, 1991.

[84] F.J. Gommers and V.H. Dropkin. Quantitative histochemistry of nematode-induced transfer cells. *Phytopathology*, 67:869–873, 1977.

[85] W.T. Gorham. The energetic and nutritional contribution of glucose and glycine taken up from natural sea water by adult marine mussels. *Marine Ecology*, 9:1–14, 1988.

[86] F. Grundler, M. Betka, and U. Wyss. Influence of changes in the nurse cell system (syncytium) on sex determination and development of the cyst nematode *Heterodera schachtii*. 1. total amounts of proteins and amino acids. *Phytopathology*, 81:70–74, 1991.

[87] K. Hamburger, F. Møhlenberg, A. Randløv, and H.U. Riisgård. Size, oxygen consumption and growth in the mussel *Mytilus edulis*. *Marine Biology*, 75:303–306, 1983.

[88] R.J.F. van Haren. Quantifying feeding rates of the potato cyst nematode *Globodera pallida* by image analysis of apoplastic applied fluorescine. *submitted*, 1995.

[89] R.J.F. van Haren, F. Arntzen, and H.J. Atkinson. Growth of vermiform nematodes compared with growth and fecundity of the potato cyst nematode *Globodera pallida* on different hosts, a model approach. *submitted*, 1995.

[90] R.J.F. van Haren, E.M.L Hendrikx, and H.J. Atkinson. Growth curve analysis of sedentary plant parasitic nematodes in relation to plant resistance and tolerance. In J. Grasman and G. van Straten, editors, *Predictability and nonlinear modelling in natural sciences and economics*, pages 172–184, Kluwer, Dordrecht, 1994.

[91] R.J.F. van Haren, E.M.L. Hendrikx, F. de Ruijter, and M. van Oijen. Responses of field-grown potato cultivars to cyst nematodes, at three levels of soil compaction. 3. nematode density estimation in soil and root. *in preparation*, 1995.

[92] R.J.F. van Haren and S.A.L.M. Kooijman. Application of a dynamic energy budget model to *Mytilus edulis* (l.). *Netherlands Journal of Sea Research*, 31(2):119–133, 1993.

[93] R.J.F. van Haren, H. Regeer, and M. van Oijen. Modelling population dynamics of the potato cyst nematode *Globodera pallida* based on individual energetics and root dynamics: a study into intraspecific competition. *submitted*, 1995.

[94] R.J.F. van Haren, H.E. Schepers, and S.A.L.M. Kooijman. Dynamic energy budgets affect kinetics of xenobiotics in the marine mussel *Mytilus edulis*. *Chemosphere*, 29:163–189, 1994.

[95] R.J.F van Haren, J. Van der Meer, and M.B. de Vries. Cadmium and copper accumulation in the common mussel *Mytilus edulis* in the Western Scheldt estuary:a model approach. *Hydrobiologia*, 195:105–118, 1990.

[96] A.J.S. Hawkins and B.L. Bayne. Seasonal variations in the balance between physiological mechanisms of feeding and digestion in *Mytilus edulis* (bivalvia, mollusca). *Marine Biology*, 82:233–240, 1984.

[97] W.L. Hayton and B.C. Barron. Rate limiting barriers to xenobiotic uptake by the gill. *Environmental Toxicology and Chemistry*, 9:151–157, 1990.

[98] W.J.M. Hegeman. Comparison of theoretical and experimental hydrophobicity dependent parameters of polycyclic aromatic hydrocarbons (PAH's). in preperation:, 1995.

[99] T.J. Hilbish and K.M. Zimmerman. Genetic and nutritional control of the gametogenetic cycle in *Mytilus edulis*. *Marine Biology*, 98:223–229, 1988.

[100] C. Hogstrand and C. Haux. Binding and detoxification of heavy metals in lower vertebrates with reference to metallothionein. *Comparative Biochemistry and Physiology*, 100C:137–141, 1991.

[101] E. Honkoop. Meerjaren plan gewas bescherming. *Groenten + Fruit*, week 1, 6 jan.:16–18, 1995.

[102] H.J. Horstmann. Sauerstoffverbrauch und trockengewicht der embryonen von *Lymnaea stagnalis* l. *Zeitschrift fur Vergleichende Physiology*, 41:390–404, 1958.

[103] O.C. Huisman. Interrelations of root growth dynamics to epidemiology of root invading fungi. *Annual Review of Phytopathology*, 20:303–327, 1982.

[104] H. Hummel, J.P. UitOudeGroeneveld, J. Nieuwenhuize, J.M. van Liere, R.H. Bogaards, and L. de Wolf. Relationship between PCB concentrations and reproduction in mussels *Mytilus edulis*. *Marine Environmental Research*, 28:489–493, 1989.

[105] H.H. Jansen and N. Scholz. Uptake and cellular distribution of cadmium in *Mytilus edulis*. *Marine Biology*, 55:133–141, 1979.

[106] Madulu J.D. and D.L. Trudgill. Influence of temperature on the development and survival of *Meloidogyne javanica*. *Nematologica*, 40:230–243, 1994.

[107] M.J. Jeger. The influence of root growth and inoculum density on the dynamics of root disease epidemics: theoretical analysis. *New Phytologist*, 107:459–478, 1987.

[108] A.L. Jensen, S.A. Spigarelli, and M.M. Thommes. Pcb uptake by five species of fish in lake michigan, green bay of lake michigan, and cayuga laken new york. *Canadian Journal of Fisheries and Aquatic Sciences*, 39:700–709, 1982.

[109] R.N. Johnson and D.R. Vigliercho. Sugar beet nematode (*Heterodera schachtii*) reared on axenic *Beta vulgaris* root explants. 2. selected environmental and nutritional factors affecting development and sex-ratio. *Nematologica*, 15:144–152, 1969.

[110] F.G.W. Jones and J.N. Perry. Modelling populations of cyst-nematodes NEMA-TODA:HETERODERIDAE. *Journal of Applied Ecology*, 15:349–371, 1978.

[111] M.G.K. Jones. Host cell responses to endoparasitic nematode attack: structure and function of giant cells and syncytia. *Annals of Applied Biology*, 97:353–372, 1981.

[112] M.G.K. Jones. Movement of solutes from host to parasite in nematode infected roots. In I.F. Wardlaw and J.B. Passioura, editors, *Transport and Transfer processes in Plants*, pages 65–71, Academic Press, New York, 1976.

[113] M.G.K. Jones and V.H. Dropkin. Scanning electron microscopy of nematode induced giant transfer cells. *Cytobios*, 15:149–161, 1976.

[114] M.G.K. Jones and D.H. Northcote. Nematode induced syncytium, a multinucleate transfer cell. *Journal of Cell Science*, 10:789–809, 1972.

[115] C.B. Jørgensen. *Bivalve filter feeding: hydrodynamics, bioenergetics, physiology and ecology*. Olsen & Olsen, Fredensborg, 1990.

[116] C.B. Jørgensen. Growth efficiencies and factors controlling size in some mytilid bivalves, especially *Mytilus edulis* l.: review and interpretation. *Ophelia*, 15:175–192, 1976.

[117] O.P. Judson. The rise of the individual-based model in ecology. *Trends in Ecology and Evolution*, 9:9–14, 1994.

[118] N. Kannan, S. Tanabe, R. Tatsukawa, and D.J.H. Phillips. Persistency of highly toxic coplanar pcbs in aquatic ecosystems: uptake and release kinetics in green-lipped mussels (*Perna viridis* linnaeus). *Environmental Pollution*, 56:65–76, 1989.

[119] N. Kautsky. Growth and size structure in a baltic *Mytilus edulis* population. *Marine Biology*, 68:117–133, 1982.

[120] N. Kautsky. Quantitative studies on gonad cycle, fecundity, reproductive output and recruitment in a baltic *Mytilus edulis* population. *Marine Biology*, 67:143–160, 1982.

[121] U. Kerstan. Die beeinflussung des geschlechterverhaltnisses in der gattung *Heterodera*, 2 minimallebensraum - selektive absterberate der geschlechter - geschlechterverhaltnis *Heterodera schachtii*. *Nematologica*, 15:210–228, 1969.

[122] T. Kiørboe, F. Møhlenberg, and O. Nøhr. Effect of suspended bottom material on growth and energetics in *Mytilus edulis*. *Marine Biology*, 61:283–288, 1981.

[123] T. Kiørboe, F. Møhlenberg, and O. Nøhr. Feeding, particle selection and carbon absorption in *Mytilus edulis* in different mixtures of algae and resuspended bottom material. *Ophelia*, 19:193–205, 1980.

[124] O. Klepper. *A model of carbon flows in relation to macrobenthic food supply in the Oosterschelde estuary (S.W. Netherlands)*. PhD thesis, Agricultural University, Wageningen, the Netherlands, 1989.

[125] S.A.L.M. Kooijman. *Dynamic energy budgets in biological systems, Theory and applications in ecotoxicology*. Cambridge University Press, Cambridge, 1993. 350 pp.

[126] S.A.L.M. Kooijman. Energy budgets can explain body size relations. *Journal of Theoretical Biology*, 121:269–282, 1986.

[127] S.A.L.M. Kooijman. Population dynamics on the basis of energy budgets. In J.A.J. Metz and O. Diekmann, editors, *The Dynamics of Structured Populations. Lecture Notes in Biomathematics*, pages 266–297, Springer Verlag, Berlin, 1986.

[128] S.A.L.M. Kooijman. The von Bertalanffy growth rate as a function of physiological parameters: a comparative analysis. In T.G. Hallam, L.J. Gross, and S.A. Levin, editors, *Mathematical Ecology*, pages 3–45, World Scientific, Singapore, 1988.

[129] S.A.L.M. Kooijman. What the hen can tell about her eggs: egg development on the basis of energy budgets. *Journal of Mathematical Biology*, 23:163–185, 1986.

[130] S.A.L.M. Kooijman, E.B. Muller, and A.H. Stouthamer. Microbial dynamics on the basis of individual budgets. *Antonie van Leeuwenhoek*, 60:159–174, 1991.

[131] S.A.L.M. Kooijman and R.J.F. van Haren. Animal energy budgets affect the kinetics of xenobiotics. *Chemosphere*, 21:681–693, 1990.

[132] J. Kort, H. Ross, H.J. Rumpenhorst, and A.R. Stone. An international scheme for identifying and classifying pathotypes of potato cyst nematodes *Globodera rostochiensis* and *G. pallida*. *Nematologica*, 23:333–339, 1977.

[133] F. Kruger. Zur frage der grossenabhangigkeit des sauerstoffverbrauchs von *Mytilus edulis* l. *Helgolander Wissenschaftlicher Meeresuntersuchungen*, 7:125–148, 1960.

[134] K. Kuwabara, S. Fukushima, R. Tanaka, H. Miyata, and T. Kashimoto. Relationship between shell length of blue mussel and levels of residual PCBs within the body. *Journal Japanese Soc. of Food Sanitation*, 27/5:565–569, 1986.

[135] R.W.P.M. Laane, H. Etcheber, and J.C. Relaxans. Particulate organic matter in estuaries and its ecological implication for macrobenthos. *Mitteilungen Geologisch und Paleontologisch Institut Universitat Hamburg*, 64:71–91, 1987.

[136] J.A. LaMondia, D. Rawsthorne, and B.B. Brodie. Decline of *Globodera rostochiensis* as influenced by potato root diffusate movement and persistence in soil. *Journal of Nematology*, 19:172–176, 1987.

[137] M. Langeslag, D. Mugniery, and G. Fayet. Développement embryonnaire de *Globodera rostochiensis* et *G. pallida* en fonction de la temperature, en conditions contrôlées et naturelles. *Revue de Nematologie*, 5:103–109, 1982.

[138] A. Lomnicki. Population ecology from the individual perspective. In D.L. DeAngelis and L.J. Gross, editors, *Individual-based models and approaches in ecology, Populations, communities and ecosystems*, pages 3–17, Chapman & Hall, 1992.

[139] A. Lomnicki. *Population ecology of individuals. Monographs in population biology, 25*, Princeton University Press, Princeton, 1988.

[140] R.A. Lutz. Annual growth patterns in the inner shell layer of *Mytilus edulis* l. *Journal of the Marine Biological Association U.K.*, 56:723–731, 1976.

[141] C. Magnusson and W. Golinowsky. Ultrastructural relationships of the developing syncytium induced by *Heterodera schachtii* (NEMATODA) in root tissues of rape. *Canadian Journal of Botany*, 69:44–52, 1991.

[142] A.E. Martell, R.J. Motekaitis, and R.M. Smith. Structure-stability relationship of metal complexes and metal speciation in environmental aqueous solutions. *Environmental Toxicology and Chemistry*, 7:417–434, 1988.

[143] W.T. Mason. *Biological techniques: Fluorescent and luminescent probes for biological activity: A practical guide to technology for quantitative real-time analysis*. Academic Press, london, 1993.

[144] M.A. McClure. *Meloidogyne incognita*: a metabolic sink. *Journal of Nematology*, 9:88–90, 1977.

[145] J. McDowell Capuzzo, J.W. Farrington, P. Rantamaki, C.H. Clifford, B.A. Lancaster, D.F. Leavitt, and X. Jia. The relation between lipid composition and seasonal differences in the distribution of PCBs in *Mytilus edulis*(L.). *Marine Environmental Research*, 28:259–264, 1989.

[146] H. Melakeberhan and H. Ferris. Growth and energy demand of *Meloidogyne incognita* on susceptible and resistant *Vitis vinifera* cultivars. *Journal of Nematology*, 20:545–554, 1988.

[147] F. Møhlenberg and H.U. Riisgård. Efficiency of particle retention in 13 species of suspension feeding bivalves. *Ophelia*, 17:239–246, 1978.

[148] F. Møhlenberg and H.U. Riisgård. Filtration rate, using an new indirect technique, in thirteen species of suspension-feeding bivalves. *Marine Biology*, 54:143–147, 1979.

[149] D. Mugniery. Vitesse de développement en fonction de la température de *Globodera rostochiensis* et G. pallida (nematoda: heteroderidae). *Revue de Nematologie*, 1:3–12, 1978.

[150] D. Mugniery and G. Fayet. Determination du sexe chez *Globodera pallida* STONE. *Revue de Nematologie*, 4:41–45, 1978.

[151] J. Muller, K. Rehbock, and U. Wyss. Growth of *Heterodera schachtii* with remarks on amounts of food consumed. *Revue de Nematologie*, 4:227–234, 1981.

[152] B.A. Mullin and B.B. Brodie. Effects of host resistance on the fecundity of *Globodera rostochiensis*. *Nematologica*, 20:109–112, 1988.

[153] M. Mullin. Workshop on high resolution PCB analysis. *USEPA, Large Lakes Research Station, Grosse Ile, Research station*, May 1985.

[154] J.F. Narbonne, P. Garrigues, D. Ribera, C. Raoux, A. Mathieu, P. Lemaire, J.P. Saloun, and M. Lafaurie. Mixed-function oxygenase enzymmes as tools for pollution monitoring:

field studies on the french coast of the mediterranean sea. *Comparative Biochemistry and Physiology*, 100C:37–42, 1991.

[155] M.V. Nielsen. The effect of temperature on the shell length growth of juvenile *Mytilus edulis* l. *Journal of Experimental Marine Biology*, 123:227–234, 1988.

[156] P.S. Nobel. *Physicochemical and Environmental Plant Physiology*. Academic Press, San Diego, 1991.

[157] R.J. Norstrom, A.E. McKinnon, and S.W. DeFreitas. A bio-energetics based model for pollutant accumulation by fish, simulation of pcb and methyl mercury residue levels in ottawa river yellow perch (*Perca flavescens*). *Journal of the Fisheries Research Board Canada*, 33:248–276, 1976.

[158] M. van Oijen, F.J. de Ruijter, and R.J.F. van Haren. Modelling the interaction between potato crops and cyst nematodes. In A.J. Haverkort and D.K.L. MacKerron, editors, *Ecology and Modeling of Potato Crops under conditions of limiting growth*, page , Kluwer Academic Publishers, 1995.

[159] M. van Oijen, F.J. de Ruijter, and R.J.F. van Haren. Responses of field-grown potato cultivars to cyst nematodes, at three levels of soil compaction. 2. root length dynamics and nutrient uptake. *Annals of Applied Biology*, submitted:, 1995.

[160] M. van Oijen, F.J. de Ruijter, and R.J.F. van Haren. Responses of field-grown potato cultivars to cyst nematodes, at three levels of soil compaction. 1. leaf area dynamics, photosynthesis and crop growth. *Annals of Applied Biology*, submitted:, 1995.

[161] M. Oostenbrink. Major characteristics of the relation between nematodes and plants. *Mededelingen Landbouwhogeschool Wageningen Nederland*, 66-4:3–46, 1966.

[162] K.J. Oparka. Uptake and compartimentation of fluorescent probes by plant cells. *Journal of Experimental Botany*, 42:565–579, 1991.

[163] A. Opperhuizen. Bioconcentration and biomagnification: is a distinction necessary? In R. Nagel and R. Loskill, editors, *Bioaccumulation in aquatic systems, Contributiotions to the Assessment*, pages 67–80, VCH, Weinheim, 1991.

[164] A. Opperhuizen. *Bioconcentration in Fish and other distribution processes of hydrophobic chemicals in aqueous environments*. PhD thesis, University of the City of Amsterdam, Netherlands, 1986.

[165] M.J. Orren, G.A. Eagle, H.F.-K.O. Hennig, and A. Green. Variation in trace metal content of the mussel *Choromytilus meridionalis*(Kr.) with season ans sex. *Marine Pollution Bulletin*, 11:253–257, 1980.

[166] H. den Ouden. Periodicity in spontaneous hatching of *Heterodera rostochiensis* in the soil. *Nematologica*, Suppl.2:101–105, 1960.

[167] H.M. Page and D.M. Hubbard. Temporal and spatial patterns of growth in mussels *Mytilus edulis* on an offshore platform: relationships to water temperature and food availability. *Journal of Experimental Marine Biology and Ecology*, 111:159–179, 1987.

[168] C.E. Palmer. Influence of ethephon on nitrate reductase, protein, amino and nitrate content of *Solanum tuburosum* L. *Plant Cell Physiology*, 26:407–417, 1985.

[169] J.S. Pate. Uptake, assimilation and transport of nitrogen compounds by plants. *Soil Biology and Biochemistry*, 5:109–119, 1973.

[170] R.H. Peters. *The ecological implications of body size.* Cambridge University Press, Cambridge, 1983.

[171] D.J.H. Philips. The common mussel *Mytilus edulis* as an indicator of pollution by zinc, cadmium, lead and copper. i. effects of environmental variables on uptake of metals. *Marine Biology*, 38:59–69, 1976.

[172] D.J.H. Phillips and P.S. Rainbow. Barnacles and mussels as biomonitors of trace elements: a comparative study. *Marine Ecology Progress Series*, 49:83–93, 1988.

[173] M.S. Phillips, H.J. Rumpenhorst, D.L. Trudgill, K. Evans, G. Gurr, D. Heinicke, M. Mackenzie, and S.J. Turner. Environmental interactions in the assessment of partial resistance to potato cyst nematodes, 1. interactions with centers. *Nematologica*, 35:187–196, 1989.

[174] H. Pieters, J.H. Kluytmans, D.I. Zandee, and G.C. Cadee. Tissue composition and reproduction of *Mytilus edulis* in relation to food availability. *Netherlands Journal of Sea Research*, 14:349–361, 1980.

[175] H. Pieters, J.H. Kluytmans, W. Zurburg, and D.I. Zandee. The influence of seasonal changes on energy metabolism in *Mytilus edulis* (l.) 1. growth rate and biochemical composition in relation to environmental parameters and spawning. In E. Naylor and R.G. Hartnoll, editors, *Cyclic phenomena in marine plants and animals*, pages 285–292, Pergamon Press, New York, 1979.

[176] M. Pilar-Aguirre. Biologia del mejillon (*M. edulis*) de cultivo de la ria de vigo. *Bol. Inst. Espa. Oceano. Tomo V*, 276:109–159, 1979.

[177] E. Poulsen, H.U. Riisgård, and F. Mohlenberg. Accumulation of cadmium and bioenergetics in the mussel *Mytilus edulis*. *Marine Biology*, 68:25–29, 1982.

[178] L.E. Powers, R.A. Dunn, and R. McSorley. Size differences among root-knot nematodes on resistant and susceptible alyceclover genotypes. *Journal of Nematology*, 23:243–248, 1991.

[179] L.E. Powers and R. McSorley. Energetics of *Meloidogyne incognita* on resistant and susceptible alyceclover genotypes. *Journal of Nematology*, 25:257–264, 1993.

[180] D.L.C. Procter. Form of the individual growth curve and developmental rate of the high arctic nematode *Chiloplacus* sp. *Growth*, 47:174–183, 1983.

[181] R.J. Pruell, J.L. Lake, W.R. Davis, and J.G. Quinn. Uptake and depuration of organic contaminants by blue mussels (*Mytilus edulis*) exposed to environmentally contaminated sediment. *Marine Biology*, 91:497–507, 1986.

[182] R.C. Randall, H. Lee II, J. Ozretich, J.L. Lake, and R.J. Pruell. Evaluation of selected lipid methods for normalizing pollutant bioaccumulation. *Environmental Toxiclogy and Chemistry*, 10:1431–1436, 1991.

[183] R.A. Rapaport and S.J. Eisenreich. Chromatographic determination of octanol-water partition coefficients (k_{ow}'s) for 58 polychlorinated biphenyl congeners. *Environmental Science and Technology*, 18:163–170, 1984.

[184] C. Ratsak, Kooijman S.A.L.M., and B.W. Kooi. Modelling the growth of an oligochaete on activated sludge. *Water Research*, 27:739–747, 1992.

[185] D. Rawsthorne and B.B. Brodie. Relationship between root growth of potato, root diffusate production and hatching of *Globodera rostochiensis*. *Journal of Nematology*, 18:379–384, 1986.

[186] H. Remmert. *Arctic animal ecology.* Springer Verlag, Berlin, 1980.

[187] G. Reversat. Increase of the chemical oxygen demand during the growth in *Heterodera sacchari. Revue de Nematologie*, 10:115–117, 1987.

[188] C.A. Richardson. An analysis of the microgrowth bands in the shell of the common mussel *Mytilus edulis. Journal of the Marine Biological Association U.K.*, 69:477–491, 1989.

[189] O. Richter and D. Söndgerath. *Parameter estimation in ecology, the link between data and models.* VCH, Weinheim, 1990.

[190] H.U. Riisgård, E. Bjornestad, and F. Mohlenberg. Accumulation of cadmium in the mussel *Mytilus edulis*: kinetics and importance of uptake via food and sea water. *Marine Biology*, 96:349–353, 1987.

[191] H.U. Riisgård and F. Møhlenberg. An improved automatic recording apparatus for determining the filtration rate of *Mytilus edulis* as a function of size and algal concentration. *Marine Biology*, 52:61–67, 1979.

[192] H.U. Riisgård and A. Randløv. Energy budgets, growth and filtration rates in *Mytilus edulis* at different algal concentrations. *Marine Biology*, 61:227–234, 1981.

[193] A.F. Robinson. Comparison of five methods for measuring nematode volumes. *Journal of Nematology*, 16:343–347, 1984.

[194] M.P. Robinson, H.J. Atkinson, and R.N. Perry. The effect of delayed emergence on infectivity of juveniles of the potato cyst nematode *Globodera rostochiensis. Nematologica*, 31:171–178, 1985.

[195] M.P. Robinson, H.J. Atkinson, and R.N. Perry. The influence of soil moisture and storage time on the motility, infectivity and lipid utilization of second stage juveniles of the potato cyst nematodes *Globodera rostochiensis* and *G.pallida. Revue de Nematologie*, 10:343–348, 1987.

[196] M.P. Robinson, H.J. Atkinson, and R.N. Perry. The influence of temperature on the hatching, activity and lipid utilization of second stage juveniles of the potato cyst nematodes *Globodera rostochiensis* and *G.pallida. Revue de Nematologie*, 10:349–354, 1987.

[197] M.P. Robinson, H.J. Atkinson, and Perry R.N. The association and partial characterisation of a fluorescent hypersensitive response of potato roots to the potato cyst nematodes *Globodera pallida* and *G. rosotchiensis. Revue de Nematologie*, 11:99–107, 1988.

[198] P.G. Rodhouse, J.H. McDonald, R.I.E. Newell, and R.K. Koehn. Gamete production, somatic growth and multiple-locus enzyme heterozygosity in *Mytilus edulis. Marine Biology*, 1986.

[199] P.G. Rodhouse, C.M. Roden, G.M. Barnell, M.P. Hensey, T. McMahon, B. Ottway, and T.H. Ryan. Food resource, gametogenesis and growth in *Mytilus edulis* on the shore and in suspended culture: killary harbour, ireland. *Journal of the Marine Biological Association U.K.*, 64:51–529, 1984.

[200] G. Roesijadi. Metallothioneins in metal regulation and toxicity in aquatic animals. *Aquatic Toxicology*, 22:81–114, 1992.

[201] A.H. Ross and R.M. Nisbet. Dynamic models of growth and reproduction of the mussel *Mytilus edulis* l. *Functional Ecology*, 4:777–787, 1990.

[202] G.J.S Ross and D. Trudgill. The effect of population density on the sex ratio of *Heterodera rostochiensis*: a two-dimensional model. *Nematologica*, 15:601–607, 1967.

[203] H.J. Rumpenhorst. Intracellular feeding tubes associated with sedentary plant parasitic nematodes. *Nematologica*, 30:77–85, 1984.

[204] J. Schans. *Population dynamics of potato cyst nematodes and associated damage to potato.* PhD thesis, Wageningen Agricultural University, The Netherlands, 1993.

[205] F. Schiemer. Food dependence and energetics of freeliving nematodes, 1. respiration, growth and reproduction of *Caenorhabditis briggsea* (nematoda) at different levels of food supply. *Oecologia*, 54:108–121, 1982.

[206] F. Schiemer. Food dependence and energetics of freeliving nematodes, 2. life history parameters of *Caenorhabditis briggsea* (nematoda) at different levels of food supply. *Oecologia*, 54:122–128, 1982.

[207] R. Schneider. Polychlorinated biphenyls (PCBs) in cod tissues from the western baltic: significance of equilibrium partiotioning and lipid composition in the bioaccumulation of lipophilic pollutants in gill-breathing animals. *Meeresforshung*, 29:69–79, 1982.

[208] T.W. Schoener. Population growth regulated by intraspecific competition for energy or time:some simple representations. *Theoretical Population Biology*, 4:56–84, 1973.

[209] S.M. Schrap. Bioavailability of organic chemicals in the aquatic environment. *Comparative Biochemistry and Physiology*, 100C:13–16, 1991.

[210] E.H. Schulte. Influence of algal concentration and temperature on the ltration rate of *Mytilus edulis. Marine Biology*, 30:331–341, 1975.

[211] R. Seed. The ecology of *Mytilus edulis* l. (lamellibranchiata) on exposed rocky shores. 2. growth and mortality. *Oecologia*, 3:317–350, 1969.

[212] R. Seed. The ecology of *Mytilus edulis* l. lamellibranchiata exposed rocky shores. 1. breeding and settlement. *Oecologia*, 3:277–316, 1969.

[213] L.A. Segel. *Modeling dynamic phenomena in molecular and cellular biology.* Cambridge University Press, Cambridge, 1984.

[214] J.A Seinhorst. Agronomic apsects of potato cyst infestation. In F. Lamberti and C.E. Taylor, editors, *Cyst Nematodes*, pages 211–227, NATO-ASI Series, Plenum Press, New York, 1986.

[215] J.A Seinhorst. The development of individuals and populations of cyst nematodes on plants. In F. Lamberti and C.E. Taylor, editors, *Cyst Nematodes*, pages 101–117, NATO-ASI Series, Plenum Press, New York, 1986.

[216] J.W. Seinhorst. Dynamics of populations of plant parasitic nematodes. *Annual Review of Phytopathology*, 8:131–156, 1970.

[217] J.W. Seinhorst. The regulation of the numbers of cysts and eggs per cyst produced by *Globodera pallida* and *G. rostochiensis* on potato roots at different initial egg densities. *Nematologica*, 39:104–114, 1993.

[218] J.W. Seinhorst. Relation between population density of potato cyst nematodes and measured degrees of susceptibility between this density and cyst content in the new generation. *Nematologica*, 30:66–67, 1984.

[219] M.K. Seymour. The feeding pump of *Ditylenchus dipsaci* (NEMATODA: TYLENCHIDA). *Nematologica*, 29:171–189, 1983.

[220] P.C. Sijmons, H.J. Atkinson, and U. Wyss. Parasitic strategies of root nematodes and associated host cell responses. *Annual Review of Phytopathology*, 32:235–259, 1994.

[221] P.C. Sijmons, F.M.W. Grundler, N. von Mende, P. Burrows, and U. Wyss. *Arabidopsis thaliana* as a new model host for plant parasitic nematodes. *The Plant Journal*, 1:245–254, 1991.

[222] K. Simkiss. Lipid solubility of heavy metals in saline solutions. *Journal of the Marine Biological Association, U.K.*, 63, 1983.

[223] R.D. Simpson. Uptake and loss of zinc and lead by mussels *Mytilus edulis* and relationships with body weight and reproductive cycle. *Marine Pollution Bulletin*, 10:74–78, 1979.

[224] M. Singh and S.B. Sharma. Temperature effects on development and reproduction of *Heterodera cajani* on pigeonpea. *Journal of Nematology*, 26:241–248, 1994.

[225] J.F. Southey. *Laboratory Methods for Work with Plant and Soil Nematodes, reference book 402*. Ministry of Agriculture, Fisheries and Food, London: Her Majesty's Stationary Office, 1986.

[226] A. Spacie and Hamelink J.L. Alternative models for describing the bioconcentration of organics in fish. *Environmental Toxicology and Chemistry*, 1:309–320, 1982.

[227] M. Sprung. Physiological energetics of mussel larvae (*Mytilus edulis*) 1. shell growth and biomass. *Marine Ecology Progress Series*, 17:283–293, 1984.

[228] J.M. Stanton and M Sartori. Hatching and reproduction of the potato cyst nematode *Globodera rostochiensis*, from potato fields in western australia as influenced by soil temperature. *Nematologica*, 36:457–464, 1990.

[229] A.R. Stone. *Heterodera pallida* N. SP. (NEMATODA: HETERODERIDAE), a second species of potato cyst nematode. *Nematologica*, 18:591–606, 1972.

[230] G.W. Storey. Spatial population dynamics of potato cyst nematode *Globodera rostochiensis* (WOLL.) in sandy and peaty loam during the course of a growing season. *Nematologica*, 28:219–232, 1982.

[231] R.M.J. Storey. The initial lipid reserves of juveniles of *Globodera* spp. *Nematologica*, 29:144–150, 1983.

[232] R.M.J. Storey. The relationship between neutral lipid reserves and infectivity for hatched and dormant juveniles of *Globodera* spp. *Annals of Applied Biology*, 104:511–520, 1984.

[233] T. Strömgren and C. Cary. Growth in length of *Mytilus edulis* l. fed on different algal diets. *Journal of the Marine Biological Association U.K.*, 76:23–34, 1984.

[234] J. Stronkhorst. Trends in pollutants in blue mussel *Mytilus edulis* and flounder *Platichtys flesus* from two dutch estuaries, 1985-1990. *Marine Pollution Bulletin*, 24:250–258, 1992.

[235] S. Tanabe, R. Tatsukawa, and D.F.H. Philips. Mussels as bioindicators of PCB pollution: a case study on uptake and release of PCB isomers and congeners in green-lipped mussels (*Perna viridis*) in hong kong waters. *Environmental Pollution*, 47:41–62, 1987.

[236] B.T. Theisen. The growth of *Mytilus edulis* l. (bivalvia) from disko and thule district, greenland. *Ophelia*, 12:59–77, 1973.

[237] B.T. Theisen. Variation in size of gills labial palps and adductor muscle in *Mytilus edulis* l. (bivalvia) from danish waters. *Ophelia*, 21:49–63, 1982.

[238] R.J. Thompson. Production, reproductive effort, reproductive value and reproductive cost in a population of the blue mussel *Mytilus edulis* from a subarctic environment. *Marine Ecology Progress Series*, 16:249–257, 1984.

[239] R.J. Thompson and B.L. Bayne. Active metabolism associated with feeding in the mussel *Mytilus edulis* l. *Journal of Experimental Marine Biology and Ecology*, 9:111–124, 1972.

[240] R.J. Thompson and B.L. Bayne. Some relationships between growth, metabolism and food in the mussel, *Mytilus edulis*. *Marine Biology*, 27:317–326, 1974.

[241] J.H.M. Thornley and J.J. Hesling. Models describing sex ratio dat in *Heterodera rostochiensis*, I environmentally determined sex. *Nematologica*, 18:563–570, 1972.

[242] D. Trudgill. The effect of environment on sex determination in *Heterodera rostochiensis*. *Nematologica*, 13:263–272, 1967.

[243] D. Trudgill. Resistance and tolerance of plant parasitic nematodes in plants. *Annual Review of Phytopathology*, 29:167–192, 1991.

[244] J.E. Tucker, D. Mauzerall, and E.B. Tucker. Symplastic transport of carboxyfluorescine in staminal hairs of *Setcreasea purperea* is diffusive and includes losses to the vacuole. *Plant Physiology*, 90:1143–1147, 1989.

[245] M.T. Tyree and P.M.L. Tammes. Translocation of uranin in the the symplasm of staminal hairs of *Tradescantia*. *Canadian Journal of Botany*, 53:2038–2046, 1975.

[246] O. Vahl. Efficiency of particulate retention of *Mytilus edulis* (l.). *Ophelia*, 10:17–25, 1972.

[247] P.M. Verbost. *Cadmium toxicity: interaction ofcadmium with cellular calcium transport mechanisms*. PhD thesis, Katholic University Nijmegen, Netherlands, 1989.

[248] J.H.G. Verhagen. A distribution and population model of the mussel *Mytilus edulis* in lake grevelingen. In W.K. Lauenroth, G.V. Skogerboe, and M. Flug, editors, *Analysis of ecological systems: State of the art in ecological modelling*, pages 373–383, Elsevier Scientific, Amsterdam, 1983.

[249] A. Viarengo, M.N. Moore, G. Mancinelli, A. Mazzucotelli, R.K. Pipi, and S.V. Farrar. Metallothioneins and lysosommes in metal toxicity and acccumulation in marine mussels: the effect of cadmium in the presence and absence of phenanthrene. *Marine Biology*, 94:251–257, 1987.

[250] A. Viarengo, S. Palermo, G. Zanicchi, R. Capelli, R. Vaiserre, and M. Orunesu. Role of metallothioneins in cd and cu accumulation and elimination in the gill and digestive gland cells of *Mytilus galloprovinciales* lam. *Marine Environmental Research*, 16:23–36, 1985.

[251] C.H. Walker. Kinetic models to predict bioaccumulation of pollutants. *Functional Ecology*, 4:295–301, 1990.

[252] S.A. Ward, R. Rabbinge, and H. den Ouden. Construction and preliminary evaluation of a simulation model of the population dynamics of the potato cyst nematode *Globodera pallida*. *Netherlands Journal of Plant Pathology*, 91:27–44, 1985.

[253] W. van der Werf, R. Rabbinge, and W. Heijbroek. Spring invasion of *Heterodera schachtii* in sugarbeet: a simulation study. *Netherlands Journal of Plant Pathology*, 92:33–42, 1986.

[254] J. Widdows. Combined effects of body size, food concentration and season on the physiology of *Mytilus edulis*. *Journal of the Marine Biological Association U.K.*, 58:109–124, 1978.

[255] J. Widdows. The effect of temperature on the metabolism and activity of *Mytilus edulis*. *Netherlands Journal of Sea Research*, 7:387–398, 1973.

[256] J. Widdows and B.L. Bayne. Temperature acclimation of *Mytilus edulis* with reference to its energy budget. *Journal of the Marine Biological Association U.K.*, 51:827–843, 1971.

[257] J. Widdows, P. Fieth, and C.M. Worral. Relationship between seston, available food and feeding activity in the common mussel *Mytilus edulis*. *Marine Biology*, 50:195–207, 1979.

[258] J. Widdows and A.J.S. Hawkins. Partitioning of rate of heat dissipation by *Mytilus edulis* into maintenance, feeding and growth components. *Physiological Zoology*, 62:764–784, 1989.

[259] K.J. Williams and J.M. Fisher. Development of *Heterodera avenae* woll. and host cellular responses in susceptible and resistant wheat. *Fundamental and Applied Nematology*, 16:417–423, 1993.

[260] J.E. Winter. The filtration rate of *Mytilus edulis* and its dependence on algal concentrations, measured by a continuous automatic recording apparatus. *Marine Biology*, 22:317–328, 1973.

[261] J.E. Winter. A review on the knowledge of suspension-feeding in lamellibranchiate bivalves, with special reference to artificial aquaculture systems. *Aquaculture*, 13:1–33, 1978.

[262] R.T. Wright, R.B. Coffin, C.P. Ersing, and D. Pearson. Field and laboratory measurements of bivalve filtration of natural marine bacterioplankton. *Limnology and Oceanography*, 27:91–98, 1982.

[263] U. Wyss. Observations on the feeding behaviour of *Heterodera schachtii* throughout development, including events during moulting. *Fundamental and Applied Nematology*, 15:75–89, 1992.

[264] U. Wyss and F.M.W. Grundler. The feeding behaviour of sedentary plant parasitic nematodes. *Netherlands Journal of Plant Pathology*, Suppl. 2:165–173, 1992.

[265] U. Wyss, F.M.W. Grundler, and A. Münch. The parasitic behaviour of second-stage juveniles of *Meloidogyne incognita* in roots of *Arabidopsis thalliana*. *Nematologica*, 38:98–111, 1992.

[266] P. Yodzis. *Introduction to theoretical ecology*. Harper & Row Publ. Inc., 1989.

[267] D.I. Zandee, J.H. Kluytmans, W. Zurburg, and H. Pieters. Seasonal variations in biochemical composition of *Mytilus edulis* with reference to energy metabolism and gametogenesis. *Netherlands Journal of Sea Research*, 14:1–29, 1980.

[268] C. Zonneveld. *Animal energy budgets: a dynamic approach*. PhD thesis, Free University, Amsterdam, Netherlands, 1992.

[269] C. Zonneveld and S.A.L.M. Kooijman. The application of a dynamic energy budget model to *Lymnaea stagnalis*. *Functional Ecology*, 3:269–278, 1989.

[270] C. Zonneveld and S.A.L.M. Kooijman. Comparative kinetics of embryonic development. *Bulletin of Mathematical Biology*, 55:609–635, 1993.

[271] J.J.G. Zwolsman and G.T.M. van Eck. Dissolved and particulate trace metal chemistry in the scheldt estuary, s.w.-netherlands (water column and sediments). *Netherlands Journal of Aquatic Ecology*, 27:287–300, 1993.

Samenvatting

Het onderzoek beschreven in dit proefschrift betreft de toepassing van een Dynamisch Energie Budget, DEB, model op verschillende concrete situaties. Het DEB model is ontwikkeld door Kooijman en recent uitgebreid beschreven [125]. Volgens het DEB model functioneren alle dierlijke organismen op een gelijke wijze. Het basale patroon is dat ze voedsel opnemen, dit verteren en het onverteerde voedsel weer uitscheiden. Opgenomen voedingsstoffen worden opgeslagen in een energie voorraad van waaruit het gebruikt wordt voor groei, onderhoud en voortplanting van het individu. De kwantitatieve regels voor deze processen zijn toepasbaar op vele organismen en kunnen daarom als uitgangspunt dienen voor verdere studie van een bepaald organisme in zijn omgeving.

De eerste toepassing betreft het werk aan de zoutwater mossel *Mytilus edulis*. Deze mossel wordt voor consumptie gekweekt en veelal in het buitenland verkocht. Om deze redenen wordt er veel onderzoek gedaan naar de groei van de mossel en naar de lichaamsvreemde (giftige) stoffen in het mosselvlees.

De mossel kan vrij snel lichaamsvreemde stoffen uit het water opnemen via zijn kieuwen maar ook via het voedsel. De chemische eigenschappen van deze stoffen en de hoeveelheden in het water bepalen samen met de grootte en de fysiologische conditie van de mossel de opname en uitscheidingssnelheid van deze stoffen. Er is een onderscheid te maken tussen zware metalen als cadmium en kwik, en organische verbindingen (veelal gechloreerde koolwaterstoffen) zoals PAK's en PCB's. PCB's zijn olie-achtige stoffen en een algemene regel is dat hoe olie-achtiger een chemische stof, des te sneller wordt deze stof opgenomen. Voor zware metalen geldt de oplosbaarheid als bepalende factor voor opname.

De fysiologie van de mossel is belangrijk voor de opname, de opslag en de uitscheiding van de chemische stoffen. Om deze reden is eerst het fysiologisch DEB model voor de mossel ingevuld. Gegevens van experimenten die in de wetenschappelijke literatuur beschreven zijn, zijn opnieuw geanalyseerd en gebruikt om de constanten van het DEB model te bepalen.

Een mossel blijft gedurende zijn ontwikkeling op één plaats vast zitten. De chemische stoffen die door de mossel opgenomen zijn, kunnen een lange tijd in de mossel aanwezig blijven. Daarom is de mossel te gebruiken als 'bewaker' van de waterkwaliteit. Regelmatige bemonstering is dan voldoende om een inzicht te krijgen in de hoeveelheden chemische stoffen in het water. Belangrijk is echter wel dat ook de hoeveelheid voedsel voor de mossel of de groei van de mossel gemeten wordt, de conditie van de mossel bepaald immers de hoeveelheid chemische stof in het mosselvlees.

Op verzoek van het Rijksinstituut voor Kust en Zee RIKZ van het ministerie van Verkeer en Waterstaat is het DEB model uitgebreid om de opname en afgifte van de lichaamsvreemde stoffen in de mossel te beschrijven en te voorspellen. Het model is toegepast op de situatie in de Westerschelde. De reconstructie van de cadmium concentraties in mosselen verzameld bij Terneuzen is goed. Ook de reconstructies van andere stoffen zoals PAK's en PCB's is bevredigend.

De tweede toepassing van het DEB model betreft de populatiedynamica van het aardappelcysteaaltje. Aardappelcysteaaltjes *Globodera pallida* en *G. rostochiensis* zijn de oorzaak van aardappelmoeheid. Aardappelcysteaaltjes zijn kleine glasachtige rondwormen (nema-

toden) die in het infectieve stadium 0.02 mm breed en 0.5 mm lang zijn. In het infectieve stadium dringen ze de wortel binnen en maken ze een overdrachtcel aan die ze van voedsel voorziet dat uit de vaatbundels van de wortel gehaald wordt. De aaltjes hechten zich aan deze cel vast en kunnen zich vervolgens niet meer verplaatsen. De aaltjes ontwikkelen zich verder tot of bolvormige vrouwtjes, met een diameter van 0.5 mm, die uiteindelijk uit de wortel barsten of tot wormvormige mannetjes die als volwassene de wortel verlaat en de uit de wortel gebarsten vrouwtjes bevruchten. De gevormde eitjes blijven in het vrouwtje waarvan de huid na haar dood uithardt en een beschermende laag om de eitjes vormt. De zo gevormde cyste kan jaren in de bodem blijven en de eitjes in deze cyste kunnen maximaal 30 jaar infectief blijven.

Het is duidelijk dat aardappelmoeheid moeilijk te bestrijden is. Daarom wordt er op grote schaal grondontsmetting toegepast, 60% van alle pesticiden wordt gebruikt voor grondontsmetting. In deze tijd is het gebruik van gifstoffen politiek niet meer haalbaar en daarom wordt er veel onderzoek uitgevoerd naar alternatieve bestrijdingsmethoden.

Een alternatieve bestrijdingsmethode is het verbouwen van resistente en partieel resistente aardappelen in een optimale gewasrotatie. Hiervoor is het belangrijk dat de aardappelcysteaaltjes niet in aantal toenemen en bij voorkeur zelfs in aantal afnemen. Daarom moeten er betrouwbare populatiedynamische modellen ontwikkeld worden die de aantallen aaltjes goed kunnen voorspellen. Hier wordt het DEB model toegepast. In eerste instantie wordt in dit proefschrift de groei van het aaltje bestudeerd op één aardappelwortel met een techniek die is overgenomen van prof. Atkinson van de Universiteit van Leeds in het Verenigd Koninkrijk. Het individuele model wordt geschikt gemaakt om de groei en het aantal eitjes per vrouwtje te voorspellen voor verschillende aardappelrassen. Mannetjes zijn in de populatiedynamica niet van belang en worden daarom niet gemodelleerd. Vervolgens wordt er een model ontwikkeld om het binnendringen van de aaltjes in de wortel en de hoeveelheid voedsel die ze aan de aardappelplant onttrekken te voorspellen. De combinatie van deze modellen wordt geschikt gemaakt om de metingen aan aardappelplanten die in het veld en in bloempotten uitgevoerd zijn te beschrijven. Het blijkt dat het model de populatiedynamica van de aaltjes in het veld en in de bloempotten goed beschrijft. Op deze manier is een verband gelegd tussen groeimetingen aan aaltjes die eenvoudig in het laboratorium uitgevoerd kunnen worden en de processen die in het veld moeilijk te meten zijn. Dit is een verbetering van de bestaande technieken en zal bijdragen aan het optimaliseren van rassenkeuze en gewasrotaties.

Nawoord

In dit late uur waarop ik onder druk van de tijdslimiet de laatste hand aan mijn proefschrift leg, moet juist een van de belangrijkste taken vervuld worden. Mijn dank te uiten aan allen die mij geholpen hebben dit proefschrift tot stand te brengen.

In de eerste plaats dank ik Bas Kooijman, Cees Booij en Howard Atkinson. Zij vormden voor mij een voortdurende bron van inspiratie.
Bas, jij hebt mij de mogelijkheden in handen gegeven om dit proefschrift te maken. Wat mij vooral in je trof, was naast het vertrouwen dat je in je mensen stelde, de openheid waarbinnen discussies gevoerd konden worden.
Cees, de vrijheid die me op het IPO werd veroorloofd, heb ik grotendeels aan jou te danken. De dagelijkse werkbesprekingen bij de koffie waren voor mij onmisbaar en bijzonder stimulerend.
Howard, I am grateful for your friendly and inspiring cooperation and for giving me the privilege to learn techniques in your laboratory.

Veel dank ben ik verschuldigd aan Esther Hendrikx voor haar inzet en motivatie. Zij gaf een belangrijke bijdrage aan het onderzoek en zorgde voor een prettige werksfeer op het lab.

Marcel van Oijen, Hetty Regeer en Frits Arntzen wil ik danken voor de samenwerking in gemeenschappelijke experimenten en het bespreken van elkaars ideeën.
Hierbij wil ik Hans Schepers noemen die onder grote tijdsdruk het projekt voor DGW heeft afgerond op het moment dat ik aan mijn onderzoek op het IPO begon en Gonnie van Bussel die als studente veel werk heeft verzet voor de verwerking van veldproeven.

Het goede werkklimaat waarvoor vele collegas bij de Dienst Getijdewateren, Theoretische Biologie en het Instituut voor Planteziektenkundig Onderzoek hebben gezorgd, wil ik hier niet onvernoemd laten. Het is altijd een stimulerende bijdrage geweest waarvoor ik jullie allen erkentelijk ben.
Verder dank ik alle anderen die op enigerlei wijze deelname hebben gehad aan de totstandkoming van dit proefschrift.

Tot slot wil ik Katinka noemen, de vrouw van wie ik het meeste hou, die met haar eigen perspektief het hele proces van onderzoek heeft ingekleurd.

Hopend dat ik in deze laatste zinnen voor ieder van jullie het juiste dankwoord heb gevonden, wil ik hierbij mijn proefschrift beëindigen.

CURRICULUM VITAE

Rob J.F. van Haren werd op 23 juni 1961 geboren te Nijmegen. Aldaar bezocht hij het Dominicus College. In juni 1979 werd het diploma Atheneum B behaald. In september van hetzelfde jaar werd begonnen met de studie Biologie aan de Landbouw Universiteit te Wageningen, waar in april 1987 het doctoraal examen werd afgelegd.

Doctoraalvakken werden gevolgd in de dierecologie en de wijsbegeerte. In 1983-1984 werd het inhaalprogramma filosofie aan de faculteit filosofie van de Katholieke Universiteit Nijmegen gevolgd en met goed gevolg afgesloten. De stages werden doorgebracht bij het Proefstation voor Tuinbouw onder Glas te Naaldwijk en bij het Nederlands Instituut voor Onderzoek der Zee.

Van mei 1987 tot april 1989 werd hij aangesteld als toegevoegd onderzoeker bij het Rijksinstituut voor Kust en Zee (RIKZ) van het Ministerie van Verkeer en Waterstaat. Gedurende deze periode ontwikkelde hij wiskundige modellen voor toxico-kinetiek van zware metalen, PCB'S en PAK'S in de mossel *Mytilus edulis* in kader van het project Systeem Analyse Westerschelde (SAWES).

Van mei 1989 tot oktober 1990 werd hij op fondsen van het RIKZ in kader van het project SAWES als toegevoegd onderzoeker aangesteld bij de vakgroep Theoretische Biologie ten behoeve van het ontwikkelen van een toxico-kinetisch model voor de mossel op basis van de Dynamische Energie Budget (DEB) theorie. Het in het eerste gedeelte van dit proefschrift beschreven onderzoek is daar het resultaat van.

Van oktober 1990 tot november 1994 werd hij aangesteld op het Instituut voor Planteziektenkundig Onderzoek (IPO-DLO) te Wageningen als onderzoeker/projektleider met als opdracht het ontwikkelen van populatie-dynamische modellen voor het aardappelcysteaaltje *Globodera pallida* op basis van de DEB theorie ten behoeve van teelt-management systemen. Het in het tweede gedeelte van dit proefschrift beschreven onderzoek is daar het resultaat van.

Thans is hij werkzaam als post-doc onderzoeker aan de Landbouw Universiteit te Wageningen bij de vakgroep Terrestrische Oecologie en Natuurbeheer, sectie bodembiologie met als opdracht de effekten van wortelherbivorie door macro-evertebraten op de nutriënten dynamiek in de bodem en competitie tussen grassen in een verschralingssuccessie van graslanden langs de Drentse A te bestuderen.

PUBLICATIONS

Scientific publications

1. R.J.F. van Haren, M.M. Steenhuis, M.W. Sabelis & O.M.B. de Ponti, 1987, Tomato stem trichomes and dispersal succes of *Phytoseiulus persimilis* relative to its prey *Tetranychus urticae, Experimental and Applied Acarology*, **3**, 115-121.

2. R.J.F. van Haren, J. van der Meer & M.B. de Vries, 1990, Cadmium and copper accumulation in the common mussel *Mytilus edulis* in the Western Scheldt estuary: a model approach, *Hydrobiologia*, **195**, 105-118.

3. S.A.L.M. Kooijman & R.J.F. van Haren, 1990, Animal energy budgets affect the kinetics of xenobiotics, *Chemosphere*, **21**, 681-694.

4. R.J.F. van Haren & S.A.L.M. Kooijman, 1993, Application of a dynamic energy budget model to *Mytilus edulis* (L.), *Netherlands Journal of Sea Research*, **31(2)**: 119-133.

5. R.J.F. van Haren, E.M.L. Hendrikx & H.J. Atkinson, 1994, Growth curve analysis of sedentary plant parasitic nematodes in relation to plant resistance and tolerance, in: *'Predictability and Nonlinear Modelling in Natural Sciences and Economics'*, eds: J. Grasman & G. van Straten, Kluwer, Amsterdam, pages 186-197.

6. R.J.F. van Haren, H.E. Schepers & S.A.L.M. Kooijman, 1994, Dynamic energy budgets affect kinetics of xenobiotics in the marine mussel *Mytilus edulis, Chemosphere*, **29**:163-189.

7. M. van Oijen, F.J. de Ruiter & R.J.F. van Haren, 1995, Modeling the interaction between potato crops and cyst nematodes, Ecology and Modeling of Potato Crops under conditions of limiting growth, Eds: Haverkort, A.J. and MacKerron, D.K.L., Kluwer Academic Publishers, in press.

8. M. van Oijen, F.J. de Ruiter & R.J.F. van Haren, 1995, Responses of field-grown potato cultivars to cyst nematodes, at three levels of soil compaction, 1. Leaf area dynamics, photosynthesis and crop growth, *Annals of Applied Biology*, submitted.

9. M. van Oijen, F.J. de Ruiter & R.J.F. van Haren, 1995, Responses of field-grown potato cultivars to cyst nematodes, at three levels of soil compaction, 2. Root length dynamics and nutrient uptake, *Annals of Applied Biology*, submitted.

10. R.J.F. van Haren, F. Arntzen, & H.J. Atkinson, 1995, Growth of vermiform nematodes compared with growth and fecundity of the potato cyst nematode *Globodera pallida* on different hosts, a model approach. *Fundamental and Applied Nematology*, submitted.

11. R.J.F. van Haren, 1995, Quantification of apoplastic feeding rates of the potato cyst nematode *Globodera pallida* by Image Analysis, *Fundamental and Applied Nematology*, submitted.

12. R.J.F. van Haren, H. Regeer & M. van Oijen, 1995, Modelling population dynamics of potato cyst nematodes based on individual dynamic energy budgets and potato root dynamics: a study into intraspecific competition, in preparation.
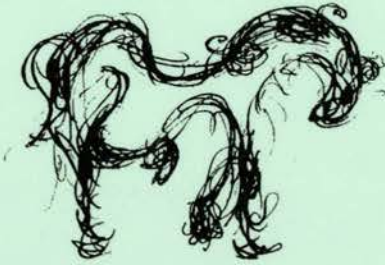
Reports

1. R.J.F. van Haren, 1988, Het Eems-Dollard model verkwikt., NIOZ rapport 1988-9, Nederlands Instituut voor Onderzoek der Zee, Ecologisch Onderzoek Noordzee en Waddenzee, Texel, the Netherlands.

2. R.J.F. van Haren, 1988, Minder PCB's, meer zeehonden in de Waddenzee? Een prognose voor 1995., Nota GWAO-88.011, Ministry of Public Works and Transport, Tidal Waters Division, The Hague, the Netherlands.

3. R.J.F. van Haren, 1988, Accumulatie model voor zware metalen in de mossel *Mytilus edulis*. Een black-box model en een fysiologisch gestructureerd model., Nota GWAO-88.049, Ministry of Public Works and Transport, Tidal Waters Division, The Hague, the Netherlands.

4. R.J.F. van Haren & M.B. de Vries, 1989, UPTiMUM, een dynamisch model voor de opname van zware metalen door *Mytilus edulis*. Rapportage van modelontwikkeling, calibratie en validatie. Report T0252, Delft Hydraulics, Delft, The Netherlands.

5. R.J.F. van Haren, H.E. Schepers & S.A.L.M. Kooijman, 1990, Application of a one-compartiment toxico kinetic model to artificial and environmental contaminated marine mussels (*Mytilus edulis*) in the Western Scheldt. Final report prepared for the Ministry of Public Works and Transport, Tidal Waters Division, The Hague, The Netherlands, from the department of Theoretical Biology, Free University, Amsterdam, The Netherlands.

6. R.J.F. van Haren & H.E. Schepers, 1990, Handleiding voor accumulatie-eliminatie modellen voor de mossel *Mytilus edulis* en de wadpier *Arenicola marina* in de SENECA omgeving. Final report prepared for the Ministry of Public Works and Transport, Tidal Waters Division, The Hague, The Netherlands, from the department of Theoretical Biology, Free University, Amsterdam, The Netherlands.

Abstracts

1. R.J.F. van Haren & E.M.L Hendrikx, 1992, Population dynamic models of potato cyst nematodes based on dynamic energy budgets, *Nematologica*, **38**: 414

2. R.J.F. van Haren & E.M.L. Hendrikx, 1995, Feeding, growth and reproduction of potato cyst nematodes, *Nematologica* in press.

3. E.M.L. Hendrikx, E.M.J. Meijer & R.J.F. van Haren, 1995, A biochemical method for calibration of lipid determination techniques for potato cyst nematodes, *Nematologica* in press.

4. A.H.M. van Bussel, R.J.F. van Haren & M. van Oijen, 1995, A model for the interaction between root growth of potato cultivars and the population dynamics of the potato cyst nematode (PCN), *Nematologica* in press.